Energy Research and Development Division
FINAL PROJECT REPORT

# ASSESSMENT OF CALIFORNIA'S NATURAL GAS PIPELINE VULNERABILITY TO CLIMATE CHANGE

## White Paper from the California Energy Commission's Climate Change Center


Prepared for: California Energy Commission
Prepared by: University of California, Berkeley



JANUARY 2017
CEC-500-2017-008

**PREPARED BY:**

***Primary Authors:***
John D. Radke
Greg S. Biging

***Co-Authors:***
Martine Schmidt-Poolman, Howard Foster, Emery Roe,
Yang Ju, Olivier Hoes, Tessa Beach, Amna Alruheil,
Liam Meier, Wei-Chen Hsu, Rosanna Neuhausler,
William Fourt, Wei Lang, Uriel Garcia, Ian Reeves

University of California, Berkeley
College of Environmental Design
College of Natural Resoruces
101 Sproul Hall
Berkeley, CA 94720
Phone: 510-642-5215

***Contract Number: 500-11-016***

***Prepared for:***

**California Energy Commission**

Susan Wilhelm
***Contract Manager***

Aleecia Gutierrez
***Office Manager***
***Energy Generation Research Office***

Laurie ten Hope
***Deputy Director***
***ENERGY RESEARCH AND DEVELOPMENT DIVISION***

Robert P. Oglesby
***Executive Director***

# ACKNOWLEDGEMENTS

This work was funded by the Public Interest Energy Research (PIER) program of the California Energy Commission, grant UCB 500-11-016 to the University of California, Berkeley. Guido Franco has been critical in providing the vision for this work as well as for the entire Public Interest Energy Research Program project. We gratefully acknowledge Dr. Dan Cayan and Dr. Peter Bromirski at Scripps Institute of Oceanography, for discussions on sea-level rise and extreme storms.

We would like to acknowledge Amy Micka Lindblom, Principal and Asset Management Specialist at PG&E Gas Transmission Asset & Risk Management. Without her commitment and follow-through our research collaboration would not have been possible. Teddy Atkinson, Gas Technical Specialist (GIS) in PG&E's Integrity Management was also instrumental in taking the GIS results and working through implications for the Transmission Asset Family in Gas Operations. We also especially thank Andy Wenzel, Supervisor in PG&E Gas Control, who made it possible to visit the transmission side of the Gas Control Center; he also provided valuable insights into real-time Gas Operations, both its history and current status.

We are grateful to the following people for their input: Esfandiar Imani, Risk Manager, PG&E Gas Operations (particularly for his help regarding the research NDA with PG&E and our visits to its Gas Operations Control Center); Bronson Ingemansson, Gas Engineer, Transmission Integrity Management Program (TIMP) Risk Management; Jonathan Rigotti, Senior Engineer, Corrosion Engineering Services; Troy Rovella, Principal Business Analyst, Transmission Investment Planning; and particularly Alex Quintana, Risk Analyst in PG&E Gas Operations, for his insights and logistical assistance. Finally, we would like to thank Christine Cowsert Chapman, Senior Director of Asset Knowledge & Integrity Management and Chris Benjamin, Director, Corporate Sustainability at PG&E for their input and comments on this report.

We would like to acknowledge Kinder Morgan Energy Partners, L.P. staff for their input: Peter G. Murphy, Operations Manager (KM Richmond Station) for his time and follow-through; Nicole Stewart (Area Manager, KM Brisbane Terminal) and Darrell Donaho (GIS-PODS Manager, Pipeline Integrity) for their discussions and guidance on the impact of inundation on their liquids pipeline system; and Matt Wickland (Wickland Pipelines LLC) and Donald Scott, (General Manager, Swissport Fueling Services) for their help in understanding the jet fuel side of the hazardous liquids system in the Bay Area.

At the San Francisco Airport, we benefited from the jet-fuel insights of: John Pickens (Operating SFO Fuel CO, LLC); Rosalyn Yu and Nixon Lam of the SFO's Environmental Affairs; Dave Maas, Deputy Planning Director; Sandra Oberle, Supervising Property Manager, and Michael Zimmerman, Manager, Environmental and Airfield Program.

We would like to thank Paul R. Schulman who participated in some of the early interviews and whose discussion and observations were particularly helpful.

We gratefully acknowledge Simone Brant and Dr. Susan Wilhelm, our project managers at the PIER Program at the California Energy Commission, for their guidance and patience during the execution of this research. This research work is made stronger by their collective input and we are grateful to them for sharing their expertise with us. Any mistake in this research document is the responsibility of the authors alone.

Finally, the modeling undertaken in this research was compute-intensive and was processed on numerous computers. We acknowledge the support provided by the Beatrix Farrand Research Fund, Department of Landscape Architecture, University of California at Berkeley for support of this computing. In addition, we gratefully acknowledge the support of Apple Inc. in the form of an Apple MacPro, with very capable processing speed, that arrived just-in-time for some of the heavy lifting.

# PREFACE

The California Energy Commission Energy Research and Development Division supports public interest energy research and development that will help improve the quality of life in California by bringing environmentally safe, affordable, and reliable energy services and products to the marketplace.

The Energy Research and Development Division conducts public interest research, development, and demonstration (RD&D) projects to benefit California.

The Energy Research and Development Division strives to conduct the most promising public interest energy research by partnering with RD&D entities, including individuals, businesses, utilities, and public or private research institutions.

Energy Research and Development Division funding efforts are focused on the following RD&D program areas:

- Buildings End-Use Energy Efficiency
- Energy Innovations Small Grants
- Energy-Related Environmental Research
- Energy Systems Integration
- Environmentally Preferred Advanced Generation
- Industrial/Agricultural/Water End-Use Energy Efficiency
- Renewable Energy Technologies
- Transportation

*Assessment of California's Natural Gas Pipeline Vulnerability to Climate Change* is the final report for the project (contract number 500-11-016) conducted by the University of California, Berkeley. The information from this project contributes to Energy Research and Development Division's Environmental Area Program.

When the source of a table, figure or photo is not otherwise credited, it is the work of the author of the report.

For more information about the Energy Research and Development Division, please visit the Energy Commission's website at www.energy.ca.gov/research/ or contact the Energy Commission at 916-327-1551.

# ABSTRACT

One of California's greatest concerns related to global and regional climate change is the vulnerability of infrastructure to the effects of extreme storm events and long-term sea level rise. California's natural gas transmission system, much of which is located along the state's waterways, is particularly vulnerable to damage caused by inundation (flooding).

To assess potential effects of climate change on natural gas infrastructure, researchers created computer simulations of water level fluctuations in the San Francisco Bay, the Sacramento-San Joaquin River Delta Region, and the Coast. They integrated a high-resolution earth surface model created using publically available geographical information system data with dynamic three-dimensional water modeling based on historical observed near-100-year storm events coupled with various increments of sea level rise. This novel modeling method allowed researchers to analyze both the realistic flow of water across the landscape during a storm event and the effects of inundation on infrastructure at regional and local scales. This method included dynamic influences of tides and storm surges as well as surface objects that impede water flows, such as buildings.

By comparing the location, depth, and duration of inundation from these simulations against the locations of existing natural gas transmission infrastructure, researchers were able to characterize the system's vulnerability to inundation associated with the coupling of sea level rise and storms. The research team also collaborated with natural gas pipeline operators to better understand the risks of damage and structural failure. Research results provide valuable input for gas operation programs, plans, and investments to develop adaptation strategies for lessening the impact of potential flood damage.

**Keywords:** climate change, sea-level rise, flooding, inundation, extreme storm surge, peak water levels, natural gas transmission pipeline infrastructure vulnerability, digital elevation model, DEM, digital surface model, DSM, LiDAR, hydrodynamic model, and 3Di.

Please use the following citation for this paper:

Radke, J. D., G. S. Biging, M. Schmidt-Poolman, H. Foster, E. Roe, Y. Ju, O. Hoes, T. Beach, A. Alruheil, L. Meier, W. Hsu, R. Neuhausler, W. Fourt, W. Lang, U. Garcia I. Reeves (University of California, Berkeley). 2016. ***Assessment of Bay Area Natural Gas Pipeline Vulnerability to Climate Change***. California Energy Commission. Publication number: CEC-500-2017-008

## TABLE OF CONTENTS

## LIST OF FIGURES

## LIST OF TABLES

# EXECUTIVE SUMMARY

## Introduction

Uninterrupted supply of natural gas is vital to California's economy and the well-being of the state's population. Natural gas meets nearly one-third of California's total energy demand, and natural gas-fired generation is the dominant source of electricity in the state, accounting for approximately 43 percent of all generation in 2012. Given the state's reliance on this resource, the pipeline infrastructure and facilities designed to store, transmit, and distribute natural gas throughout the region are critical.

Nevertheless, this infrastructure may be at increasing risk of damage caused by long-term sea-level rise (SLR) and more frequent and intense storms—changes associated with global and regional climate change. In locations where California's natural gas transmission system is located along the state's waterways, it is especially vulnerable to inundation (flooding) of increased frequency, duration, and depth. Such inundation may cause increased hydrostatic pressure, erosion, disruption of supporting materials, and exposure to saline conditions. These conditions have the potential to accelerate structural failures and threaten the functionality of California's natural gas transmission system as a whole without appropriate resilience measures.

## Project Purpose

Researchers were motivated to assess the vulnerability of California's natural gas transmission system vulnerability after analyzing the flood damage caused by Hurricane Katrina to the natural gas transmission system in the New Orleans region. The 2005 storm inundated the region's natural gas pipeline systems with salt-and-brackish water, causing the pipeline system owner to replace 486 kilometers (302 miles) of pipeline out of concern for corrosion damage. With this in mind, researchers set out to develop a comprehensive, high-resolution hydrodynamic model that would enable them to identify how much of California's natural gas transmission system might be at risk for damage caused by extreme storm surges and rising sea-levels resulting from climate change. The main goal of this research was to provide a baseline of high-quality data to inform planners and policymakers in their efforts to develop strategies to lessen potential damage from SLR.

## Project Process and Results

Researchers used computer models to simulate different flooding scenarios in three primary regions: the San Francisco Bay Area, the Sacramento-San Joaquin River Delta, and California's full coastline. They then analyzed the location of existing natural gas transmission pipelines and associated infrastructure to identify locations of possible vulnerability to inundation damage associated with extreme storms and various increments of long-term SLR.

High-resolution surface elevation models of the three regions were created by combining high resolution airborne laser scan LiDAR point clouds with publically available geographic information systems (GIS) data. The models incorporated surface objects (such as buildings) that may affect the movement of water over the landscape. These regional surface models were integrated with a hydrodynamic model called 3Di to simulate different locations and depths of flooding. In the Bay and Delta regions, the flood simulation was calibrated using actual observed time series of water level data from a past near-100-year storm event coupled with four levels (0.0, 0.5, 1.0, and 1.41 meters) of SLR.

According to modeling results, SLR greater than 1.0 meter would, with current infrastructure and surface features, be expected to cause portions of the natural gas infrastructure system in California to fall within areas of inundation during extreme storm events. To better understand potential risks to the state's pipeline system, the research team shared data and collaborated with natural gas pipeline operators. Discussions where held with both PG&E gas pipeline operators to analyze the potential risks to their pipeline systems in areas identified as being inundated in the flooding simulations.

Researchers and PG&E staff collaborated to address utility's primary concern regarding climate change-induced inundation—risk to their pipelines caused by the weight of water on the landscape during and after a storm surge. Under a non-disclosure agreement, researchers shared the results of several scenarios including 1.41 meters of SLR coupled with a near 100-year storm event, for the Bay Area and Delta regions. Based on the modeled inundation predictions, researchers and PG&E gas pipeline operators formulated preliminary cost estimates and strategies for avoiding and lessening damage to PG&E-operated natural gas infrastructure.

By integrating their sophisticated spatial modeling with the pipeline operators' risk analysis framework for operation, program, and planning purposes, researchers presented pipeline operators with a critical opportunity to plan the redesign, replacement, and/or retrofit of infrastructure to mitigate possible effects, thereby facilitating climate change adaptation in the energy sector.

### Benefits to California

The research team successfully demonstrated an improved SLR and storm surge modeling technique that produced the most detailed and dynamic simulation of inundation in the Bay Area, Delta Region, and coastal region at the time of this project's completion. This innovative modeling method has the potential to help California develop realistic strategies to strengthen and better manage its natural gas infrastructure to prepare for emergencies. The models can also be used to simulate other potential inundation scenarios. Furthermore, the results of this study will inform PG&E's ongoing efforts to better understand, plan for, and respond to climate change risks.

# CHAPTER 1: Introduction

One of the greatest concerns related to global and regional climate change is the potential for impacts to infrastructure from extreme storm events coupled with long-term sea-level rise (SLR). In California, the natural gas transmission system is a critical infrastructure system and at risk with much located along the state's waterways. This makes the system vulnerable to impacts from a greater frequency, duration, and depth of inundation.[1] Such inundation may result in increased hydrostatic pressure, erosion, debris flows, disruption of supporting materials, and exposure to saline conditions. These conditions have the potential to accelerate structural failures and potentially threaten the functionality of California's natural gas transmission system as a whole.

In this study, researchers characterized the vulnerability of the natural gas transmission system to SLR by simulating where assets are likely to be affected by inundation and collaborate with system operators to analyze the risks that this inundation poses to the system. The analysis integrated geographic information systems (GIS) and a state-of-the art hydrodynamic model, 3Di, to simulate the location and depth of potential inundation in California under realistic extreme storm events coupled with various increments of SLR.[2] Researchers analyzed the location of natural gas transmission pipelines and associated infrastructure in relation to inundation projections to identify vulnerable locations. Results demonstrate that under projected SLR greater than one meter, significant portions of the natural gas infrastructure system in California would fall within areas of inundation. The research team provided this data to sophisticated risk assessment pipeline operators at Pacific Gas and Electric Company (PG&E), who voluntarily agreed to assess the risk such inundation poses to their assets and help inform efforts to design mitigation strategies.

This research is unique and innovative in its dynamic spatial detail and the fact that it incorporates time-series water level data from real past (near 100-year) storm events to capture the dynamic effect of storm surges[3] in modeling inundation. The novel modeling methodology incorporates higher spatial land surface resolution as the complexity of the landscape increases,

---

[1] The term *inundation* is used throughout this report to refer to lands that are flooded during a storm event. Some of this land will remain permanently inundated, some land will eventually dry, while other lands, over time, will eventually be pumped dry as a result of land management practices. The research team's concern was to report the location and the maximum inundation depth of water that came into contact with gas transmission pipeline infrastructure during the storm event.

[2] Increments of SLR are modeled to calculate Peak Water Levels (PWL) that are originally calibrated with PWL measured at gauging stations during real near 100-year storm events. Although the near 100-year storm events take place during El Nino, the team did not additionally factor in King Tides or the Pacific Decadal Oscillation phase that may contribute to base sea levels.

[3] In this report, storm surge is refered to as storm-induced elevated high tides.

thereby allowing researchers to cover an extensive spatial region while accurately capturing potential inundation of transmission system infrastructure at a local or very high resolution spatial scale. In contrast to the majority of SLR studies that rely on static water levels, this study integrated time-series water level data for entire storm events from numerous monitoring stations into the 3Di hydrodynamic model.[4] The analysis provides a more comprehensive, realistic simulation of inundation location and depth for the duration of a storm event under SLR conditions than has been done heretofore. Such accurate and realistic characterization of the system's vulnerability at this resolution is extremely valuable for planners and policymakers developing strategies to mitigate potential energy sector impacts from SLR. At the time of this study, the research team was aware of no other studies that used the expertise of sophisticated pipeline operators to elucidate the risks such inundation processes pose to their assets.

## 1.1 Importance of Natural Gas Transmission System

Uninterrupted supply of natural gas is vital to California's economy and the well-being of the state's population. However, the state's natural gas pipeline infrastructure may be at increasing risk from impacts associated with climate change, particularly those due to sea-level rise. Natural gas supplies meet nearly one-third of California's total energy requirement and natural gas fired generation is the dominant source of electricity in the state, accounting for approximately 43% of all generation in 2012 (California Energy Commission, 2014). Other primary end uses of the fuel include industrial processes and residential space and water heating. Given the state's reliance on this resource, the pipeline infrastructure and facilities designed to store, transmit, and distribute natural gas throughout the region are critical. The reliability and safety of this system are of primary concern to the State's Energy Commission, Public Utilities Commission, Legislature, utilities and general public (Kennedy et al., 2014). However, the natural gas pipeline system has been engineered and built for current climate regime and researchers posit that it is unlikely, without further improvement, to be resilient to future climate change.[5]

California's intrastate pipeline system through which natural gas is transported is vast, consisting of approximately 16,900 kilometers (km; 10,500 miles) of onshore transmission pipeline in addition to gathering and distribution lines (Pipeline and Hazardous Materials Safety Administration (PHMSA, 2014)). The transmission pipeline system is the critical link between the State's gathering and distribution systems, making it possible for natural gas to be transported between production and end-users. The transmission system is made up of

[4] The USGS developed a Coastal Storm Modeling System (CoSMoS) that predicts storm-induced coastal flooding, erosion and cliff failures accounting for the dynamic nature of tides and storms and shoreline change (Barnard et al. 2014). In their model, "storm events inside the Bay were derived from numerically modeled wind-wave heights driven by down-scaled wind projections derived from one GCM (Geophsyical Fluid Dynamics Laboratory [GFDL] Earth System Model [ESM] 2M)." This model differs by not predicting shoreline change and by being calibrated using real extreme storm events.

[5] PG&E is currently addressing this issue to better understand, plan for, and respond to climate change risks (PG&E, 2016).

pipelines, equipment, and facilities necessary to transport natural gas. Besides pipes, this includes taps, valves, pumps or compressors, metering stations, inspection device launchers and receivers, breakout tanks, storage tanks, and compressor stations. While transmission pipelines are generally buried underground, their associated facilities are generally located aboveground (FERC, 2010). Figure 1 provides a conceptual model of a typical pipeline system from production (on the left) to user (on the right).

**Figure 1: Conceptual Model of the Organization of a Typical Pipeline System**

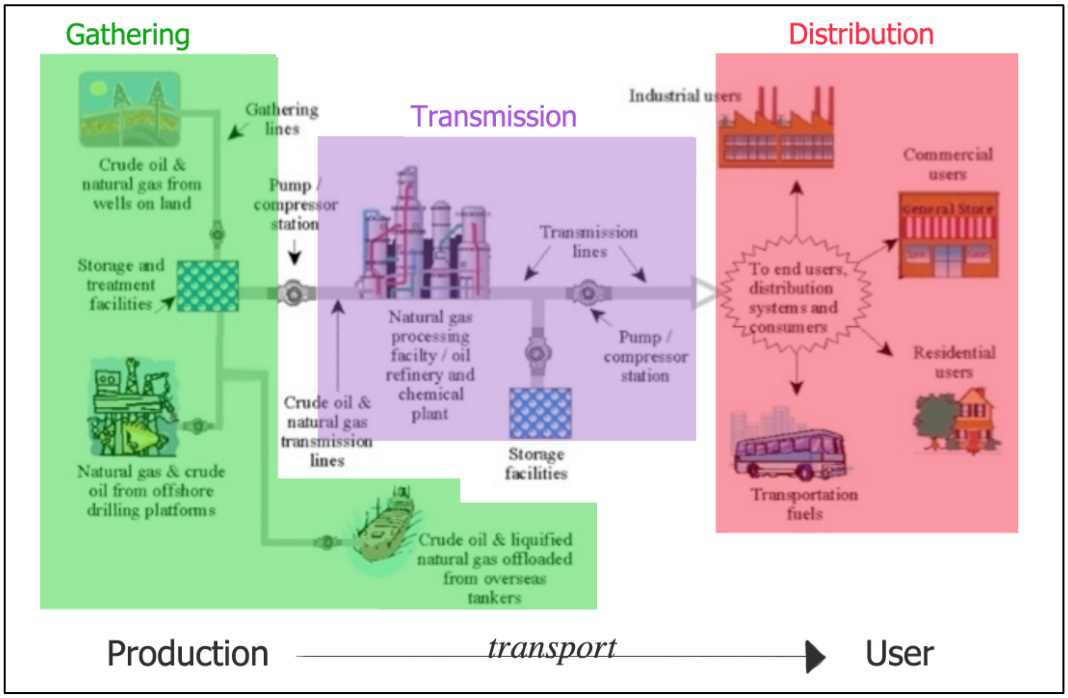


Source: adapted from PHMSA, 2011b

## 1.2 Effect of Sea-Level Rise and Storm Surge on Pipelines

Rising sea levels, along with more intense and/or frequent storms under climate change, are expected to cause more frequent and damaging floods as well as increase the size of the current floodplain (Heberger, Cooley, Herrera, Gleick, & Moore, 2009). These conditions have the potential to impact natural gas pipelines and associated infrastructure—both above and below ground— that they were never designed to withstand (Needham, Brown, & Carter, 2012). Natural gas pipelines located in the current floodplain may experience a greater frequency, duration, and/or depth of inundation, while pipelines previously outside the floodplain may become newly inundated.

Such conditions have the potential to accelerate structural failures in pipelines or cause damage to other components that make up the transmission system, such as aboveground infrastructure. Hurricane Katrina’s flood damage to coastal infrastructure provides an illustration of the problems that are likely to be incurred by natural gas transmission systems under increased sea-level rise and storm frequency. Katrina’s surge and powerful waves damaged many power plants and pipelines (Harris and Wilson, 2008).[6] Widespread flooding due to the hurricane inundated portions of New Orleans's natural gas pipeline system with salt-and-brackish water.[7] This compelled Entergy, the pipeline system owner, to replace 486 km (302 miles) of pipeline infrastructure out of concern for damage due to corrosion (Entergy, 2015).

Although gas transmission systems have built-in redundancy, in the event of widespread flooding, the consequences of a failure such as a levee breach could be long-term. Designing and building pipeline systems that are resilient to future climate change is imperative.

## 1.3 Modeling Inundation and Analyzing Risk

In this study, researchers modeled the location and depth of potential flood/inundation in California under realistic extreme storm events coupled with various increments of long-term SLR. They then analyzed the location of natural gas transmission pipelines and associated infrastructure in relation to their inundation projections in order to identify locations of possible vulnerability in the system. By characterizing the system's vulnerability the team sought to provide a baseline to inform planners and policymakers in their efforts to develop strategies to mitigate potential impacts from SLR.

The inundation modeling focused on three regions: the San Francisco Bay (the Bay), the Sacramento-San Joaquin River Delta Region (the Delta), and the California Coast (the Coast). To simulate the location and depth of inundation in these regions, GIS was integrated with a hydrodynamic model called 3Di. High-resolution modeling of inundation based on a real near 100-year storm event coupled with 0.0, 0.5, 1.0, and 1.41 meters of SLR, respectively, was performed in the Bay and Delta regions. Inundation along California's coast was simulated at a more coarse resolution owing to its large spatial scale and use data from three separate near 100-year storm events coupled with the same four increments of SLR. These potential SLR increments were based on those used in previous California climate change impact studies that project local SLR based on forecasts of relevant weather and climate parameters (see Chapter 3). By comparing the location, depth, and duration of inundation from these simulations to locations of existing natural gas transmission infrastructure, the team was able to characterize the inundation vulnerability posed to the system by SLR.

Finally, to understand what risk this inundation creates for pipeline systems researchers collaborated with natural gas and hazardous liquid (for comparison purposes) pipeline operators. The team integrated their spatial modeling with the operators' risk analysis

---

[6] Hurricane Katrina is used as an example of salt water mixing with and compromising the integrity of gas pipeline infrastructure; there is no intention to compare the magnitude of a hurricane such as Katrina to an extreme storm event on the west coast of California.

[7] In this study, the terms flooding (dry areas becoming temporarily wet) and inundation (dry areas being permanently submerged) are used, as both conditions occur with SLR (Flick et al., 2012), contribute risk to pipeline infrastructure, and must be addressed in SLR and extreme storm surge scenarios. For example, in the case of a levee failure in the Delta, flooded land could remain inundated for months and possibly a year before pumping could return the land mass to dry status.

frameworks for operation, program, and planning purposes and held discussions with both PG&E gas operations and Kinder Morgan, a hazardous liquids pipeline operator, to understand the risk that the simulated inundation results might pose to their pipeline systems. This process of assessing the risk posed to the transmission systems by inundation from SLR and storm surge under climate change presented operators with a critical opportunity to plan the redesign, replacement, and/or retrofit of infrastructure to mitigate possible effects, thereby facilitating climate change adaptation in the energy sector.

## 1.4 Innovative Approach

This study adds to and improves on previous SLR impact research for the California Energy Commission in numerous ways. Overall, it focuses on potential impacts to natural gas pipeline system infrastructure, a topic that to date has received little specific attention. For example, Sathaye et al. (2011) and Heberger et al. (2009) analyze impacts of SLR inundation on California's energy systems but focus largely on electricity production and transmission infrastructure, and Biging et al. (2012) analyze impacts to transportation infrastructure. Moreover, unlike other research, this study accounts for the dynamic influence of tides and storm surges on inundation location and depth.[8] The majority of existing SLR impact studies incorporate only static water level data, to which projected SLR is added. Such studies therefore do not take into account the dynamic nature of tides and storm events. The research team calibrated the model using data from a near 100-year storm event and do not attempt to model shoreline erosion over time.[9] By integrating the 3Di hydrodynamic model and calibrating it to a real storm event, the analysis provides a more comprehensive, realistic simulation of inundation location, depth, and duration throughout a storm event.

This study is also innovative in that it provides an extensive yet accurate characterization of inundation by using both a "pathway" framework to characterize floodplain extent – which contributes to an efficient process in constructing a more realistic earth surface model – and a variable resolution (dynamic quadtree) modeling method to increase the model resolution as the complexity of the landscape increases. As a result, researchers were able to analyze:

1. A large area encompassing the Bay, the Delta, and the Coast in order to provide insight into inundation at a regional scale, while also capturing the impacts to pipeline infrastructure at a high resolution at a local scale.
2. How water flows realistically across the landscape during an event. This is done by integrating very high-resolution digital surface models of objects on the earth's surface

---

[8] CoSMoS (Barnard et al. 2014) also accounts for the dynamic influence of tides and storm surges.

[9] It is possible that some shoreline areas will experience significant erosion over this century and that the impacts of SLR and storms might be underpredicted by this research. However, calibrating the model with a single real near 100-year storm event does not allow shoreline erosion to be accurately modeled. Conversely, if seawalls, levees, or other protective structures are enacted in specific locations the research could overestimate the impacts of SLR and storms.

likely to impede the flow of water (such as buildings) with hydrodynamic simulation of water level fluctuations.

In contrast to this approach, the majority of inundation models analyzing sea level change at a regional scale uses a coarse resolution and makes assumptions that, while appropriate for covering large areas, are inappropriate for analyzing impacts to infrastructure at a high resolution or local scale. By using a variable resolution (a quadtree) method to incorporate finer resolution where the landscape is more complex (and coarser resolution when it is less complex), the analysis maintains computational feasibility but also has a high degree of local accuracy across the entire region. Similarly, by capturing flow pathways and impediments at a local scale, this study captures their effects when estimating the extent and depth of inundation more accurately than models that ignore these surface features.

Lastly, this approach adds significant value by integrating SLR spatial modeling and operator risk analysis. In particular, PG&E has developed a sophisticated risk management framework where asset and operation risks are identified, ranked, and then serve as input for gas operation programs, plans, and investments. Their framework has already identified and ranked risks of flooding and soil erosion due to weather-related operating factors and this study's modeling results allow them to add or modify climate-change risks in their official risk register. This is critical in advancing infrastructure operations to become more robust and resilient to climate change.

## 1.5 Structure of the Report

This report documents the research team's methodology and findings. Chapter 2 describes the physical vulnerabilities of the natural gas pipeline system; Chapter 3 describes data and methodology; and Chapters 4 and 5 detail the results, discussion, and conclusions. The four appendices describe the technical details and accomplishments of the research. Appendix A describes the data assembling and construction of the Elevation Surface Models. Appendix B describes the analysis and modeling schema along with the selection process of the extreme near 100-year storm event data. Appendix C describes the 3Di hydrodynamic model employed to simulate storm surge, and Appendix D details the process undertaken to determine the initial water level data for each of the tile simulations.

# CHAPTER 2: Impacts of Inundation and Vulnerability of the Natural Gas Transmission System

Most energy infrastructure in the United States today has been engineered and built for past or current climate conditions[10] and may not be resilient to climate changes and SLR over the long term (US GAO, 2014). There is wide consensus that climate changes including increases in average mean temperature, the number of warm days over mid- to high-latitudes, and precipitation and temperature extremes are likely to bring about melting of sea ice and glaciers, a warmer and expanded body of ocean water, and some degree of SLR, resulting in greater flooding and higher storm surges (Biging, Radke, & Lee, 2012; IPCC, 2014). Wilbanks (2009) argues that energy resource systems in the United States are particularly vulnerable to impacts from SLR and previous research for the California Energy Commission (Sathaye et al., 2011; Stoms, Franco, Raitt, Wilhelm, & Grant, 2013) suggests that the State's energy infrastructure is likely to be threatened by inundation associated with SLR.[11]

For the natural gas transmission pipeline system in particular, storm surge coupled with higher mean sea levels may lead to corrosion associated with inundation or damage associated with increased external loading, erosion, debris flows, and/or disruption of surrounding materials. The vulnerability of the infrastructure that makes up the natural gas transmission system will depend not only on its location but also the age, design, and installation characteristics of the components. The consequences of infrastructure failure, on the other hand, will depend largely on the role of the failed components in system operation as well as the component location.

## 2.1 Effects of Inundation on Pipeline Infrastructure

Inundation has the potential to cause damage to natural gas transmission pipelines and associated above or belowground infrastructure through increased hydrostatic load, erosion, debris flow, and/or corrosion.

### 2.1.1 Increased Hydrostatic Load

Sea-level rise enables greater extents and depths of inundation during (extreme) storm events, which can immerse buried pipelines and associated above ground infrastructure in water. Gokhale & Rahman (2008) suggest that during storm surge flooding, non-traditional loading from hydrostatic head can be transferred through soils onto buried pipelines leading to potential failure modes, such as cracking, fracturing or buckling. Such surges may also inflict

---

[10] According to PG&E, they are making investments to build a more modern and resilient gas and electric system that can better withstand extreme weather and natural disasters (PG&E, 2015).

[11] Earthquakes, or other disasters, could cause failure of shoreline protection devices (e.g. levees, especially in the Delta), but since they are not the focus of this research they were not modeled here. Only levees or object overtoppings were considered as a compromise of shoreline protection devices.

increased levels of force on above ground system infrastructure causing buckling, cracking, fractures, or other damage.

### 2.1.2 Erosion/Scouring/Debris Flow

Storm surge associated with increased mean sea levels has the additional potential to impact natural gas transmission infrastructure by causing washouts or scouring of surrounding materials and damage due to movement of debris in flooding events. In addition, there is potential for negative impacts to facility assets, such as stations and valves. A United States Government Accountability Office report (US GAO; 2014) on climate change risks to energy infrastructure suggests hazardous liquid and natural gas pipelines are highly vulnerable to such impacts. For instance, in Montana in 2011 an oil pipeline buried beneath the Yellowstone riverbed circumferentially failed due to stress placed on the pipeline by debris flowing in the river associated with several flood events (US DOT, PHSMA, OPS, 2012). In Maryland, pipeline system owner Baltimore Gas and Electric Company (BGE) has raised concerns that the proximity of their system to the Chesapeake Bay makes it susceptible to floodwaters from coastal surges that could erode the ground around buried utilities and cause breaks in gas mains (BGE, 2015). Erosion, scouring, and debris flow may also disrupt the concrete coating that provides negative buoyancy for many pipelines causing damage to the pipes as they become positively buoyant. Moreover, Gokhale & Rahman (2008) suggest the shifting of aboveground system components on their foundations during surge and flooding events can rupture rigid connections to buried pipelines.

### 2.1.3 Corrosion

Inundation with saline or brackish water can impact pipeline infrastructure by contributing to pipeline corrosion. According to PHMSA (2015b) approximately 8% of significant pipeline incidents[12] among onshore, intrastate natural gas transmission pipelines in California between 1994-2013 were associated with corrosion. Major storm events such as Hurricane Katrina (in 2005) have also revealed the vulnerability of belowground pipeline infrastructure to corrosion. The widespread flooding due to Katrina inundated portions of New Orleans's natural gas pipeline system. This drove the utility Entergy to launch the Rebuild Project in 2007, an ongoing effort to replace cast iron and steel pipes with high-density polyethylene pipelines to prevent the corrosive effects of the saltwater from degrading the pipelines and causing service interruptions for years to come ("After Katrina, New Orleans Gas Rebuild Ahead of Pace," 2009; Bahr, 2007; Entergy, 2015; Thompson, 2010). Entergy's Gas Rebuild Project highlights that the corrosive effect of inundation can extend over a longer period of time than just after the inundation event.

---

[12] Significant incidents are defined by PHMSA as those that cause any of the following: fatality or injury requiring in-patient hospitalization; $50,000 or more in total costs; highly volatile liquid releases of 5 barrels or more or other liquid releases of 50 barrels or more; or liquid releases resulting in an unintentional fire or explosion.

### 2.1.4 Access

Storm surge and sea level rise have also been shown to impact transportation infrastructure and may also disrupt an operator's ability to access utility infrastructure (Biging et al., (2012).

## 2.2 Pipeline Vulnerability

The location, age, construction, and installation of pipelines and associated infrastructure will affect their vulnerability to damages associated with additional hydrostatic loads, corrosion, and erosion caused by inundation.

### 2.2.1 Location

Pipelines located in areas projected in this analysis to experience new or increased levels of inundation under sea-level rise and storm surge conditions are most vulnerable to the effects of inundation. In general, these pipelines are likely to be located in proximity to coastal or inland waterways within the state. Results predict that, under projected SLR greater than one meter, a small fraction of the natural gas infrastructure system in California could be inundated.[13] This is further discussed in Chapters 4 and 5.

However, pipeline infrastructure in areas not projected to be inundated according to the analysis may still be vulnerable. For example, the analysis considers only the potential for overtopping of levees in the study regions, under the assumption that such levees will sustain themselves given SLR and storm surge conditions. Yet, it is possible that these levees may break under such conditions, leaving the infrastructure behind them susceptible to inundation. Sathaye et al. (2011) suggest that the nexus of energy infrastructure systems along the western islands of California's Delta region should be of significant concern in terms of potential impacts from SLR and storm surge. Much of the land harboring that energy infrastructure already resides below sea level (Figure 2), and levees protecting the islands might experience increased hydrostatic pressure and increased likelihood of failure during storms coupled with SLR (DRMS, 2008). Moreover, the failure of one of the systems may have cascading effects on other co-located systems (although the understanding of "cascading failure" across infrastructures remains in very early stages [Roe & Schulman, Forthcoming]).

[13] In this report it is acknowledged there are uncertainties due to assumptions in SLR, that future extreme storm events will be of the same magnitude as existing events, and that current infrastructures will remain the same. To signify that there are model uncertainties, qualifiers such as *may*, *could*, and *shall* are used to indicate there are uncertainties from multiple sources within the projections.

**Figure 2: Natural Gas Pipeline and Storage Facilities – Above and Below Sea Level in California's Delta Region**

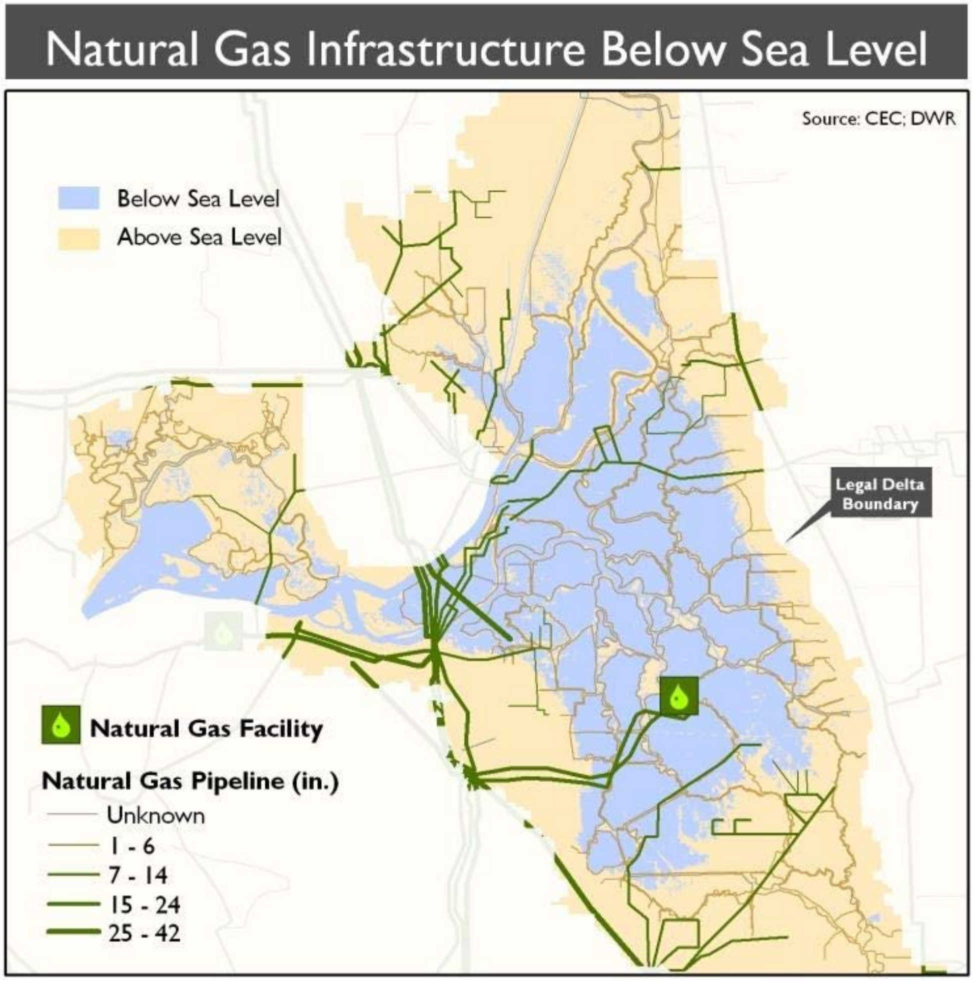


Source: adapted from Sathaye et al. 2011

### 2.2.2 Construction Characteristics

#### *2.2.2.1 Pipeline Material and Diameter*

The material from which pipelines are constructed and their diameter can affect their vulnerability to inundation. Cast iron and steel pipes are more prone to the degrading corrosive effects of inundated saltwater than are high-density polyethylene pipelines (Pipeline and Gas Journal, 2009). However, natural gas transmission pipelines are made of steel and are often coated and almost always additionally cathodically protected to combat corrosion from moisture, corrosive soils, and construction induced defects. Based on data in operator annual reports submitted to PHMSA (2015), 99.5% (16,808 km/10,444 miles) of intrastate transmission pipelines in California as of 2013 are both coated and cathodically-protected to combat corrosion. In theory, if these protective measures are correctly installed and are not compromised, inundation should have a minimal impact due to corrosion.[14]

In addition to the material from which they are constructed, the diameter of a pipeline determines whether or not it is constructed with seams, and the presence of seams can play a role in pipeline vulnerability. Certain seam types are more prone to external corrosion; these are typically vintage seam types such as low frequency electric resistance welded, flash welded, or oxy-acetylene welded seam types (PHMSA, 2011a ; Clark et al., 2004 ; Kiefner & Rosenfeld, 2012). Natural gas transmission pipelines generally measure between 6 and 48 inches (15 - 122 cm) in diameter (Folga, 2007). Line pipe is produced in specialized steel mills, and production techniques differ depending on the diameter of the pipe. Large-diameter pipes ranging from 20 to 42 inches (51 – 107 cm) are produced from sheets of metal folded into a tube shape with the ends welded together to form a seam. Small-diameter pipe can be produced seamlessly by heating a metal bar to very high temperatures and punching a hole through the middle to produce a hollow tube.

Since flaws in seams can grow over time and may become points of corrosion or breaks, pipes with seams may be more vulnerable to impacts from corrosion or failure due to additional external hydrostatic loads associated with inundation. Data from PHMSA (2015b) suggest that between 1994 and 2013, 12% of significant pipeline incidents among onshore, natural gas transmission pipelines in California were due to material, weld, and/or equipment failure. However, the PHMSA dataset from 1984-2001 does not separate equipment failures from material failures. Figure 3 provides a 2013 breakdown of intrastate natural gas pipelines in California by diameter based on data from annual operator reports submitted to PHMSA (PHMSA, 2015a). Approximately 47% of these pipelines (by length) are greater than 20 inches (51 cm) in diameter, and one could imply that almost half of the transmission pipelines in the State are constructed with seams, however, diameter to seam type is not necessarily a consistent correlation. Not all of these pipes are within the inundation area.

[14] However, increased hydrostatic pressure may disrupt supporting materials and alter the original protection, leading to conditions of possible corrosion.

**Figure 3: California Natural Gas Transmission Lines by Pipeline Diameter (2013)**

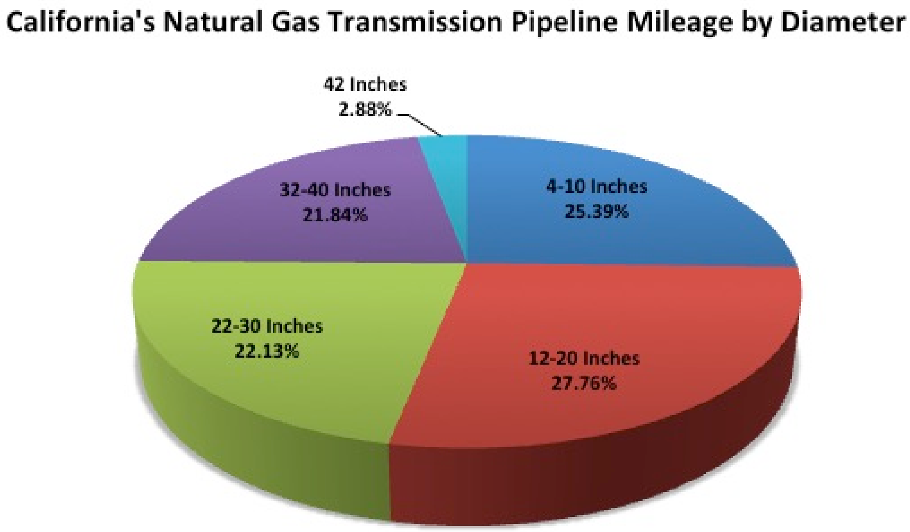


Data Source: PHMSA, 2015a

#### *2.2.2.2 Pipeline Age*

Older pipelines are also more likely to be susceptible to damage associated with inundation from SLR and storm surge. Gokhale & Rahman (2008) analyze pipeline data collected in the aftermath of hurricanes Katrina and Rita and find that damages to pipe systems were concentrated in parts of New Orleans that not only were closer to waterfronts, but also had older pipe networks. They theorize that this result occurred because these older pipelines were already in a state of partial deterioration. As pipelines age, their weld points and valves can weaken over time, making them increasingly susceptible to breakage under disturbances such as increased hydrostatic loads, debris flows, or erosion. Figure 4 presents a breakdown of California's intrastate natural gas transmission lines existing in 2013 by decade installed based on data submitted to PHMSA by pipeline operators (PHMSA, 2015a). At least 69% of transmission lines (by mileage) are 30 or more years old (installed during or before the 1970s).

**Figure 4: California Natural Gas Transmission Lines by Decade of Installation (2013)**

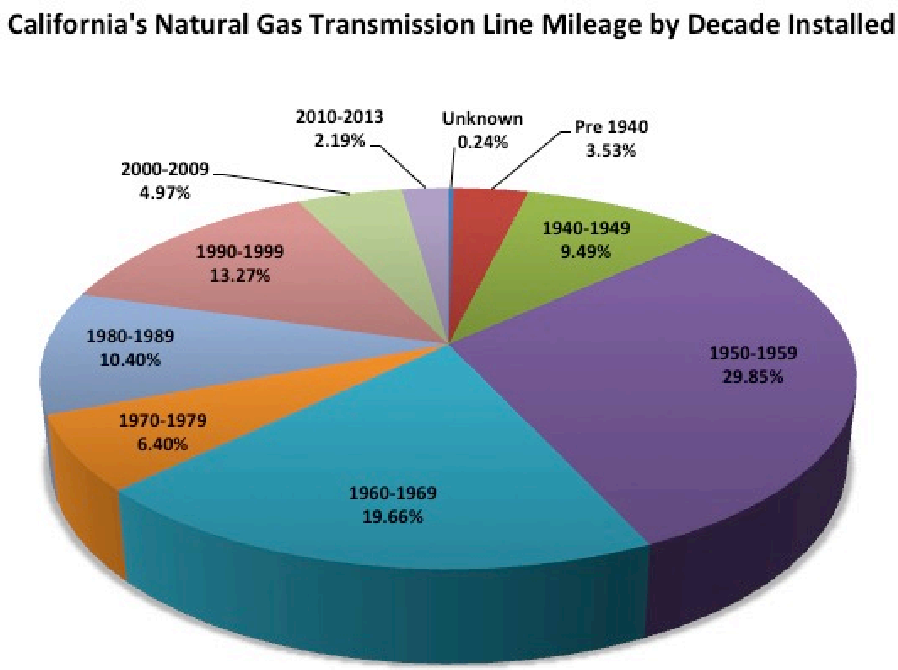


Data Source: PHMSA, 2015a

### *2.2.2.3 Pipeline Depth*

Burial depth and conditions can affect pipeline vulnerability to impacts from SLR and storm surge. While burial depth generally depends on local conditions along the pipeline route, depth requirements for transmission pipelines are normally a minimum of 30 to 36 inches (76 to 91 cm) below the surface (Folga, 2007 ; Federal Code 49 CFR Part 192.327). The depth and type of material under which a pipeline is buried affects rates of erosion or scour and what type of debris may impact the pipeline during debris flows.

Inundation can also bring about changes in coverage of submerged pipelines. Pipelines are inspected to ensure they are buried at appropriate depths when installed; however, flooding can change their coverage and cause potential risks to the pipeline infrastructure and navigation. For example, in March 2013 a tugboat struck a submerged pipeline at Bayou Perot Louisiana because the pipeline was no longer at an appropriate depth when it was struck (National Transportation Safety Board, 2014).

## 2.3 Risks of Pipeline Failure to Transmission System Operation

One of several misconceptions about critical infrastructure systems is the assumption that every component has the same criticality: lose one element and the entire system is at jeopardy. That assumption, however, does not hold everywhere and must be confirmed empirically, case-by-case. The electricity transmission grid, for instance, has been designed and built to an "n-2" contingency standard, meaning that the grid could lose a major transmission line and still be able to provide electricity grid-wide, all else being equal (Roe & Schulman, 2008). The research team's discussions with PG&E indicate that the natural gas infrastructure is also managed for contingencies, such that if one element were to be lost or disrupted, the gas provision system as a whole should not fail, assuming all else remains equal. Thus, it cannot be assumed that every segment of an infrastructure system is a chokepoint, which if compromised would bring the infrastructure into systemwide disruption or outright failure.

Given that every segment of PG&E's natural gas transmission system is not equally critical, it cannot be assumed that losing any one element of the system because of climate-change induced inundation or the effects thereof will necessarily have an effect on systemwide transmission of natural gas. Researchers found that the issue of climate change impact on PG&E's natural gas transmission is complicated by "constrained transmission" areas for load pockets such as San Francisco, San Jose, and Sacramento.[15] In these constrained areas, inundation could have an impact on any natural gas transmission system, but that too is an empirical question depending on where the specific impacts occur and what resulting threat(s) they pose— i.e. is the impact moderate, severe, or catastrophic. Certainly, the fact that the research predicts that approximately 308 km (191 miles) of transmission pipeline may be inundated under the high-end scenario (a 1.41 meter SLR[16] coupled with a near 100–year extreme storm event) in the Bay-Delta, cannot be interpreted as meaning that PG&E would, or even should, find all that pipeline under equal threat as explained in Chapter 4: Results.

These are important issues, if only because far more media and regulatory attention has been given to the damage around a system element which can be substantial than on the damage that did not happen because the rest of the system was managed to prevent wider failure and impacts.

### 2.3.1 Effects on Interconnected/Other Infrastructure Systems

Critical infrastructures define modern society in important respects. Large-scale water supplies and the energy infrastructures for electricity and natural gas, among others, have altered and determined population and demographic patterns profoundly in California as well as elsewhere (Roe & Schulman, Forthcoming). Society, in turn, expects these infrastructures to be highly reliable and interconnected at the same time. The infrastructure systems must provide their critical services safely and continuously even under adverse conditions. Simultaneously, various infrastructure systems rely on one another to function. For example, PG&E's natural gas and electricity operations, each being a separate line of business at the company, are

[15] "Constrained" is a term of art used to describe a location where the transmission system is unable to transmit power or natural gas due to congestion at one or more parts of the transmission network.

[16] The high-end SLR scenario (1.41 meter SLR) used in this study conforms with California's Climate Change Assessments to date, which are estimated for California under the A1B and A2 emission scenarios (Bromirski et al. 2012). There is uncertainty regarding the upper-bound or high-end for SLR by the end of the century and other studies have predicted higher estimates (NRC, 2012) of as much as 1.67 meters (CO-CAT 2013, p.2)

functionally interoperable in the sense that both depend on each other in terms of their functionality. Not insignificantly, other energy infrastructure depends on this interoperability: Kinder Morgan, has assets that depend on PG&E's electricity, which in turn depend on PG&E's natural gas operations.

The expectation that these systems be both reliable and interconnected has made the design and management of critical infrastructures intensely complex and challenging to understand. Even infrastructure operators, risk analysts, regulators and policymakers can find difficulty anticipating important system‑to‑system vulnerabilities and the likelihood of reciprocal failure. California certainly experienced this with the 2001 electricity crisis.

In principle, interactive complexity intensifies with the increasing interconnectivity of critical infrastructures. In practice, however, great care must be exercised when assuming "everything is connected to everything else" by virtue of infrastructural interconnectivity. First, no overarching, generally accepted theory or framework exists in the peer-reviewed literature for demonstrating the consequences of infrastructures that are spatially and/or functionally interconnected at the cross-system level (Roe & Schulman, Forthcoming).

Moreover, publically available databases on inter-infrastructural disruptions underscore that fewer dependent and interdependent interactions are present than many, including regulators and policymakers, might suppose. Far fewer "cascades" (failure in one infrastructure causing failures in other infrastructures) actually happen than are possible, though it appears the incidents in energy infrastructure, including that for natural gas, are more likely to affect other infrastructures or to be caused by other infrastructure incidents. For example, one frequently cited study (Zimmerman, 2004) found that gas pipeline failures were more likely to be caused by other infrastructure failures rather than initiate failure elsewhere. Another study (Luiijf, Nieuwenhuijs, Klaver, van Eeten, & Cruz, 2008), with a much larger and more recent database, found: "most cascades originate from only a limited number of critical sectors (energy, telecom)."

A major reason why intra-infrastructural incidents do not spill over into other infrastructures more frequently is that individual infrastructures are managed by their control room operators to dampen active interconnectivity. Dependencies among infrastructures, write Luiijf, Nieuwenhuijs, Klaver, van Eeten, & Cruz (2010) in their analysis, "are anything but unmanaged."Van Eeten, Nieuwenhuijs, Luiijf, Klaver, & Cruz, (2011, p. 396) similarly note:

> "The cascades that we find point to dependencies that are anything but unmanaged. Very few organizations operating in [critical infrastructures] are unaware of their dependency on energy or telecommunication. Even the most rudimentary processes of risk assessment would bring these vulnerabilities to light. Organizations experience these dependencies with a clear regularity. In 25 percent of all cases, an incident triggers another incident, that is, it brings to light a dependency. This relatively high frequency makes it unlikely that operators are unaware of this problem. Of course, mistakes still occur. There are many examples where backup power generators did initially manage to prevent a cascade, but they later failed because the organization was unable to organize

> the refueling of the generators. In other words, these dependencies require persistent efforts to mitigate their impacts, but they are hardly 'unmanaged'."

Accordingly, when it comes to assessing an infrastructure systems' vulnerability to cascading failure from interconnected systems, there is no substitute for knowing how the infrastructure systems involved are actually managed to prevent or otherwise mitigate such events.

# CHAPTER 3:
# Data and Methods

This study simulated near 100-year storm events coupled with various amounts of SLR in California's San Francisco Bay, Sacramento-San Joaquin Delta, and coastal regions (Figure 5) in order to characterize the potential risk of flooding and inundation of gas pipelines and associated system infrastructure. This chapter describes the primary inputs necessary to simulate potential flooding and inundation of these regions. This includes the "as is" physical situation made up of a surface (elevation) model and the natural gas infrastructure model, which provides the location data for the pipeline system infrastructure. On top of the "as is" situation, 100-year storm events and sea-level rise (SLR) scenarios were projected on the study area. These scenarios were derived from actual storm event water level data and projections of potential SLR world-wide. The simulated flooding and inundation of the study area were described using the 3Di hydrodynamic model. The results were reported as a raster layer with each cell reporting the maximum Peak Water Level (PWL) during the modeling process. This PWL prediction proves useful for infrastructure managers to assess impact. Clearly, changes to the built environment cannot be anticipated 100 years into the future, so the current surface elevation was used in the simulation of future events, and potential shoreline changes were not modeled. Likewise, current digital elevation models were used in the simulation of future events since changes to the built environment over time were not simulated.

## 3.1 Elevation Surface and Natural Gas Infrastructure Models

### 3.1.1 Elevation Surface Data Models

Since there are many physiographic subregions in California, researchers developed three separate elevation surface models for this analysis: a San Francisco Bay model (Bay model), a Sacramento-San Joaquin Delta model (Delta model), and a California Coast model (Coast model) (Figure 5). While there are slight differences in the underlying process used to build the Bay and Delta land surface models, each combined bare ground height data (digital elevation model; DEM), bathymetry data, and surface object elevations (built structures such as buildings) to represent the land surface or inundation environment. While the research team followed a similar procedure for the California Coast, they did not include surface objects such as buildings in the final land surface models because they planned and necessarily modeled the coastal inundation at a coarser spatial resolution of 50 $m^2$ owing to its very large extent.

**Figure 5: Study Areas**

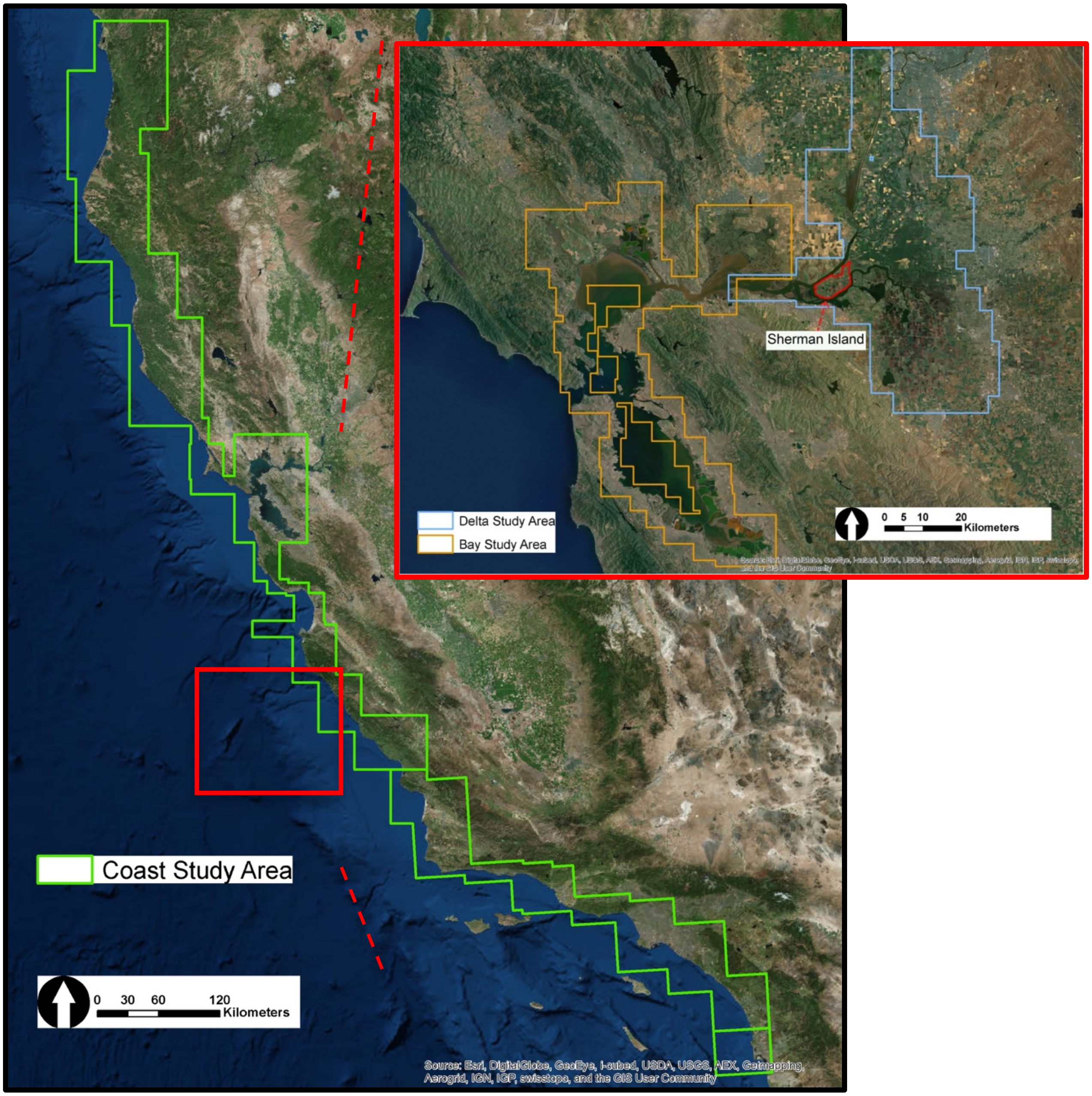


For all surface models developed, researchers began by first mosaicing the best available public domain bathymetric data with the land surface elevations from the National Elevation Dataset (NED). Along all coastlines – where they sought to improve the accuracy and predictability of inundation – they employed very high-resolution Light Detection and Ranging (LiDAR) data (more than eight billion data points in all) to build 1m$^2$ horizontal resolution surfaces and then integrated them into the final elevation surface model (Table 1).[17] Figure 6 illustrates the process of integrating the data used to construct the final earth surfaces. All elevation values used in this study were transformed into units of meters, and were referenced to the North American Vertical Datum of 1988 (NAVD 88).

**Table 1: SF Bay, Delta and Coastal LiDAR Datasets Used for Inundation Analysis**

| Study Area | Name | Projection | | Accuracy | |
|---|---|---|---|---|---|
| | | **Vertical** | **Horizontal** | **Fundamental Vertical** | **Horizontal** |
| North Bay | **NOAA** California Coastal LiDAR Project | NAVD88 | NAD83, UTM Zone 10N | 0.05 meters at 95% confidence level | 2.0 meters at 95% confidence level |
| South Bay | **USGS** California Coastal LiDAR Project | NAVD88 | NAD83, UTM Zone 10N | 0.12 meters at 95% confidence level | 2.0 meters at 95% confidence level |
| Sacramento - San Joaquin Delta | **DWR** California Department of Water Resources LiDAR survey | NAVD88 | NAD83, UTM Zone 10N | 0.18 meters at 95% confidence level | 0.3 meters at 95% confidence level |
| Califirnia Coast | **NOAA** California Coastal LiDAR Project | NAVD88 | NAD83, UTM Zones 10N & 11N | 0.094 meters at 95% confidence level | 0.5 meters at 95% confidence level |

[17] The vertical accuracy of the highest resolution LiDAR based data (the surfaces that were inundated during the flood modeling performed in this study) ranges from 0.05 to 0.12 meters at a 95% confidence level.

**Figure 6: Conceptual Model of Elevation Data Sources Used**

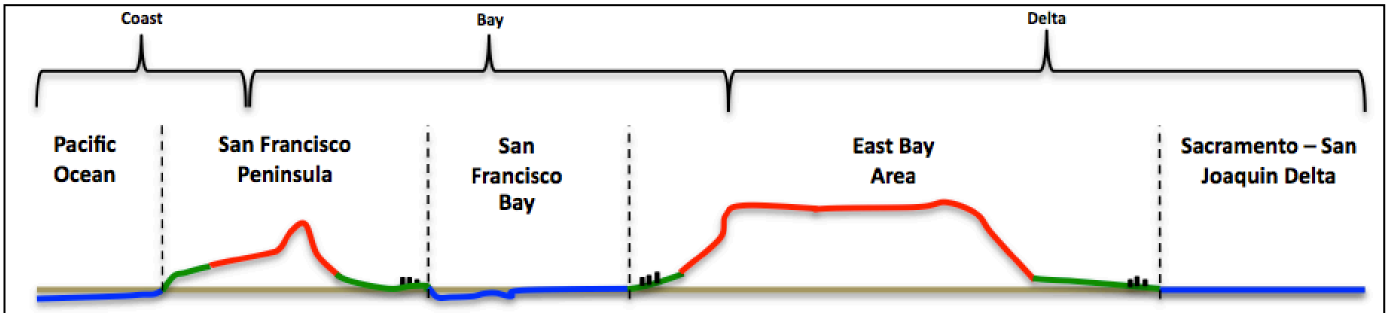


Data Sources

| | Coast | Bay | Delta |
|---|---|---|---|
| Bathymetry | 200m California Department of Fish and Wildlife Bathymetry (2007) | 10m Department of Water Resources Bathymetry (Wang and Ateljevich, 2012) | 10m Department of Water Resources Bathymetry (Wang and Ateljevich, 2012) |
| LiDAR | 1m California Coastal Conservancy LiDAR (Furgo EarthData Inc, 2011) | 1m NOAA and USGS LiDAR from the California Costal LiDAR Project (Dewberry 2011a,b) | 1m Department of Water Resources LiDAR (DWR, 2007) |
| NED | Approximately 10m (1/3 Arc Second) NED | | |
| DSM | N/A | 1m derived From NOAA and USGS LiDAR from the California Costal LiDAR Project (Biging et al., 2012) | 1m derived from Department of Water Resources LiDAR (DWR, 2007) |

Data sources used with references to sources for each region

### *3.1.1.1 Bay and Delta Region Surface Models*

To develop elevation surface models for the Bay and Delta regions, researchers first used GIS to build a high-resolution digital elevation model (DEM) and digital surface model (DSM) for the region from LiDAR point cloud data. While a DEM represents bare-ground elevations, a DSM contains information about the height of bare ground as well as the surface elevations of objects on the ground (such as buildings, trees, and levees). It was assumed that only certain surface objects, namely buildings, were likely to play a significant role in diverting the path of water, and their heights were extracted from the DSM using data delimitating object (building) footprints. Finally, the extracted surface object heights were combined with the DEM and bathymetry data to create an elevation surface model that accurately represents the environment to be inundated by the 3Di hydrodynamic model.

The DEM, DSM, bathymetry and the final land surfaces for the Bay, Delta and Coast are described generally below. Detailed descriptions of the input data and technical process for creating land surfaces for each region are included in Appendix A.

<u>Digital Elevation Models (DEM)</u>

The DEM surfaces were built by first using 1/3 arc-second (~ 10 $m^2$) data from the USGS National Elevation Dataset downloadable from the USGS National Map Seamless Server. With this base, researchers ensured that all land surfaces were covered by a DEM to support the requirements and integrity of the inundation modeling. They then inserted, or mosaicked, onto this surface much higher resolution datasets to enhance the DEM. For the San Francisco Bay, they incorporated a DEM produced by Biging et al. (2012) as part of their analysis of the impacts of SLR and extreme storm events on transportation infrastructure in the region. Biging et al. (2012) obtained and processed two, high spatial resolution LiDAR datasets covering areas of the San Francisco, San Pablo, and Suisun Bays that fall north of the Bay Bridge (National Oceanic and Atmospheric Adminsitration (NOAA) Lidar) and south of the Bay Bridge (United States Geologic Survey (USGS) LiDAR), respectively. Both datasets were collected as a part of the California Coastal LiDAR Project (CCLP), and their format and accuracy are discussed in Appendix B. Biging et al. (2012) processed the LiDAR data sets into a $1m^2$ horizontal resolution DEM for the San Francisco Bay Region (Appendix B). The resulting DEM was used in this analysis.

For the Sacramento-San Joaquin Delta, researchers downloaded and processed $1m^2$ resolution DEM tiles from the California Department of Water Resources (DWR) to create a $1m^2$ horizontal resolution DEM of the Delta region for this analysis. The DEM tiles downloaded from DWR were created from high spatial resolution LiDAR ground elevation data commissioned by the Delta-Suisun Marsh office, and collected via aerial survey between late January and February 2007 (DWR, 2007). The format, accuracy, and processing of the LiDAR data and resulting DEM tiles from DWR are discussed in Appendix B.

### Digital Surface Models (DSM) and Building Surface Objects

In order to extract the heights of surface objects (buildings), researchers obtained and derived DSMs of the Bay and Delta regions respectively for this analysis. For the Bay region, a DSM produced by Biging et al. (2012) was incorporated. In order to accurately model all surface objects (not just the ground), Biging et al. (2012) used all classes of LiDAR points when creating their DSM. Using this method, they produced a DSM with $1m^2$ horizontal resolution for the entire Bay region that the research team incorporated into this analysis. For the Delta region, the team produced a DSM using the LiDAR point cloud data obtained from DWR. This is the same LiDAR dataset that was used by DWR to generate the Delta DEM tiles processed into the Delta DEM for this analysis. Appendix B describes the processing of the LiDAR into the final $1m^2$ horizontal resolution Delta DSM researchers produced for this analysis.

To create a land model containing objects or features likely to play a significant role in diverting inundation, namely buildings, vector-based object (building) footprints were used to extract object heights from the DSMs for the Bay and Delta. Object footprints are polygons representing the area on the Earth's surface covered by a solid structure such as a building. An enormous number of object (building) footprints would be needed to represent every object in these two study regions. For the purposes of this analysis, the object footprints included in the analysis were limited to areas falling within the likely extent of inundation using the process described in Appendix B. Object footprints for the areas falling within the inundation extents were either obtained from existing city or county datasets, derived by automated feature extraction, or hand-digitized from very high resolution orthoimagery. The resulting dataset of vector object footprints within the inundation extent was used to extract from the DSMs a $1m^2$ resolution raster containing the elevation values within each object's footprint. Figure 7 provides an example of the extracted building heights from a DSM in the region of Alameda California.

**Figure 7: Image of the Extraction of Building Heights from the DSM**

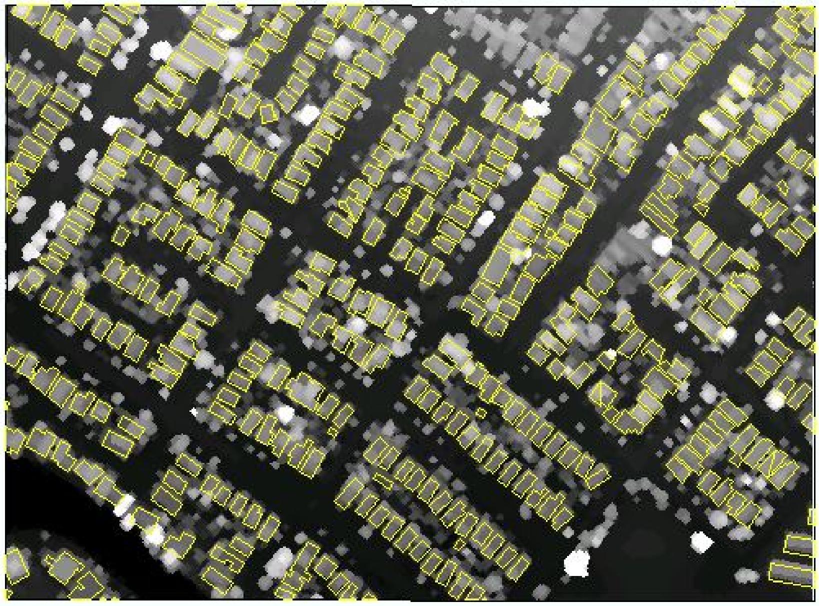

Building height extractions produced by Biging et al. (2012) (black to white background) using vectorized building footprint dataset (yellow outlines) for Alameda, CA.

<u>Bathymetry Models</u>

Bathymetry data compiled by DWR was integrated with the DEMs for the Bay and Delta regions. The DWR bathymetry dataset included large $10m^2$ resolution DEM/bathymetry grids and local $2m^2$ resolution grids that together cover the entire San Francisco Bay/Delta region. In many cases, the regional and local bathymetry grids overlapped one another, and the high-resolution $2m^2$ grids were used wherever possible (two $10m^2$ regional grids were used where local $2m^2$ grids are not available). All the grids were mosaicked together, and the combined grids were resampled to a $1m^2$ horizontal resolution raster to better integrate it into the final model. Since the bathymetry values in the various products were originally in centimeters, they were converted to meters for consistency with the elevation surfaces.

#### *3.1.1.2 California Coast Surface Model*

The land surface model for the California Coast was produced using a similar method to that of the Bay and Delta regions, but without objects (such as buildings) included in the surface as the coastal inundation was modeled at a coarser spatial resolution of $50m^2$ (horizontal). Given the size of California, the State's coast was divided into two zones based on the projection applicable to data for that zone: the Universal Transverse Mercator (UTM) 10 Zone in the north and the UTM11 Zone in the south.

The same data and procedure was used to create the elevation surface model for each coastal tile. The primary DEM data used for the coast is $30m^2$ ASTER satellite-based DEM data from 2011 in GeoTiff format and a tiled-structure, which researchers obtained from the United States

Geological Survey's (USGS) EarthExplorer database. This DEM data was merged with $1m^2$ resolution 2009-2011 Coastal Conservancy LiDAR Project (CCLP) DEM data falling within a thin strip of land at the coast-shore boundary to capture more surface features at this critical interface where inundation occurs. Researchers obtained $200m^2$ bathymetry data from the California Department of Fish and Wildlife (2007). These data were processed in GIS to a $50m^2$ horizontal resolution (the final inundation modeling resolution along the Coast of California) to produce the final elevation surface representing coastal land and bathymetry (Appendix B). Figure 8 provides an example of a final coastal tile.

**Figure 8: Coastal Tile of Merged DEM and Bathymetry Data**

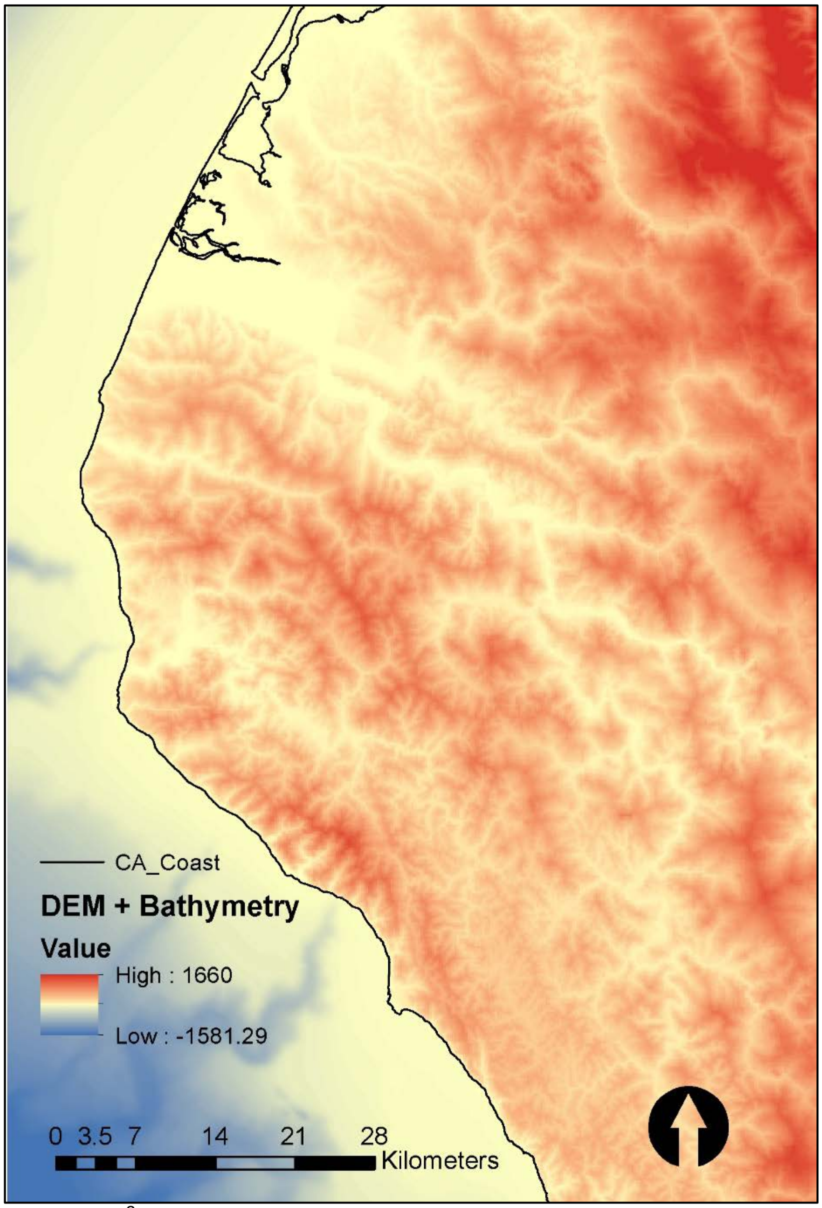


Data has a resolution of $50m^2$

### 3.1.2 Gas Infrastructure Data Model

The natural gas transmission pipeline location data in this study came from a number of authoritative sources. For gas transmission pipelines throughout the state of California, researchers used data from the National Pipeline Mapping System (PHMSA, 2013), a Web GIS of pipeline routes with attribute information including operator, length, and primary commodity transmitted. The National Pipeline Mapping System (NPMS) is maintained by Michael Baker Jr. Inc. and is hosted by PHMSA. The research team requested and received from the NPMS statewide line-route pipeline transmission data in 2012 and updates in 2013. In addition to the NPMS data, the team requested and received from PG&E Inc. natural gas transmission line data for Northern California, and line and surface facility data for central California. In addition and for pipeline operation comparison purposes, the team received spatial data for the San Francisco Bay Area from Wickland Pipelines LLC, Plains Marketing LP and Kinder Morgan Inc/SFPP for hazardous material transmission pipelines.

In order to use these datasets in the analysis, researchers entered into non-disclosure agreements (NDAs) between the University of California (UC), Berkeley and NPMS, and between UC Berkeley and the research team's industry partners. While non-public GIS data supplied by them cannot be shared with third parties, in any form, the NPMS maintains a public-access viewer, which displays some of their data at resolutions greater than 1:24,000. For example, Figure 9 displays the publically available NPMS gas transmission pipeline data for the portion of Alameda County, California that borders the San Francisco Bay.

**Figure 9: Available NPMS Gas Transmission Pipeline Data - Alameda County**

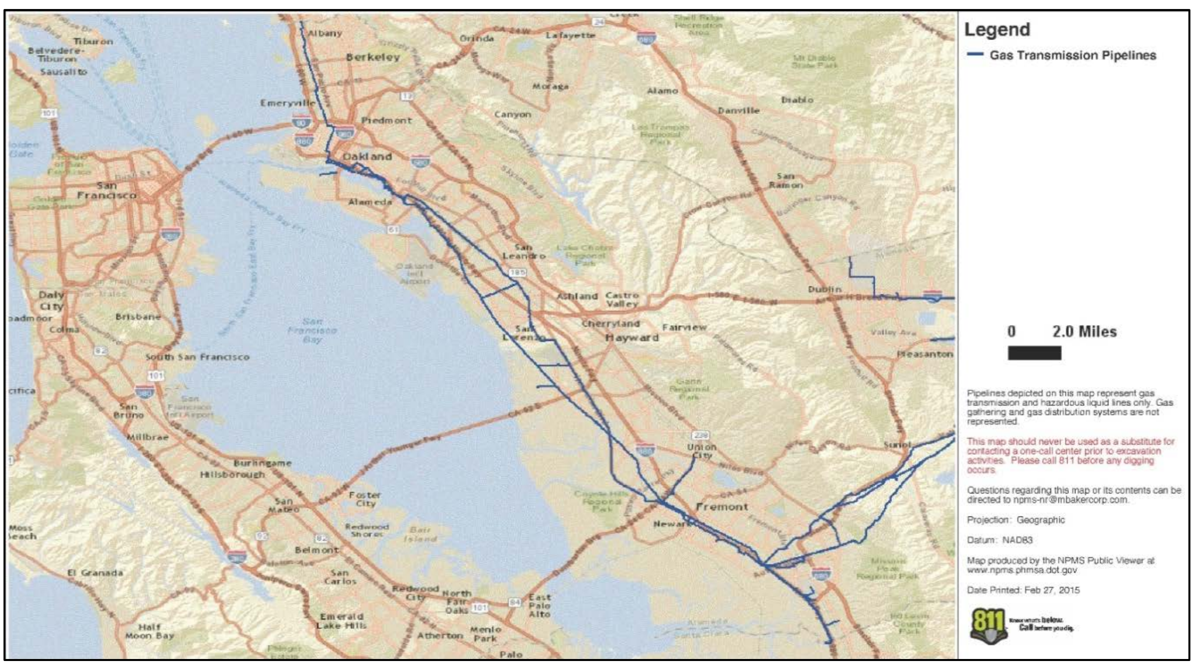


Publically available pipeline data for the portion of Alameda County, California that boarders the San Francisco Bay

Source: https://www.npms.phmsa.dot.gov/PublicViewer/

## 3.2 Applied Scenarios

To assess the potential impact of increasing sea levels and storm surge on California's natural gas transmission system, this analysis integrated the surface and gas infrastructure data models described above with projections of climate change-related SLR derived by others (Cayan et al., 2012; Bromirski et al. 2012) and time-series water level data measured at existing tide gauges during historic, near 100-year storm events. Based on these projections, researchers simulated flooding and inundation[18] impacts for California's Bay, Delta, and coastal regions under near 100-year storm conditions with 0.0, 0.5, 1.0 and 1.41meters of SLR.

### 3.2.1 Sea-Level Rise Scenarios

Sea levels along California's shoreline have been slowly, but steadily increasing over the past few decades and are projected to rise even faster in coming decades. During the last several decades, measured mean sea levels along the California coast have risen at a rate of approximately 0.17–0.20 meters per century (Cayan, Tyree, Pierce, & Das, 2012). Projections of future SLR prepared for the California Energy Commission's Vulnerability and Adaption Assessment indicate, however, that a substantially faster rate of rise is likely in the future, with a 0.9 to 1.41m increase in mean sea levels forecasted by 2100 (Cayan et al., 2012). Water levels in Northern California's San Francisco Bay and Sacramento-San Joaquin River Delta are expected to rise along with coastal mean sea levels. However, the rate of increase in the Delta is expected to follow a diminishing gradient upstream, given the existing gradient in Delta mean water levels as one moves away from the sea (Bromirski & Flick, 2008; Sathaye et al., 2011).

The increments of potential sea-level rise employed in this study were derived from previous California climate change impact studies that project local SLR based on forecasts of relevant weather and climate parameters from Global Climate Models (GCMs). Global Climate Models are numerical simulations that generate predictions of the earth's future climate (e.g. atmospheric, land, and oceanic parameters) under various greenhouse gas emission and aerosol scenarios (emission scenarios). The models are usually formulated in time dependent fashion, calibrated and validated with historic data sets, and then driven with assumed external forcing to estimate future climate changes (Biging et al., 2012). Assumed external forcing levels are based on widely-used emission scenarios developed by the Intergovernmental Panel on Climate Change (IPCC) that range from low (B1) to medium-high (A2) (Nakicenovic & Swart, 2000). The GCMs and emission scenarios from which the climate parameters used in this study are derived, are consistent with those used in other recent California Energy Commission studies, for example Biging et al., (2012), Cayan et al., (2012), and Sathaye et al., (2011).

To estimate localized climate impacts such as future SLR, the coarse outputs from GCMs were used as input variables in secondary-effect models. Given their global extent, GCMs are necessarily approximate and produce sets of future atmospheric, land, and oceanic variables

[18] Rather than draw a line between what is flooded and what is temporarily or permanently inundated, maximum water depths were reported during the duration of an extreme storm event and left to the Gas Pipeline experts to assess what conditions pose a risk to their infrastructure.

over coarse grid cells of 100–200 km horizontal distance (Biging et al., 2012). A number of studies have developed projections of future SLR for California, based on secondary-effect models using the surface air temperature projections from such GCM simulations. Cayan et al. (2008; 2012) assume SLR along the California coast will mimic global mean sea levels and derive SLR projections for California of 0.9 to 1.41m by 2100 under the IPCC's A2 and B1 emission scenarios (Figure 10, top). Bromirski et al. (2012) estimate SLR for California under the A1B and A2 emission scenarios. They project SLR of 1.2 to 1.6m by 2100 (Figure 10, bottom). Values of SLR along the same order of magnitude were estimated by Knowles' (2009) for the A2 greenhouse gas scenario and were used by Heberger et al. (2009) in a detailed analysis of SLR impacts in San Francisco Bay.

For this investigation, it was assumed that global mean sea levels will rise to a maximum of 1.41m by the end of this century. It was further assumed that SLR in the San Francisco outer Bay will closely resemble global mean SLR. This maximum mean SLR was also consistent with the maximum rise documented by Cayan et al. (2012) and the average rise under the scenarios examined by Bromirski et al. (2012). In addition to a maximum SLR of 1.41m, researchers analyzed the impacts associated with increments from 0m, 0.5m, and 1.0 m of SLR.

### 3.2.2 Storm Surges

In the Bay Area, it is estimated the 100-year storm is 2.64 m at the San Francisco NOAA tide station ID: 9414290 (Zervas, 2013). Out of the three extreme storms that occurred during El Niño years (Figure 11), the 02/06/1998 near 100-year storm event was chosen due to the number (28) of active reporting gauging stations during the event.

To capture the role of dynamic tidal and storm surge processes in the inundation simulations, sea levels during a storm event were modeled based on time-series water level data measured at tide gauges. Many existing SLR studies do not account for storm surge or tidal processes, or do so only in a static manner. Rarely have estimates of the entire tidal cycle during a storm event been completed for this study region. The exception being Bromirski & Flick (2008), who investigated the magnitude, distribution, and timing of storm-forced water propagation in the San Francisco Bay-Delta region by using water level data from a 1998 storm event.

The research team modeled the analysis of inundation in the Bay and Delta regions on the same February 1998 storm event used by Bromirski & Flick (2008) both for its extreme nature and the rich amount of water-level data from numerous gauging stations documenting the event. The 3Di hydrodynamic model employed for the inundation simulations (discussed below) required water level data for the entire tidal cycle to calibrate and simulate the movement of tides inland. Thus, the simulations for the Bay and Delta regions were based on the storm event that occurred in the region from February 5-7, 1998 where the peak water levels reached are near estimated 100-year extremes. In addition, water level data was available during the entire tidal cycle for this event.

**Figure 10: Projections of Mean Sea-level Rise by 2100**

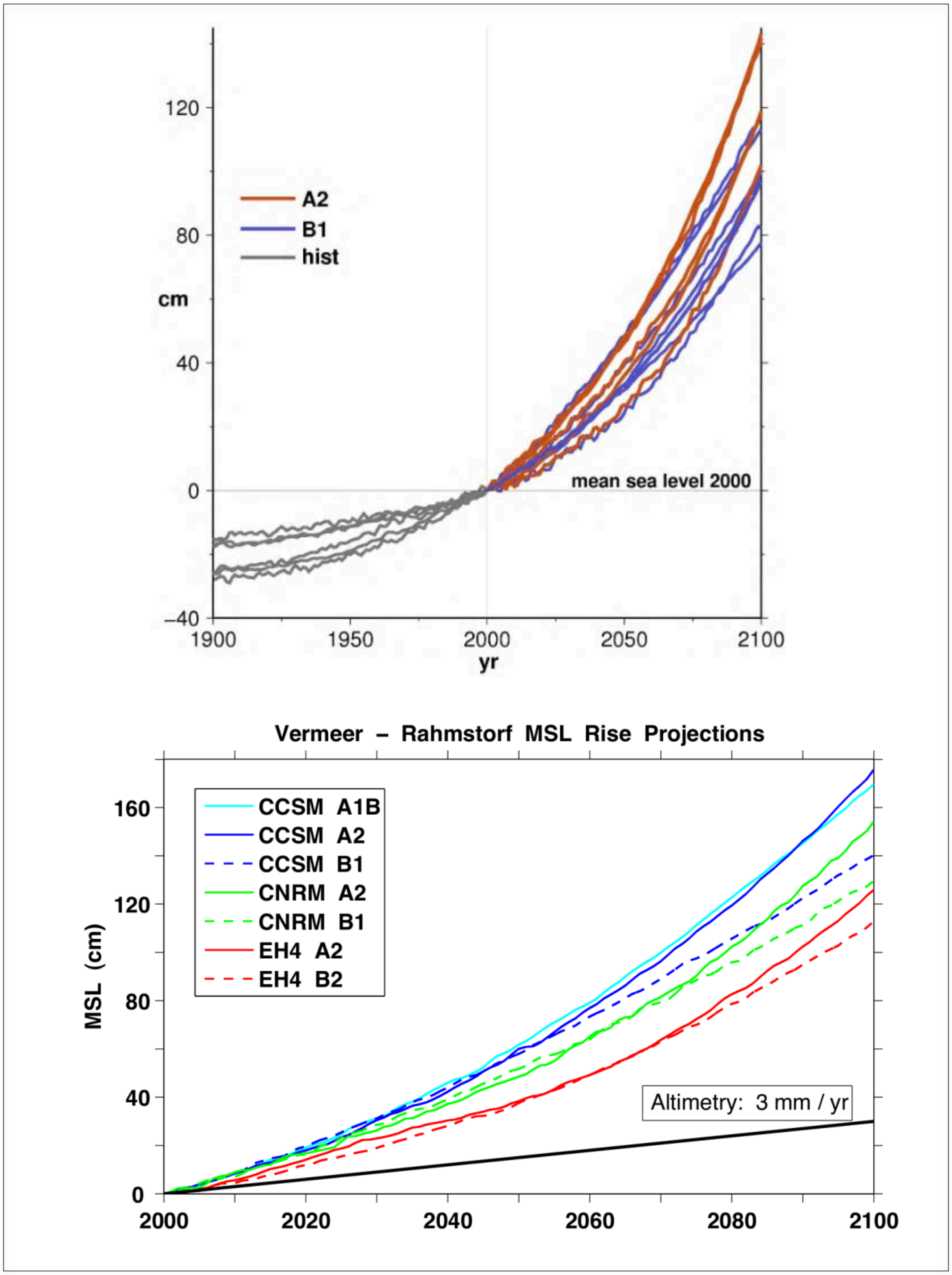


Source: Cayan et al. (2012, p.23; top) and Bromirski et al. (2012, p.4; bottom)

**Figure 11: Changes of the Oceanic Niño Index (NOI) (1950-2013)**

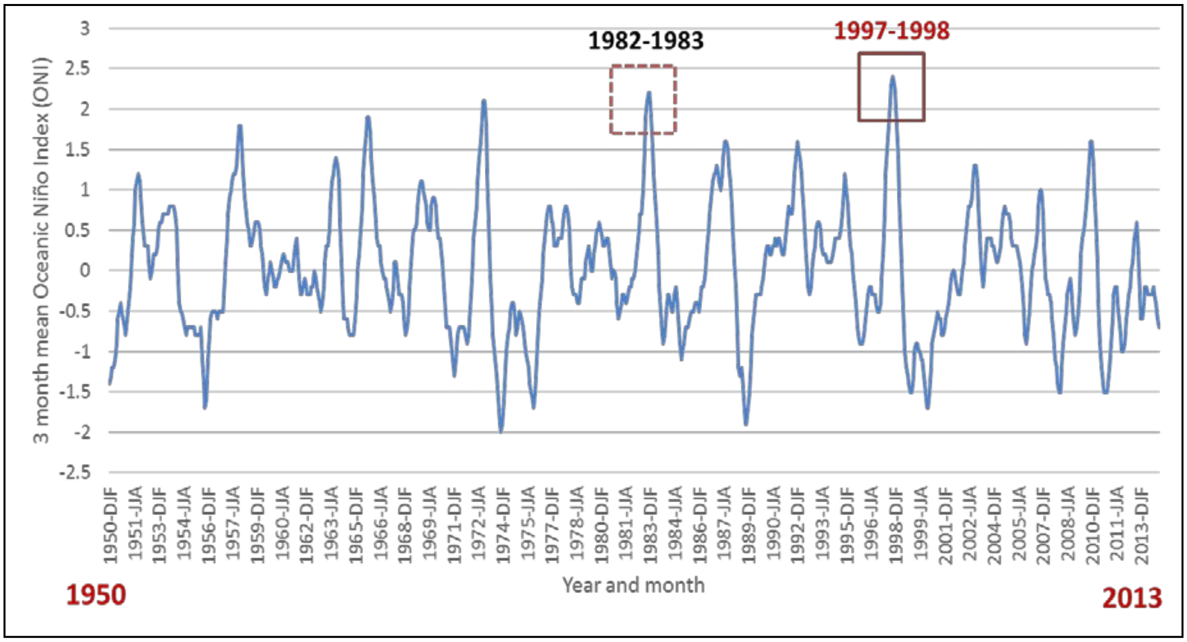


Source: Climate Prediction Center - Monitoring & Data: ENSO Impacts on the U.S. - Previous Events. (n.d.). The NOI is calculated by averaging sea surface temperature anomalies in an area in the east-central Pacific Ocean. El Nino episodes are indicated by sea surface temperature increases of more than 0.5 °C for at least five successive overlapping three-month seasons. The boxes in the figure indicate strong El Nino events.

The analysis of inundation along California's coast was modeled based on three separate but near 100-year storm events. Coastal tiles were assigned water level data recorded from NOAA Tide Gauging Stations during three separate extreme storm events that impacted different portions of the coast. In February 1998, an extreme storm impacted the central coast of California. December of 2005 produced a near 100-year event that came ashore in the Northern portions of the state, and in January 2005, southern California experienced a 100-year storm.

Appendix B provides a detailed discussion of the research team's analysis and selection of storm event data for this study as well as their collection and processing of water level data for the Bay, Delta, and California coastal regions.

## 3.3 Di hydrodynamic Model Simulation

Inundation models are used to predict the extent of flooding based on quantitative relationships between water depths and exposed land surfaces (Mcleod, Poulter, Hinkel, Reyes, & Salm, 2010). In their analysis, researchers modeled the inundation implications of climate change, tidal, and storm surge processes to approximate California's coastal and inland vulnerability to SLR. As already noted, many existing SLR studies use static projections of water depths to estimate areas of inundation. However, accurately modeling the inundation implications of sea-level rise and storm surge together is a complex exercise that should take into account the dynamic nature of tides and storm events. This was accomplished by using a hydrodynamic model, 3Di (Stelling, 2012), to dynamically simulate the movement of changing water volumes over land surfaces through time. Additionally, the analysis incorporates a flow pathway framework that takes into consideration surface feature elevations to accurately identify flow connectivity and flood zones.

### 3.3.1 The 3Di Model

The 3Di hydrodynamic model (Stelling, 2012; http://www.3di.nu/en/international/) developed in the Netherlands by Delft University of Technology, Deltares, with Nelen & Schuurmans Consultants, is a commercial model that dynamically simulates the movement of tides and flood events over digital representations of low-lying land surfaces. Model inputs include time-series water-level data and digital elevation surface data. The model simulates an entire tidal cycle and calculates, in a series of time steps, the flow direction, velocity and water depth as a flood event progresses. The user defines the time interval of the outputs and post processing to combine the results. From each time step, the inundation frequency and average inundation depth are derived. In addition, by combining the output from each time step, a flooding and inundation animation can be created to provide visual communication of potential risks, making it a valuable tool for planning and mitigation.

The 3Di model employs a state-of-the-art approach to simulating flooding, allowing it to process study regions at greater resolution (i.e. containing many more cells) and much faster speeds than existing hydrodynamic models (Van Leeuwen, 2012). As with other hydrodynamic models, 3Di solves shallow-water[19] mass and momentum preserving equations to simulate a water body volume flowing over a surface (Appendix C). The 3Di model is unique, however, in that it combines four specific methods in its solver: a quadtree tiling technique, a sub-grid method within quadrants, a bottom friction technique based on the concept of roughness depth, and a finite-volume, staggered grid method for calculating shallow water equations with rapidly varying flows (Dahm, Hsu, Lien, Chang, & Prinsen, 2014; Stelling, 2012). Each is discussed below:

1. In the sub-grid method a distinction is made between a detailed grid and a course grid. In the detailed grid (i.e. the sub-grid) all details can be taken into account at a high resolution (e.g. $1m^2$). This includes elevation, surface roughness and parameters for groundwater flow, such as interception capacity, infiltration rate and seepage rate. In the course grid the pixels are clustered for the computation of water levels and velocities (Figure 12).
2. Quadtrees detail the course grid, in which the water levels and velocities are calculated on places were the elevation grid has a high variation, such as along high and low line elements such as embankments and canals (Figure 12).

[19] The idea behind the shallow water equations is that any vertical flow is negligible compared to horizontal flow. To account for this characteristic, the distance between (quadtree) cells should be larger (or of the same magnitude) than the water depth. If the depth becomes much larger than the size of the quadtree cells, one could reduce the friction coefficient to simulate this characteristic.

3. The bottom friction technique is based on the concept of roughness depth, in which the spatial variation of the roughness in the sub-grid is taken into account in calculating the water levels and velocities in the course grid.

4. The finite-volume staggered grid method enables calculation of shallow water equations with rapidly varying flows, including semi-implicit time integration. This method ensures that the continuity equations are always solved strictly.

**Figure 12: Sub-Grid Method and Quadtree Methods in 3Di**

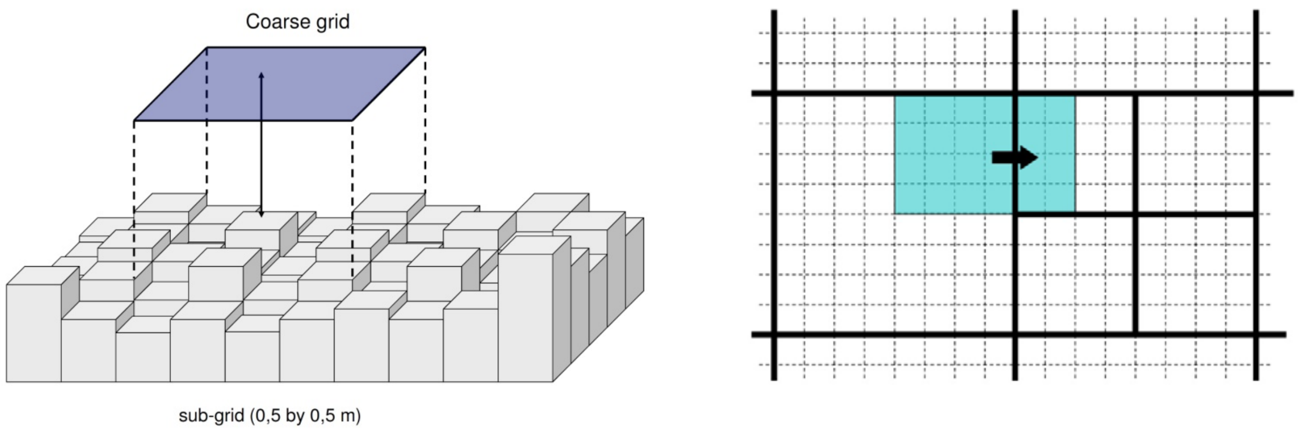


Source: Stelling, G. S. (2012).

Please read Stelling (2012) for more detailed descriptions of these components of the model formulation.

The quadtree tiling technique, and specifically the sub-grid method, results in a “flexible mesh” modeling technique that facilitates the processing of billions of cells in minutes or hours, the use of high-resolution data, and highly realistic flooding simulation (Van Leeuwen, 2012). In the research team’s specific analysis, the resolution and surface features included in the DEM surfaces, along with the 3Di model’s quadtree and sub-grid techniques, facilitate flood simulation input that follows a pathway model framework. As previously discussed, the 1m$^2$ resolution DEMs that were generated for the Bay and Delta regions contain object (mostly building) elevations by design. Given the variation in surface height in regions with these objects, 3Di’s quadtree method generates numerous, small quadrants near them (Figure 13). The model’s sub-grid calculation method, for cells within larger tiles, serves to ensure that the influence of these features on overland water flow and storage is captured in the flood simulation.

**Figure 13: Conceptional Diagram of Constructing a Ground Surface in the 3Di Model**

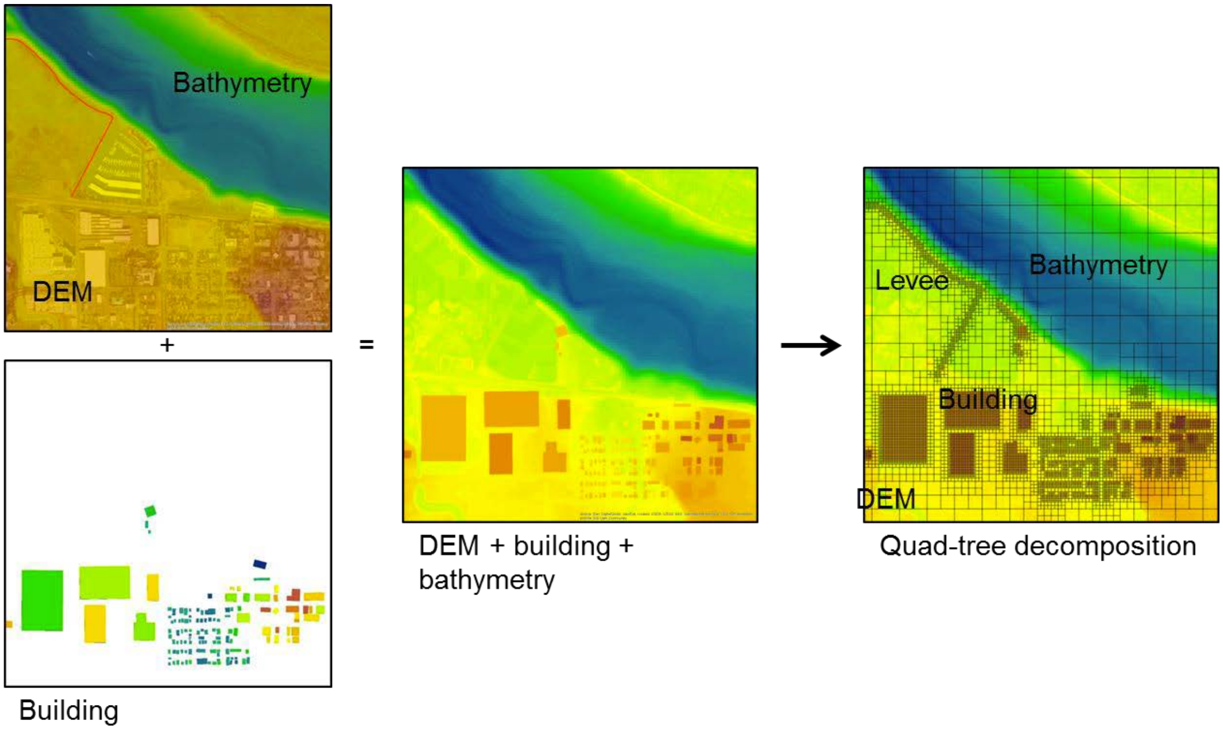


### 3.3.2 Modeling Strategy

To model inundation in each region, researchers input the applicable surface elevation model (DEM) along with combined near 100-year storm event ($NESE_{100}$) water level data and projections of potential SLR to predict a Peak Water Level (PWL). To derive peak water levels (PWLx), the four sea-level rise ($SLR_x$) scenarios {x: 0 m, 0.5 m, 1.0 m or 1.4 m} were individually added to the near 100-year extreme storm event ($NESE_{100}$) water levels ($PWL_x = SLR_x + NESE_{100}$). Researchers input the PWL into the 3Di hydrodynamic model for the four different SLR scenarios. Figure 14 provides an overview of the modeling strategy employed.

**Figure 14: Modeing Strategy Flow Chart**

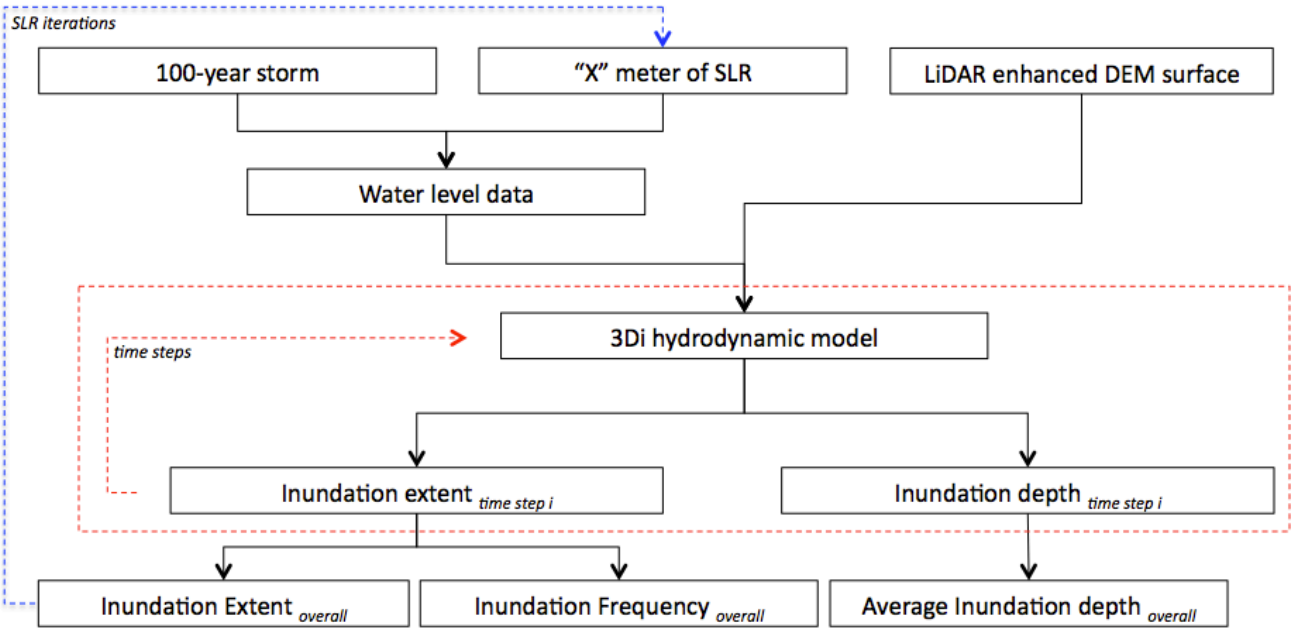


Due to the vast size and surface complexity of the study regions, and to realistically compute the model, researchers first decomposed each region (Bay, Delta and Coast) into tiles. The tiles made it possible to run 3Di simulations in a piecewise manner at very high spatial resolution (cell size) and thus improve surface accuracy. For each tile, researchers established initial water boundaries and provided initial peak water level data as required by 3Di to simulate virtual waves. The process of deriving peak water levels for individual tiles involved adding numerous virtual water level gauging stations with data simulated over the length of the storm event. Researchers used readings every 15 minutes from 28 real gauging stations[20] during the 1998 storm event to study the region, record water levels, calibrate their model during coarse-scale simulations (50 $m^2$ cells), and produce a series of virtual gauging stations for each tile in the Bay. With the input water levels and digital ground surface for each tile, 3Di was used to simulate the entire tidal cycle and calculate, in a series of one-hour time steps, the flow direction, velocity, and water depth as a flood event progresses under different SLR scenarios – all at very high spatial resolution (3 - 5 $m^2$ cells for the Bay and Delta regions)[21]. During post processing researchers combined the results from each time step to get maximum inundation extent and depth across the regions.

---

[20] The 28 gauging stations include 4 real stations in the SF Bay, 17 real stations in the Delta, and 7 real stations along the California coast.

[21] Most cells within tiles are in the 3-5 $m^2$ size range (see Figures 12 and 13), 3 tiles have cells that are slightly above this resolution (6 and 8 m), in order to include a least one complete island. One tile in the SF Bay and one tile in the Delta are 11 m in order to accommodate a complete sub watershed or island.

This modeling strategy allowed the research team to calibrate their models with real and virtual reporting gauge station data, every 15 minutes, for the entire near 100-year storm event. It also allowed them to dynamically model the entire extent of the Bay and Delta regions at unprecedented spatial resolutions producing, as Leiss (2014) points out, better forecasts through better models, a critical step in assessing risk. The quad-tree approach to surface representation allows us to embrace the fine elevation details in the surface, yet compress the databases by roughly a 120:1 ratio. This allows a huge advance in model resolution and dynamics for the region and a massive increase in the accuracy of inundation projections hitherto not achieved by alternative static and/or lower cell resolution methods.

#### *3.3.2.1 Decomposition of the Study Areas by Tiling*

Although 3Di can process a vast number of cells, it does have limitations in the total number of quadtree quadrants that it can process. Considering this computational limitation, researchers decomposed each study region into tiles and perform simulations in a piecewise manner. The size of the tiles varies across each study region, mainly based on the number and complexity of ground objects (buildings and levees) in each tile, as well as the spatial resolution of the elevation surface model. Tiles were sized to allow the model to simulate with a 3-5 $m^2$ spatial resolution and to incorporate levees and object footprints likely to be inundated. Thus, the more ground objects in an area of the study region, the more quadtree grids 3Di will create in that area, and the smaller the tile representing that area has to be. Furthermore, in the Delta region researchers took into consideration the fact that the Delta is a complex hydrologic system. To maintain a certain level of integrity in modeling this system, researchers attempted to delineate tiles that also reflect the size of the watersheds that make up the Delta. Most tiles for the Delta region cover a least one complete watershed (or island). For these tiles, researchers kept simulation results for only the complete watersheds within the tile. Results for watersheds incompletely falling within the tile are excluded.

In all, the San Francisco Bay – Delta region was divided into a total of 60 tiles (Figure 15). The Bay region has 32 tiles and the Delta region 28 tiles. The average size of a tile was 136 $km^2$, the maximum tile size is 570 $km^2$, and the minimum tile size was 36 $km^2$.

**Figure 15: Tiles Delineated for Separate 3Di model Simulations (San Francisco Bay and Sacramento-San Joaquin Delta Regions)**

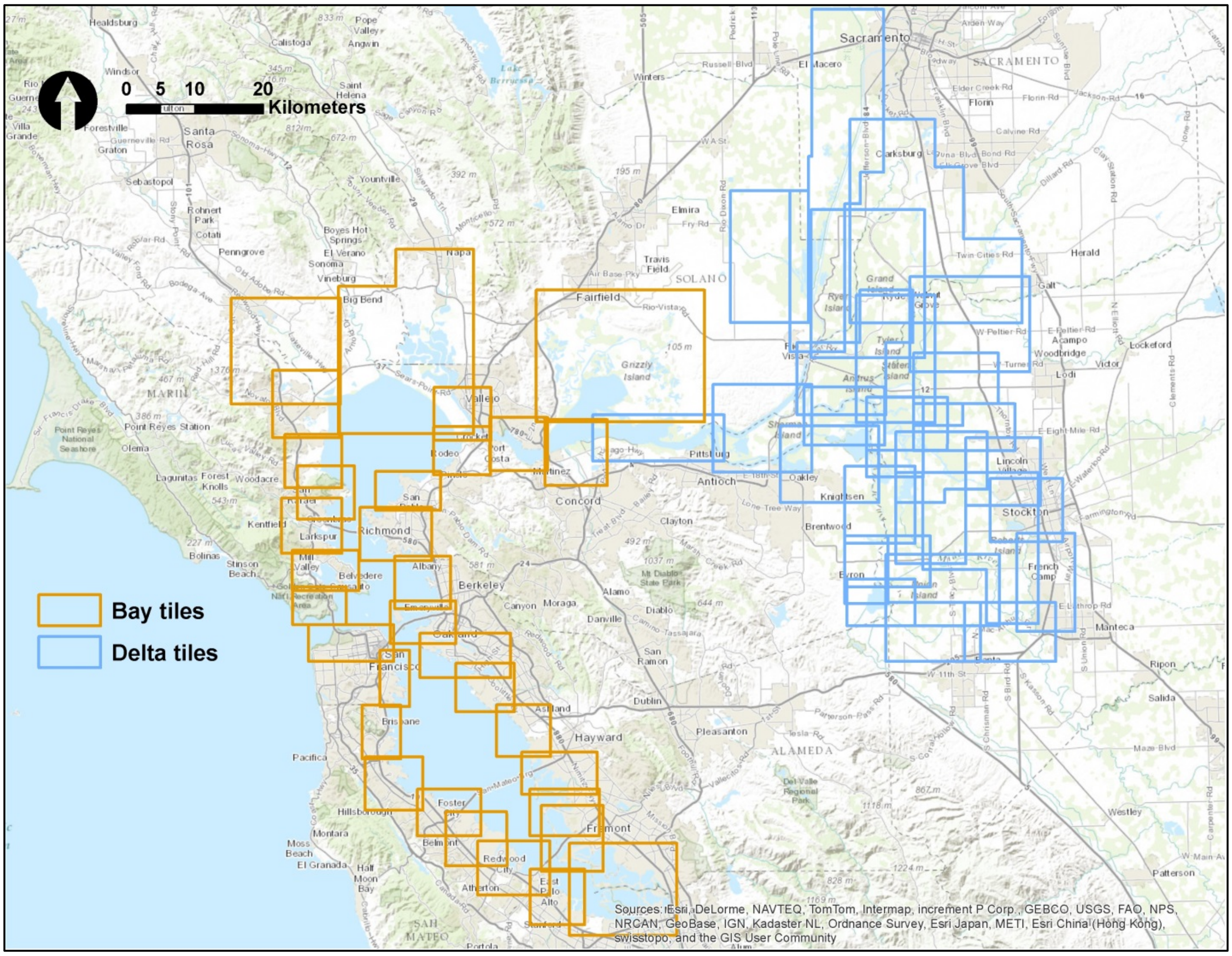


Given the size of California and the need for processing the 3Di hydrodynamic model at relatively high spatial resolution (50m²), the state's coast was divided into 33 partially overlapping tiles: 24 tiles in the northern UTM10 zone and 9 tiles in the southern UTM11 Zone (Figure 16).

**Figure 16: Tiles Delineated for Separate 3Di Model Simulations (California Coast Region)**

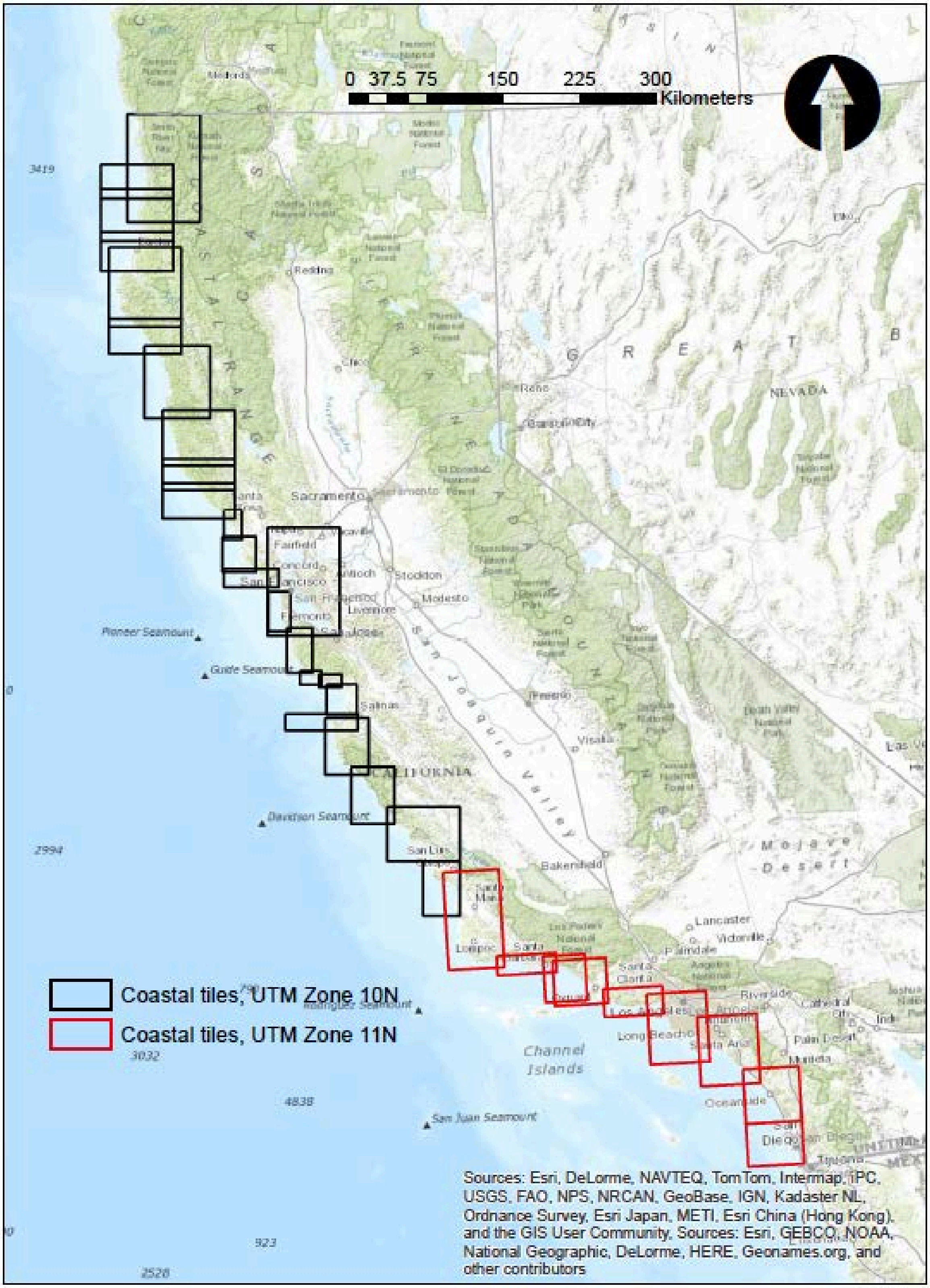

### 3.3.2.1 Initial Water Boundaries and Water Level Data for Tiles

The 3Di model requires the user to establish an initial water boundary and provide initial water level data to simulate virtual waves. Considering the differences between the Bay and the Delta, researchers took different approaches for initial boundary delineation and water level data derivation in each region.

For the Bay, the initial boundary within each tile corresponded to all the tile boundary sections that are on the water.[22] For the Delta, the initial boundaries were the tile boundary sections that are both on the water and would receive water from the Bay side (i.e. not edge sections that are on the water but would receive water from upstream as opposed to the Bay). For the northern Delta tiles, ocean water came from the southwest, so the initial inundation boundaries that required virtual gauging data were located on the south and west sides of the tile. For the southern Delta tiles, ocean water came from the northwest, so the initial boundaries were located on the north and west sides of the tile.

The initial boundaries for tiles along the coast follow the same convention as those in the Bay: the initial boundary within each tile corresponds to all the tile boundary sections are on the water.

Since the study areas are divided into tiles, water level input data for each tile must be provided. The methods used to derive water level data for each tile in the Bay, Delta, and California coast are described in detail in Appendix D.

### 3.3.2.2 3Di Modeling Bay-Delta

3Di was used to simulate the entire tidal cycle and calculate the water depth during near 100-year storm events, coupled with 0.0, 0.5, 1.0, and 1.41-meter SLR, respectively. In 3Di, the time steps for the output water-level surfaces were defined to 1-hour intervals. The output from each SLR inundation scenario included a series of inundated area grids, which allowed analysis of both spatial inundation extents and water depth every hour. In addition, results from each time step were combined to calculate inundation frequency and average inundation depth for an entire storm event.

The accuracy of the 3Di 50 $m^2$ resolution simulation of the Bay area was verified by comparing and validating the simulated water level with the measured water levels at NOAA's San Francisco, Alameda, and Point Chicago tidal gauges. The coefficient of determination ($R^2$) is the indicator of accuracy with a value close to one indicating a more accurate simulation. From Figure 17 the 3Di 50 $m^2$ resolution simulation proved to be quite accurate with the lowest $R^2$ (0.7803) at Port Chicago and the main difference between the simulated and measured water levels occurring during low tides, with the measured water levels being higher than those simulated. This is likely due to discharge from the Delta on the east side of the Bay that would

[22] For tile 26 (i.e. the tile south of Golden Gate) and tile 27 (i.e. the tile north of Golden Gate), only the west side boundary sections were used, because results from using all boundary sections that are both on the water and would receive water from the Bay obviously overestimated the inundation extent.

be expected to elevate the water level during the low tides when the tidal influence is relatively small. This indicates a strong relationship between the simulated and measured results. It should be noted that this is a limited, but important, validation of the team's water level modeling methodology. The collection of valadiation locations is small because the three gauging stations are the only ones with complete data records for these near 100-year storm events. Therefore, the virtual stations along with these NOAA stations were used to calibrate 3Di in the Bay. For the Delta and the Coastal region, a larger set of real gauging stations was used to calibrate 3Di.

**Figure 17: 3Di 50 $m^2$ Resolution Measured and Simulated Water Level Comparison (San Francisco, Alameda and Port Chicago)**

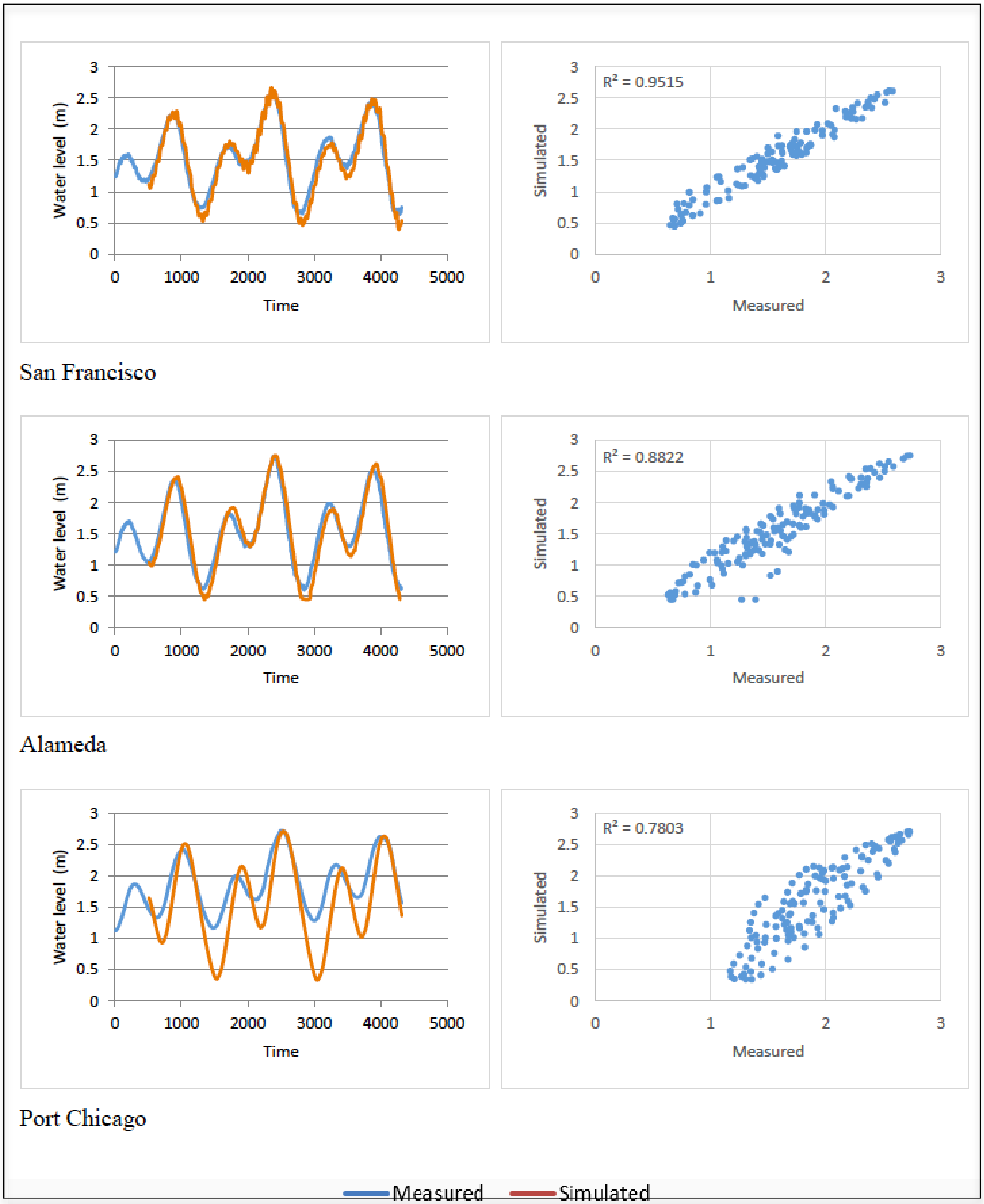

### 3.3.2.3 3Di Modeling California Coast

As stated in the intial proposal, it was necessary to model the entire coast of California at a coarser resolution. Although very high-resolution surfaces ($1m^2$) were produced, 3Di simulations were run across input surfaces constructed of $50m^2$ cells that contain ground surface elevations (DEM) but no objects. Adding objects to the input surfaces for this extensive region was beyond the scope of the research study because of the cost and time to do so. In addition, at a modeling resolution of $50m^2$, even if used as input, most of the objects would not be detected. For the California coast, input surfaces are assigned spatial reference information in the form of UTM coordinates constructed from the NAD83 horizontal datum.

Differences in the timing of extreme storm events along California's coastline forced a decomposition of the study area into three pseudo-meteorological zones (Figure 18). These zones show a rough correspondence to the Northern, Central, and Southern reaches of the California coastline. Extreme water level values were taken from a total of eight NOAA tide gauging stations located along the coast with data referenced to the NAVD88 vertical datum. Similar to the Bay-Delta models, 72-hours of water-level data were downloaded at 1-hour intervals for each near 100-year storm considered. In total, data was collected for three temporally separated events that began on the following dates: February 5, 1998; January 9, 2005; and December 30, 2005. Similar to the Bay-Delta process, water levels were assigned to the tile they are located within. For tiles that do not house a NOAA tidal gauging station, water-level values from the nearest gauging station were assigned.

The North pseudo-meteorological zone uses data from an extreme storm event recorded during December 30, 2005 - January 1, 2006. The Central pseudo-meteorological zone uses data from an extreme storm event recorded during February 5, 1998 - February 8, 1998, and the Southern pseudo-meteorological zone uses data from an extreme storm event recorded during January 9, 2005 - January 11, 2005. Figure 18 illustrates which tiles fall into each pseudo-meteorological zone.

**Figure 18: Coastal Tiles Classified by Applicable Storms Used to Model Initial Water Levels**

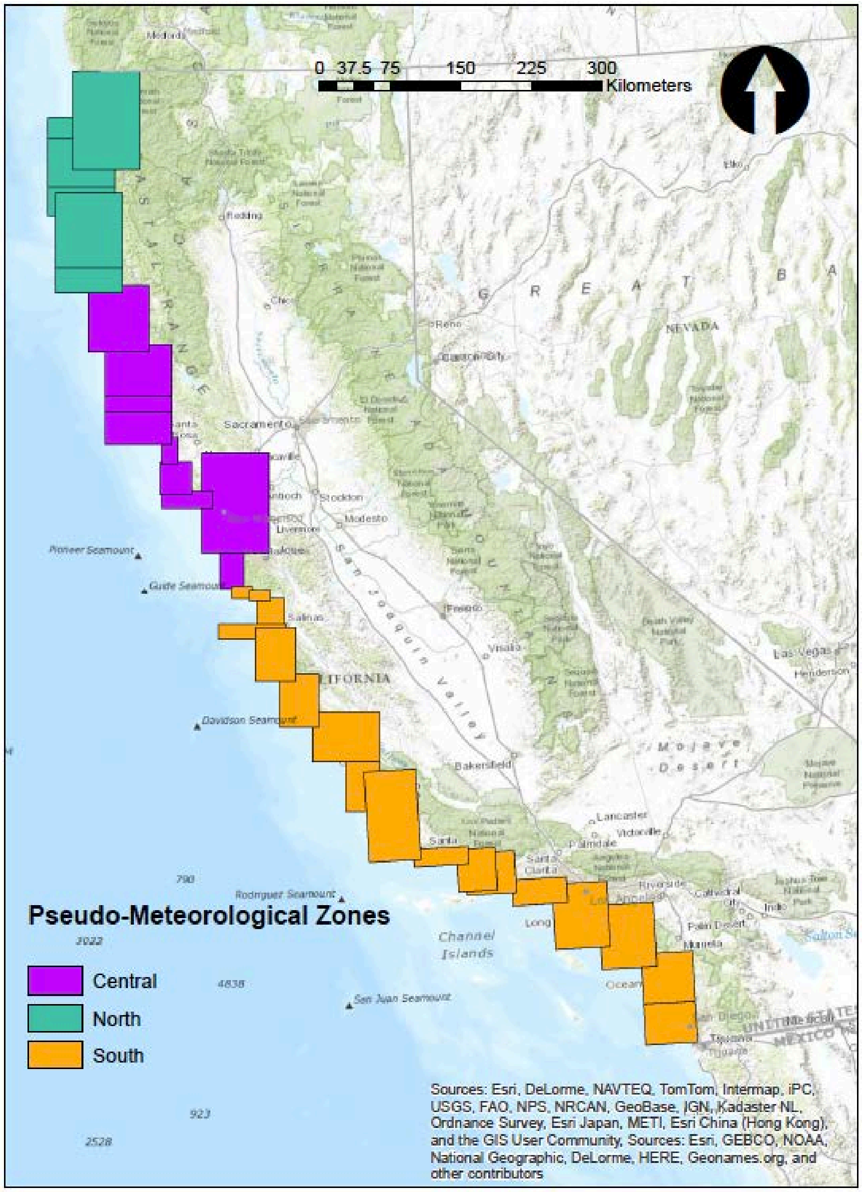


Delft's 3Di has a variety of settings that can be adjusted to match the physical conditions present within the extent of the area modeled and enhance the software's performance. These settings relate to the physics that affect the hydrological flow dynamics (i.e. friction coefficients and types), the decision rules that drive the quad-tree segmentation of input surfaces, and, among other things, the temporal resolution of the results. Flooding depths and extents produced during the simulations are printed at 1-hour intervals to a recording database. All settings were held constant for simulations run along the California Coast.

# CHAPTER 4: Results

The results fulfill the quest of better forecasts through better models.  The research team provided inundation results that were not only calculated and calibrated from real storm events, but which also provide a dynamic picture of the entire storm surge at very fine spatial resolution capturing and integrating all significant surface objects that impact and affect the movement of water. Integrating over 8 billion surface elevation data points, and simulating four scenarios of SLR, the research team's methods produced the most detailed and dynamic layers of inundation in the Bay, Delta and along the Coast of California to date. Then by intersecting the predicted inundation with a highly accurate gas transmission pipeline system for the entire State, and in cooperation with PG&E's sophisticated pipeline risk assessment operators, researchers were able to understand the potential risk such inundation poses to gas transmission assets and document design mitigation strategies and a preliminary estimate of economic costs incurred.

## 4.1 Inundation Maps and Pipelines

### 4.1.1 The Bay Inundation Output

The coastal region of the Bay Area is significantly impacted by SLR (Figure 19). With 0 m SLR, the total inundated area is 417 $km^2$ (161 $mi^2$). For 0.5 m SLR, the inundated area increases to 619 $km^2$ (239 $mi^2$), with 1.0 m SLR, this number increases to 796 $km^2$ (307 $mi^2$), and finally a 1.41 m SLR will result in 897 $km^2$ (346 $mi^2$) being inundated. Although the inundated area in the 1.41 $m^2$ SLR scenario is twice as much as the 0 m SLR scenario, due to the restricted spatial scale printed in Figure 19, the increase is difficult to visualize. This display phenomenon persists and even becomes more exaggerated in the Delta results and along the Coast. Therefore, magnified or zoomed in figures (very large scale reproductions) were included to illustrate the change in inundation over the four SLR scenarios. In the figures to follow, the maximum inundation depth in meters for each cell over the 72 hour run of the model is saved and plotted as a choropleth map.

**Figure 19: Bay Area Maximum Inundation**

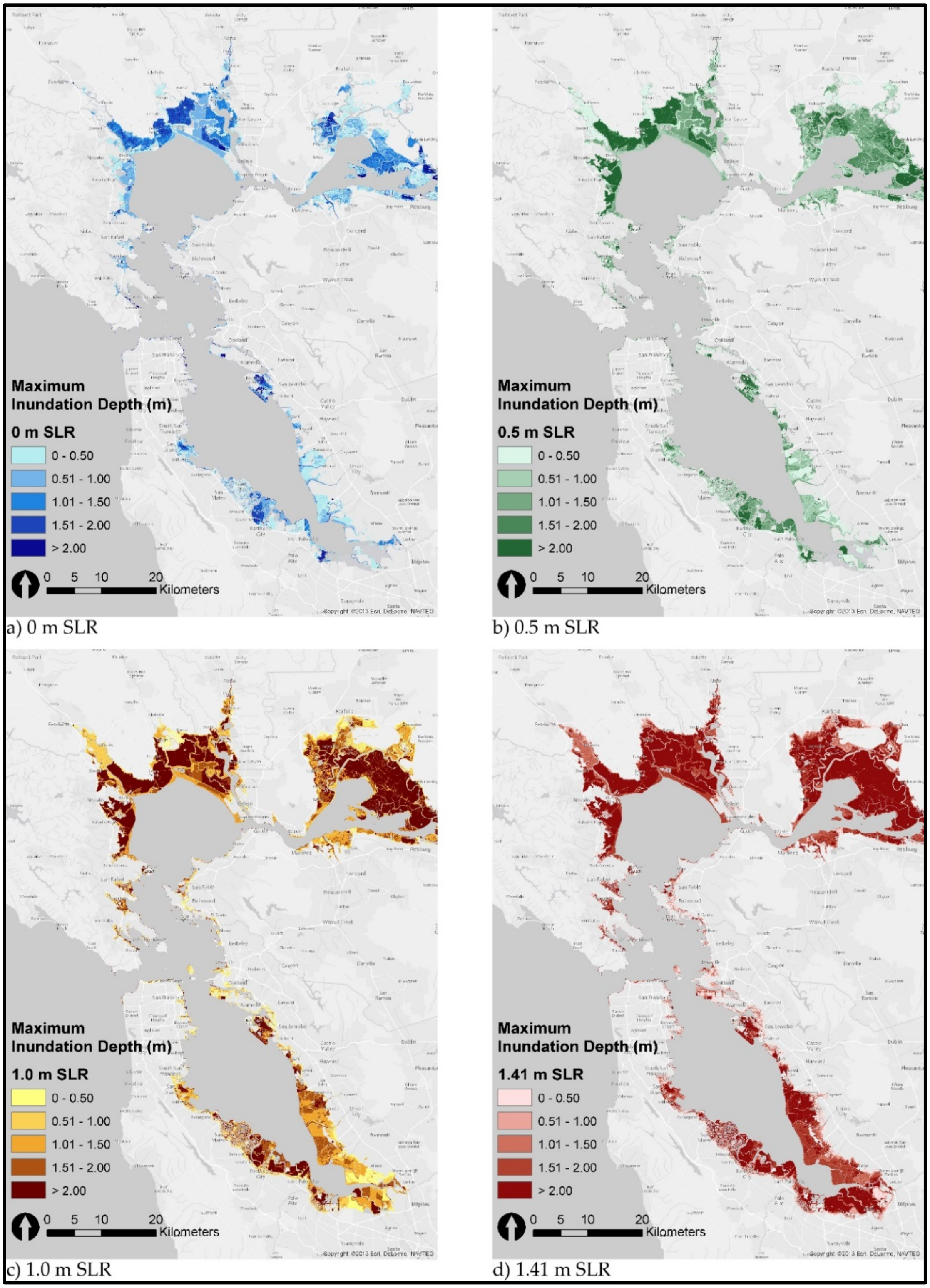


a) 0 m SLR b) 0.5 m SLR c) 1.0 m SLR d) 1.41 m SLR

Inundation through PWLx = SLRx + $NESE_{100}$ (where x = 0, 0.5, 1.0 and 1.41m)

It is useful to show the dynamics of inundation to help understand how the path of flood waters inundate a local landscape during a storm event. Figure 20 shows the simulation of the $PWL_{1.41} = SLR_{1.41} + NESE_{100}$ from Feb 1998. Dynamic representation of the impacts of SLR and storm surge helps illustrate what is a very dynamic process. The heavily inundated Foster City and Redwood Shores areas were used as an example of mapping inundation extent and depth, every two hours for a 16 hour period for the 1.41 $m^2$ SLR scenario. Figure 20 shows a large portion of Foster City inundated in the first eight hours. After eight hours water accumulated over the inundated areas, leading to deeper water levels and further damage. This zoomed in time-series output can be produced for any area in thestudy at an hourly interval and can be assembled into an animation of the inundation.  It is important to note the researchers dynamically calculated at very high spatial resolution inundation throughout the entire storm event for the entire study region.

**Figure 20: Time-series Inundation of the 100-year Storm**

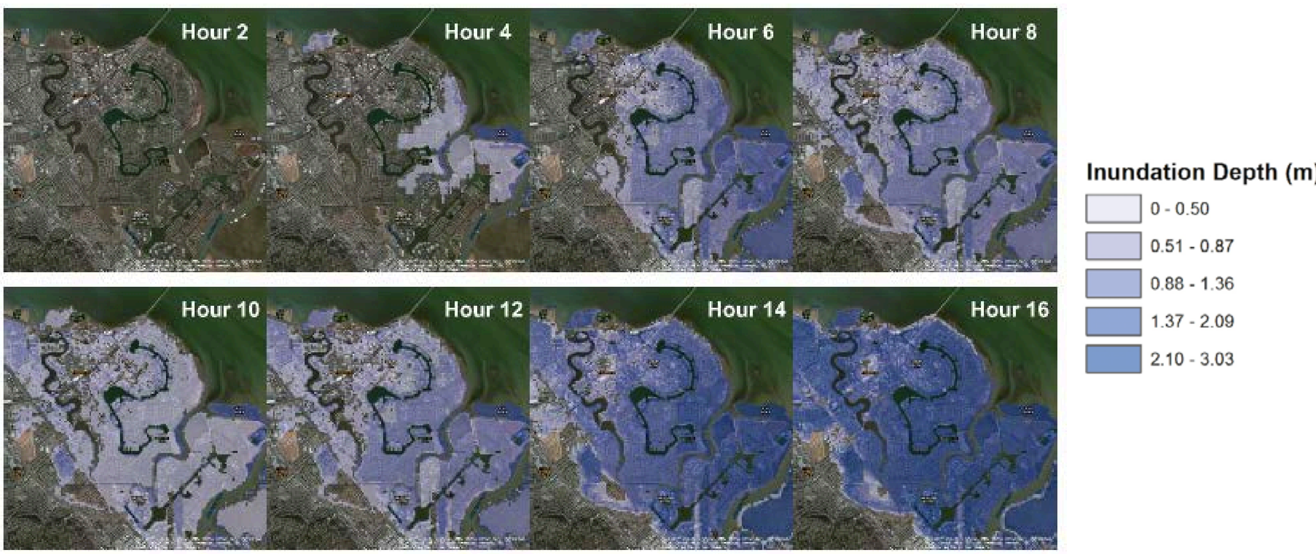


The 100-year storm is associated with 1.41m SLR in Foster City and Redwood Shores ( $PWL_{1.41} = SLR_{1.41} + NESE_{100}$).[23]

---

[23] In Figure 20 the flooding is of greater extent and depth in hour 8 than in hour 10.  This is due to oscillating tide and wave action in the simulation. In this mapped region, near Foster City and Redwood Shores, it was found that water levels continuously decreased between hour 6 and hour 10, and continuously increased between hour 10 and hour 16. In this process, hour 8 had a higher water level than hour 10, which caused the observed greater inundation extent and depth in hour 8 than in hour 10.

### 4.1.2 The Delta Inundation Output

The Delta has a completely different physiography with much of the island land surface protected by an extensive levee system in areas where elevations are well below sea level. The process of inundation in the Delta began with overtopping of an island's levee and the filling in of the islands in a relatively short period of time (Figure 21).[24]

Sherman Island (identified in Figure 5)[25] was used as an example of mapping inundation extent and depth in the Delta, every 24 hours for the duration of the February 1998 near 100-year storm event. Figure 22[26] shows Sherman Island inundation updates after the first day of the storm where, even with no sea level rise ($SLR_0$), the levee was overtopped and the western side of the island began to flood. After 48 hours during a $SLR_{1.0}$ + $NESE_{100}$ storm event, almost the entire island was inundated, and during a $SLR_{1.41}$ + $NESE_{100}$ storm event the entire island was under considerable depth of water. Figure 23 shows levee overtopping on Sherman Island during the February 1998 near 100-year storm event.

Figure 24 shows a levee break on Sherman Island during an extreme storm event in January 1969. The levee break is focused on the south side of the island yet the flood pattern resembles the inundation modeled in the $SLR_{1.0}$ + $NESE_{100}$ storm event above.

---

[24] The Delta water system is highly altered and managed by the California Department of Water Resources. During storm events when there are higher sea levels, reservoir managers release more fresh water to prevent salt water intrusion. This management leads to uncertainty in the modeling results, and although the model was calibrated to the peak water levels (as seen in Figure 17), the measured troughs are much higher than predicted. This is likely due to reservoir managers releasing more fresh water into the Sacramento and San Joaquin rivers. The model was calibrated to the PWL to ultimately predict the maximum water depth during the entire storm event.

[25] On February 9, 1998, flooding resulted in a major disaster declaration in Reclamation District 341, Sherman Island. Damage Survey Reports to fund the slope protection and levee repair and restoration efforts totaled $911,360 (https://www.fema.gov/fr/appeal/218739).

[26] This figure is meant as an illustration of the inundation or flooding process on the island, over time on one axis, and over the four SLR iterations on the other axis.

**Figure 21: The Delta Area Maximum Inundation**

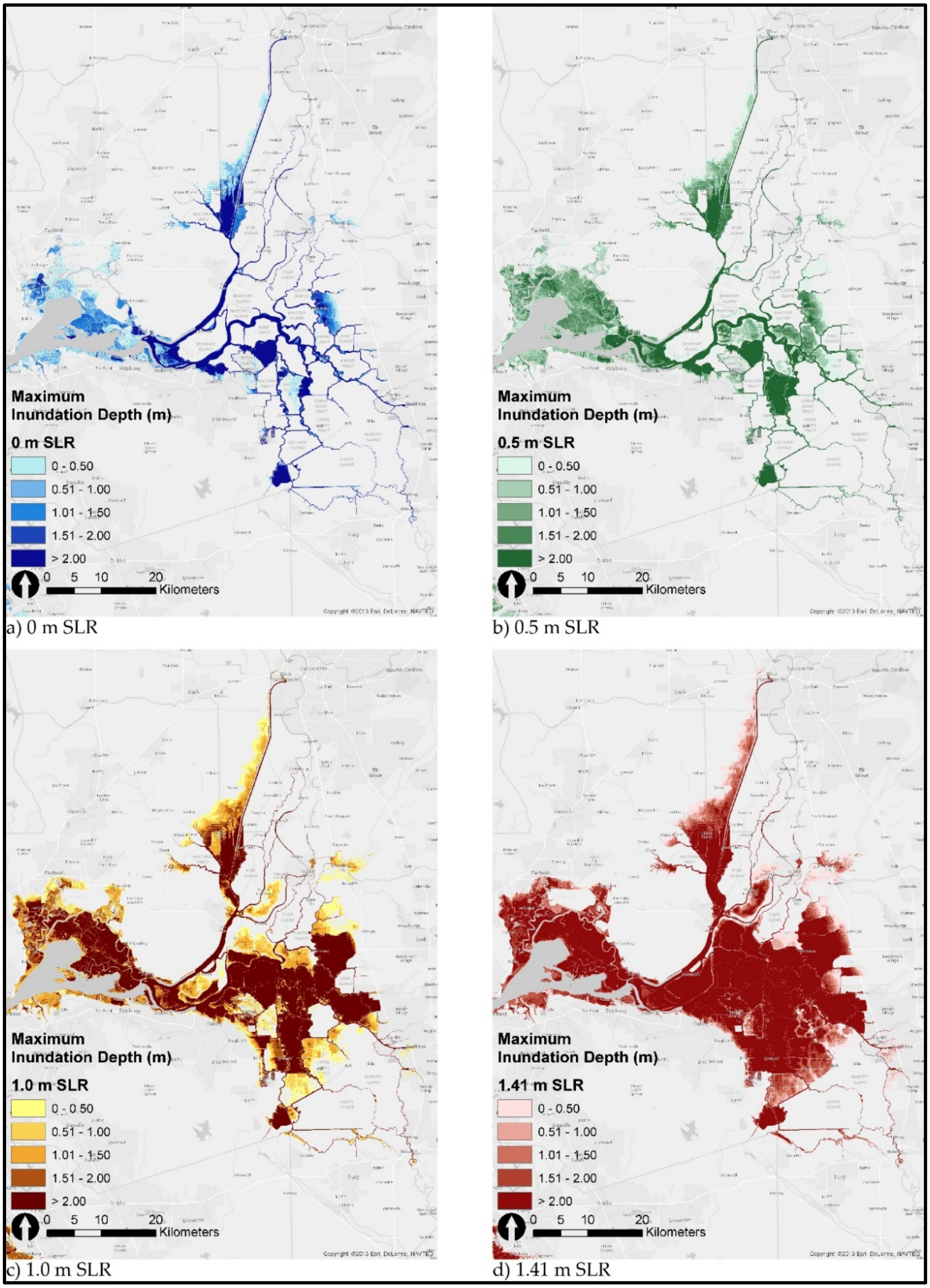


Maximum inundation through PWLx = SLRx + $NESE_{100}$ (where x = 0m, 0.5m, 1.0m, and 1.41m).

**Figure 22: Wave Wash Erosion at Levee Mile 5 on Sherman Island (February 7, 1998)**


Source: DWR staff photograph.

**Figure 23: Sherman Island Time-Series Inundation Extent and Depth**

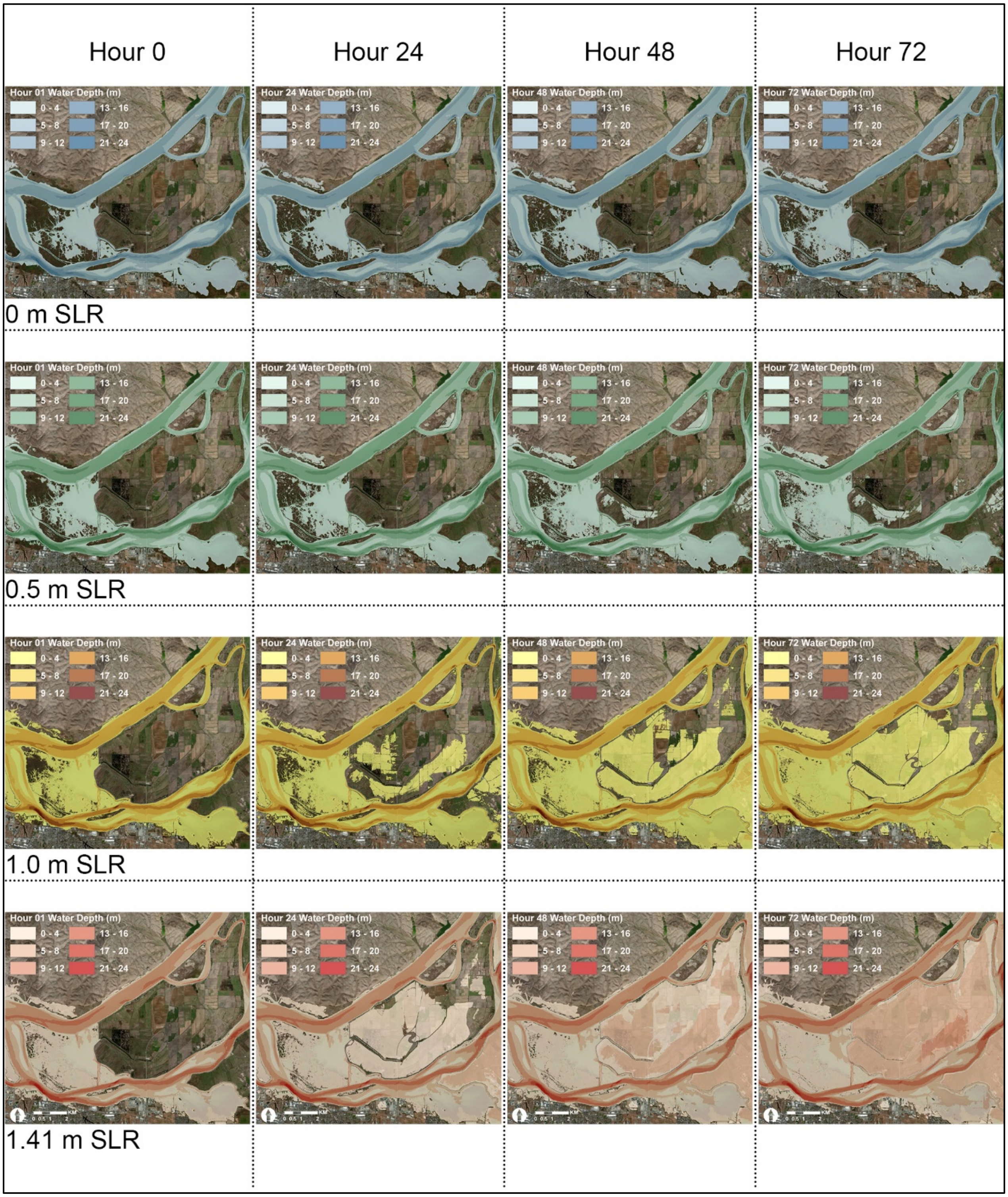


Depth through PWLx = SLRx + NESE100 (where x = 0m, 0.5m, 1.0m, and 1.41m), every 24 hours for the duration of the February 1998 NESE100

**Figure 24: Mosaic of Aerial Photographs of Sherman Island (January 21, 1969)**

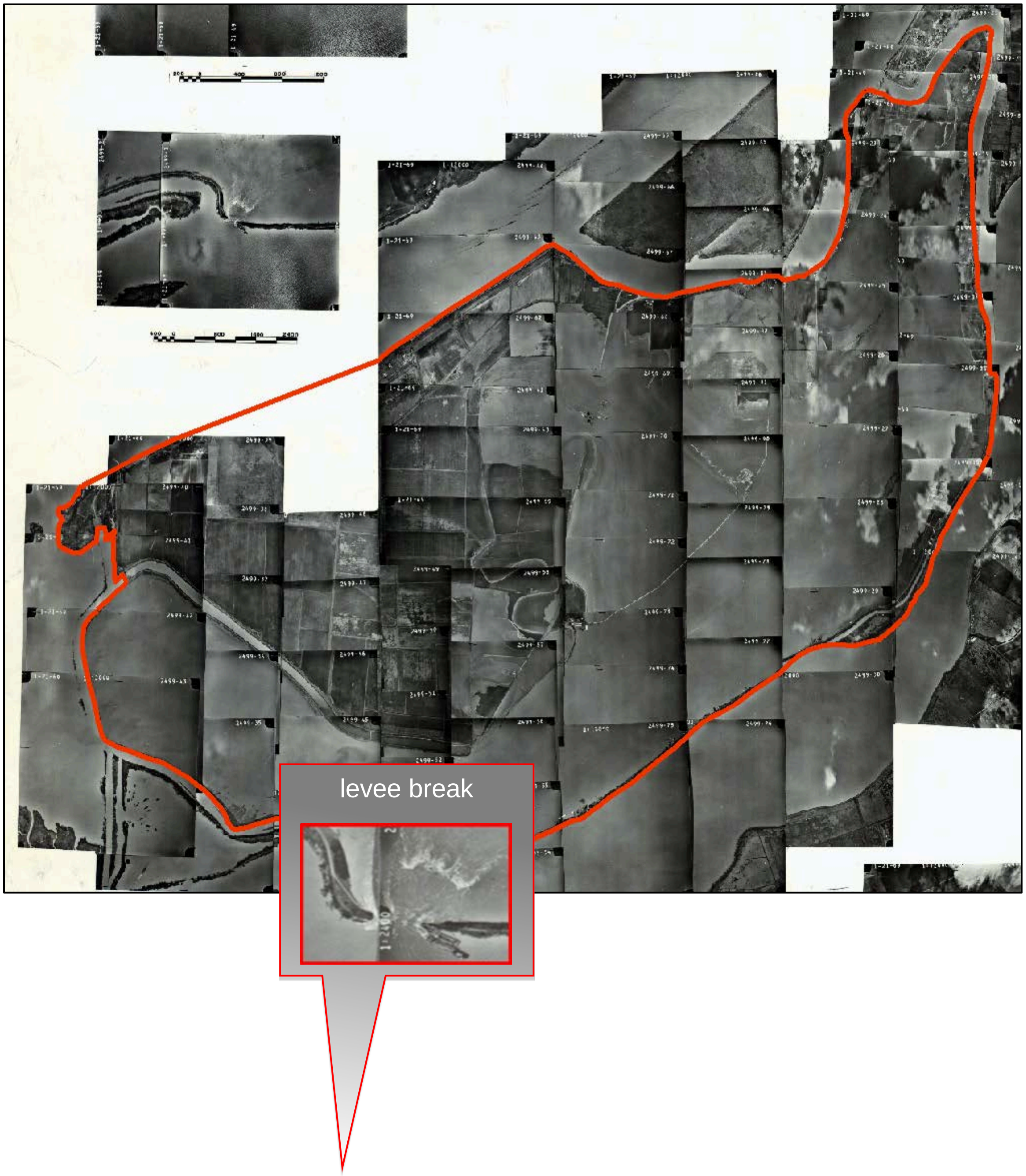


Source: DWR staff.  Photographer: G. Longton, Pilot: R. Cole.

Figure 25 shows the extent of flooding on Sherman Island during an extreme storm event in January 1969.

**Figure 25: Aerial Photograph of Sherman Island Flooding (January 21, 1969)**

Source: DWR staff. Photographer: G. Longton, Pilot: R. Cole.

### 4.1.3 The Bay-Delta Pipeline Inundation Output

There are more than 5,505 km (3,421 mi) of pipelines transecting the Bay-Delta region. Spatial scale simply impedes the researchers' ability to effectively illustrate in detail the flooded or inundated pipeline infrastructure for the Bay and Delta regions in this document. However, Figure 26 provides an effective look at the extent of the flooding and inundation over the four SLR scenarios in combination with a near 100-year storm event. At $SLR_{1.41}$ coupled with a near 100-year storm event, it is evident that the flood and inundation of pipelines in the region is quite extensive.

However, of these flooded and inundated pipelines, only 308 km (191 mi) are PG&E gas pipelines, with the balance of these transmission pipelines essentially transporting liquid fuels.

**Figure 26: Bay-Delta Pipelines Affected by Maximum Inundation and a Near 100-year Storm Event**

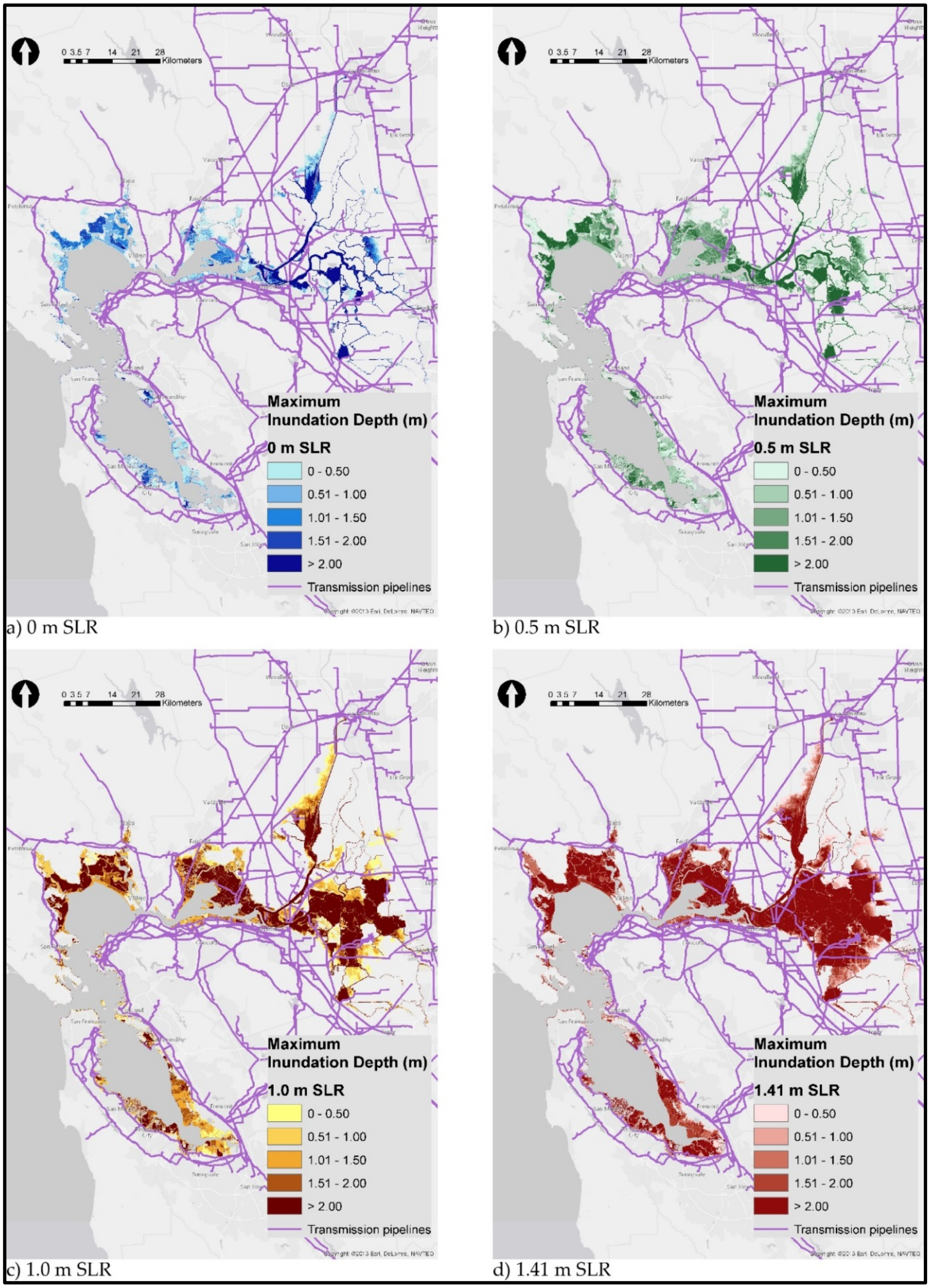


Pipelines affected by SLR of 0.0 to 1.41 m maximum inundation coupled with a near 100-year storm event

For the Bay-Delta flood and inundation simulations in Table 2, although only 124 km of pipeline are inundated under a near 100-year extreme storm event with $SLR_0$, PG&E's gas pipelines make up approximately 33% of them. In total, of all the pipelines criss-crossing the Bay-Delta region, only approximately 2.3% are predicted to be inundated under a $NESE_{100}$ with no sea level rise. However, by $SLR_{1.41}$ , approximately 11.5% of all the pipelines criss-crossing the Bay-Delta region are predicted to be inundated, and PG&E's gas pipelines make up approximately half of them.

**Table 2: Bay-Delta Pipeline Inundation Results for Four $SLR_x$ Scenarios**

| SLR Value | Total km of Pipelines Inundated in Bay-Delta Region – (between 16-18 different companies) | Total km of PG&E Gas Pipelines inundated in Bay-Delta Region | Total km of Pipelines in Bay-Delta Region |
|---|---|---|---|
| 1.41 m + 1998 storm | 633 km | 308 km | 5506 km |
| 1.0 m + 1998 storm | 413 km | 193 km | 5506 km |
| 0.5 m + 1998 storm | 225 km | 96 km | 5506 km |
| 0 m + 1998 storm | 124 km | 41 km | 5506 km |

Inundation results over four $SLR_x$ scenarios where x = 0, 0.5, 1.0 and 1.41m.

Figure 27 summarizes, for all pipeline operators, the amount of pipeline inundated by depth, or Peak Water Level (PWL) of exposure. Although the model output provides a continuous tracking of PWL over all the inundated surfaces, the results are classified here to better recognize patterns of depth across the SLR scenarios. During $NESE_{100}$ with no sea level rise, the vast majority of the inundated pipelines are predicted to experience a PWL of less than 3 meters. Even with a simulated $SLR_{1.0}$ less than 5% of the inundated pipelines are predicted to experience a PWL of more than 3.5 meters. However, with a simulated $SLR_{1.41}$ , over 50 kilometers of pipeline are predicted to be exposed to PWLs of more than 3.5 meters.[27]

[27] It is important to note that although these inundated surfaces are predicted to be exposed to various PWLs during a near 100 year storm event ($NESE_{100}$), whether they remain inundated, and to what depths, are a function of: 1) pathways and connectivity to open water sources; 2) the repair and maintenance schedules of levee systems that might protect them; and 3) emergency pumping of inundated areas. In this study, no attempt was made to account for factors 2) and 3) as they are beyond the scope of this research.

**Figure 27: Length in Kilometers of All Operator Inundated Transmission Pipelines**

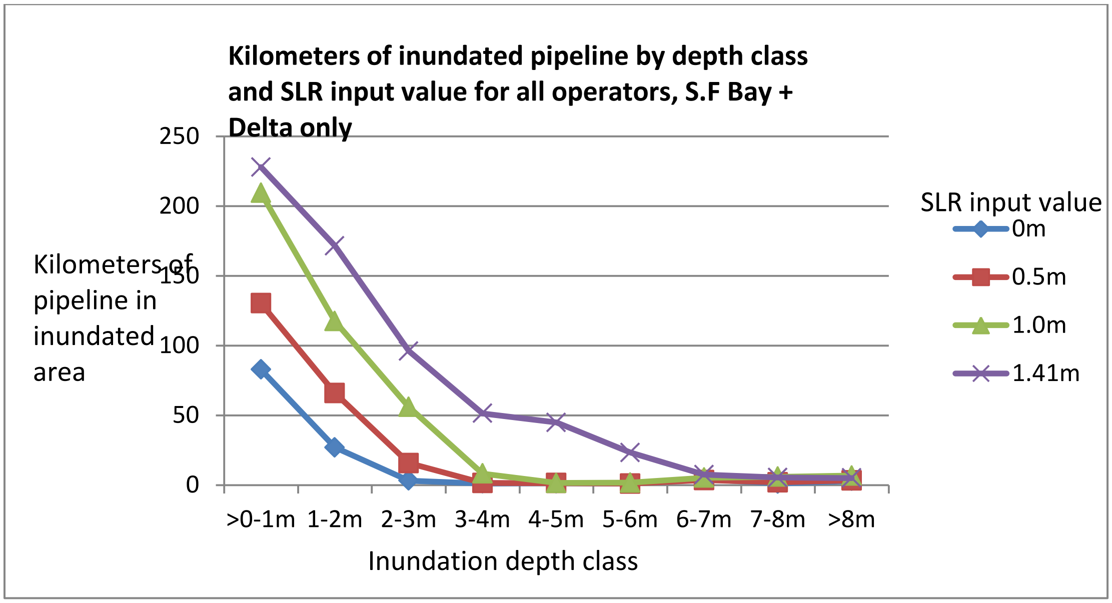


Inundated transmission pipelines by $PWL_x = SLR_x + NESE_{100}$ (where x = 0.0, 0.5, 1.0, and 1.41 m)

Figure 28 summarizes the amount of PG&E transmission pipeline that is predicted to be inundated by the depth, or Peak Water Level (PWL) of exposure. During a $NESE_{100}$ with no sea level rise, similar to all pipeline operators, the vast majority of PG&E's inundated pipelines experienced a PWL of less than 3 meters. However, with a simulated $SLR_{1.0}$, approximately 28 kilometers (17 mi) of transmission pipelines were exposed to PWLs of more than 2.5 meters but less than 5 km (3 mi) of them experience more than 3.5 meter PWLs. Although a simulated $SLR_{1.41}$ generates a similar slope to that of $SLR_{1.0}$ when mapping pipeline exposure against inundation depth, approximately 53 kilometers (33 mi) of pipeline were exposed to PWLs of more than 2.5 meters and of those, more than half (approximately 30 km or 18 mi) experienced more than 3.5-meter PWLs.

**Figure 28: Length in Kilometers of PG&E Inundated Transmission Pipelines**

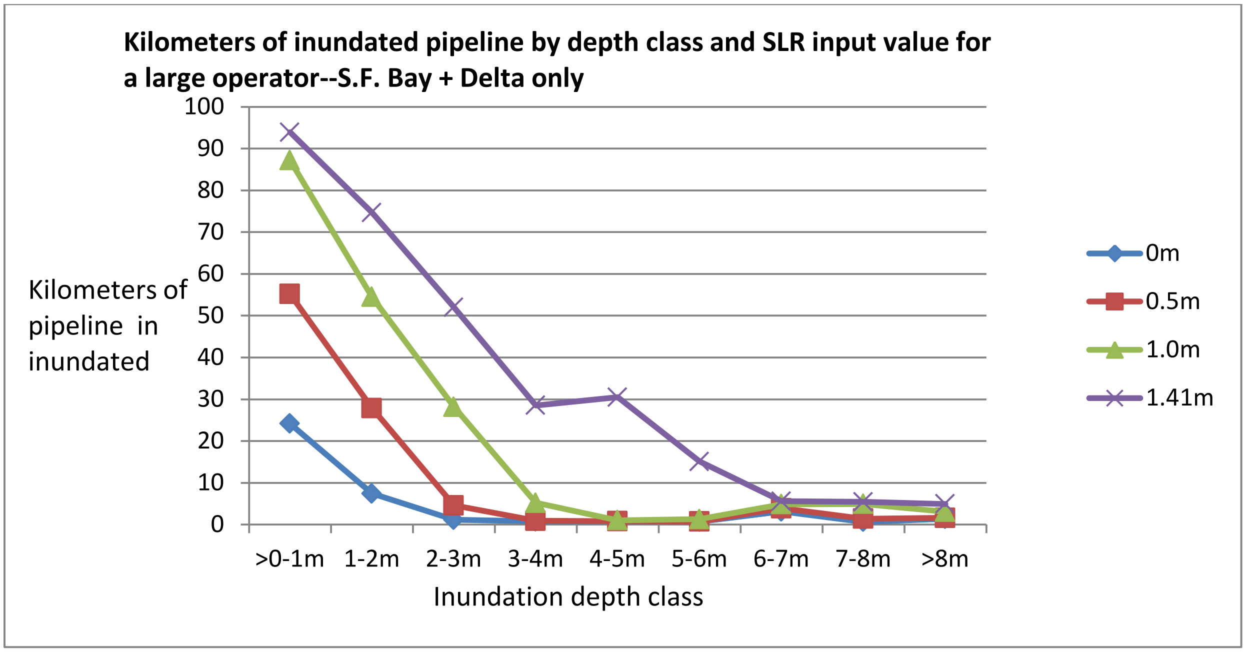


PG&E inundated transmission pipelines by PWLx = SLRx + $NESE_{100}$ (where x = 0.0, 0.5, 1.0, and 1.41m)

Figure 29 illustrates the results of the simulation modeling impacting transmission pipelines from the NPMS dataset. This zoomed in (very high resolution) image reveals the detail in the model simulations produced for the entire Bay-Delta region.

**Figure 29: Simulation Results of the Maximum Inundation Depth of NPMS Transmission Pipelines**

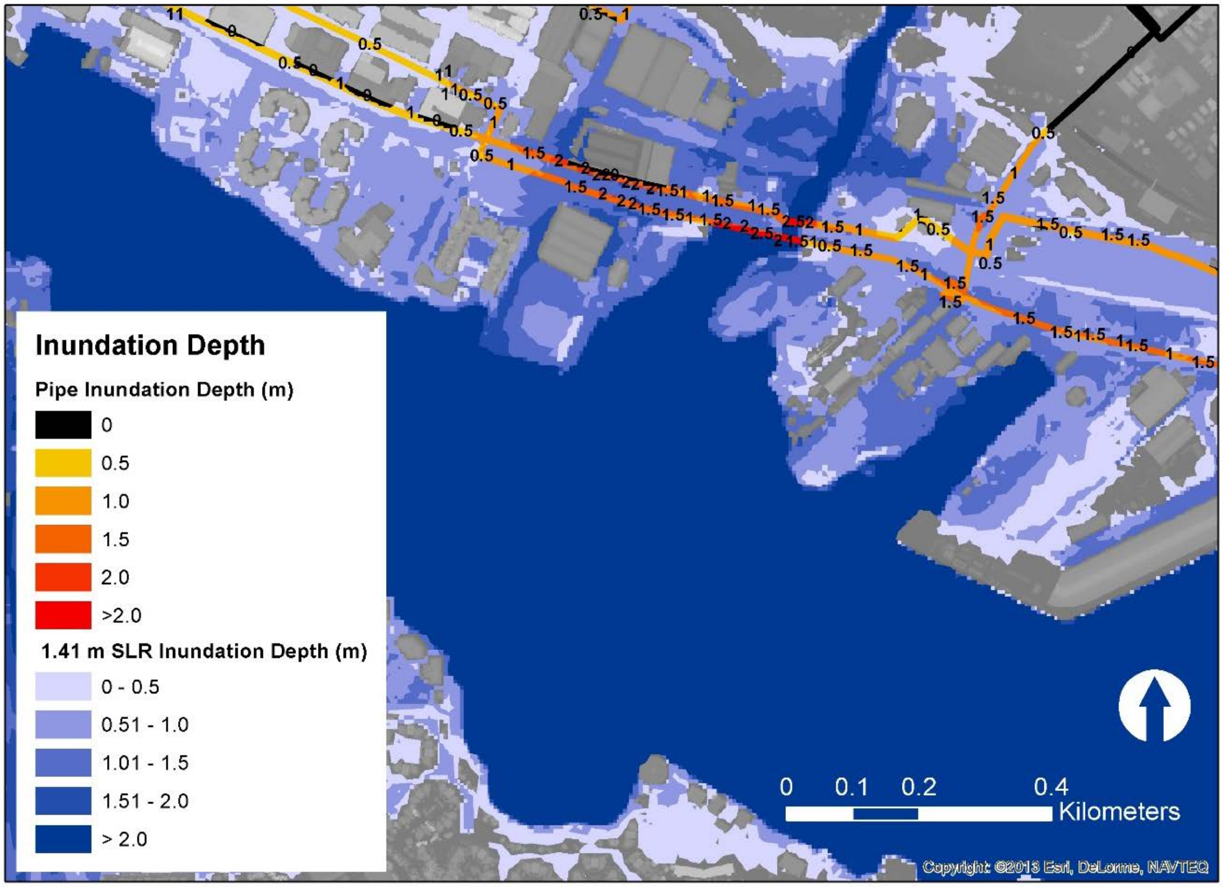


Maximum inundation depth of NPMS transmission pipelines when $PWL_{1.41} = SLR_{1.41} + NESE_{100}$ (SLR = 1.41 meters).

### 4.1.4 The Coast Inundation Output

Most of California's coast has relatively steep slopes where sea-level rise will likely erode the cliffs. Other parts of the coastal region feature low-lying outwash plains with delta like characteristics fed by rivers and streams. It is impossible to illustrate in one figure (like Figure 19 of the Bay and Figure 21 of the Delta), the inundation along the California Coast. Therefore the research team limited illustration of coastal inundation to two regions featuring a low-lying landscape and a well-mapped gas-pipeline infrastructure. Figure 30 maps inundation near Humboldt Bay along the northern California Coast, and Figure 31 maps inundation near Long Beach on the southern California Coast.

**Figure 30: The California Coast near Humbolt Bay Maximum Inundation**

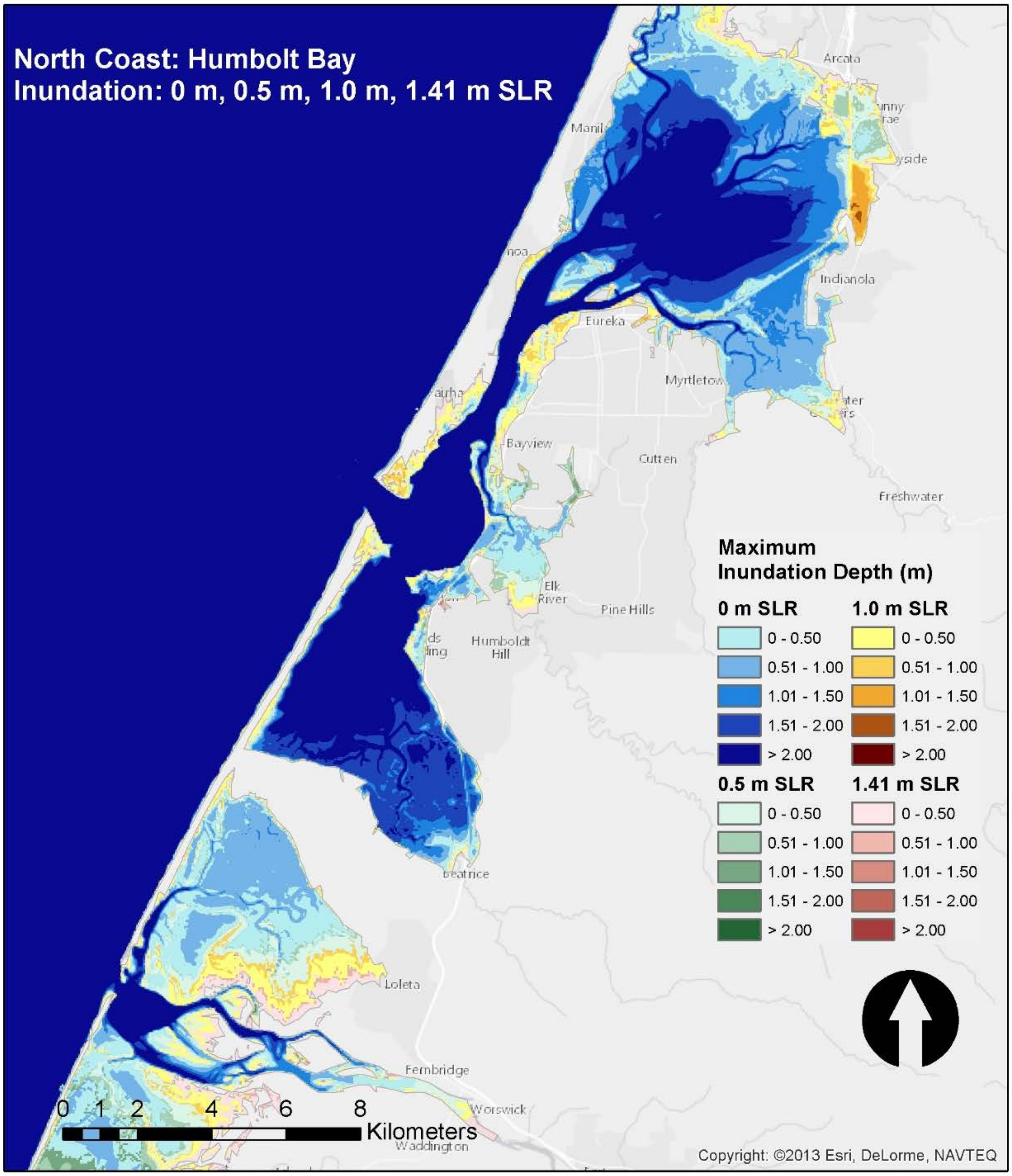


Maximum inundation through $PWL_x = SLR_x + NESE_{100}$ (where x = 0m, 0.5m, 1.0m, and 1.41m).

**Figure 31: The California Coast Near Long Beach Maximum Inundation**

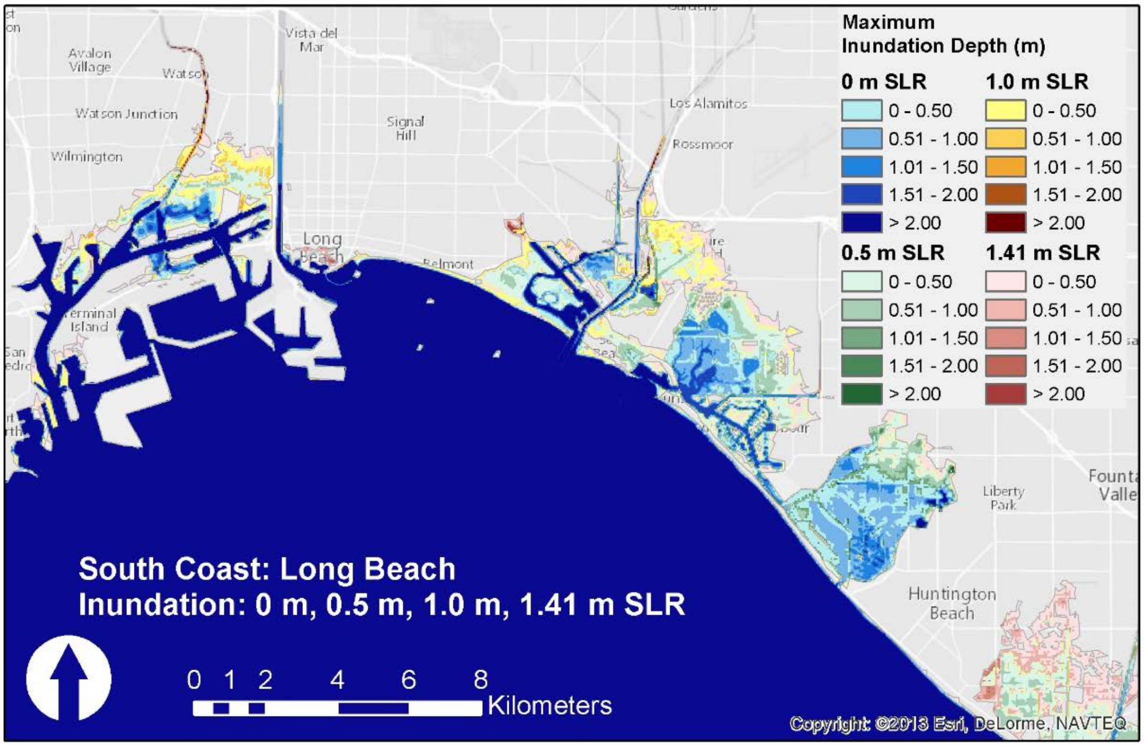


Long Beach maximum inundation through $PWL_x = SLR_x + NESE_{100}$ (where x = 0m, 0.5m, 1.0m, and 1.41m).

### 4.1.5 The Bay, Delta, and Coast Pipeline (NPMS Dataset)

The publically available National Pipeline Mapping System (NPMS) dataset delineates both the gas and liquid transmission pipelines. Figure 32 maps the dataset within California for 2013 by operator. The greatest concentration of these pipelines near the coastal regions is in the San Francisco Bay, Sacramento - San Joaquin Delta, and the Los Angeles areas.

**Figure 32: The California NPMS Line-Route Pipeline Transmission Data**


**California Underground Transmission Lines by Operator**
**UC Berkeley/California Energy Commission, John Radke & Gregory Biging Principal Investigators**

Source: from NPMS 2013 data

### 4.1.6 The California Coastal Pipeline Inundation Output

There are more than 7,088 km (4,404 mi) of pipelines along the California Coast. [28] For the California coast inundation simulations in Table 3, although only 278 km (173 mi) of pipeline were predicted to be inundated under a near 100-year extreme storm event with $SLR_0$, gas

---

[28] The definition used here for pipelines in the coastal region is the legislated Coastal Zone Boundary (https://coast.noaa.gov/czm/media/StateCZBoundaries.pdf) buffered by 20km inland.

pipelines made up approximately 19% of them. In total, of all the pipelines criss-crossing the California coastal region, less than 1% were actually inundated under a $NESE_{100}$ with no sea level rise. However, by $SLR_{1.41}$, approximately 4% of all the pipelines criss-crossing the California coastal region were predicted to be inundated.

**Table 3: California Coast Pipeline Inundation Results for Four $SLR_x$ Scenarios**

| SLR Value | Total km of Pipelines Inundated in the Coastal Region – (between 32-38 different companies) | Total km of Gas Pipelines inundated along Coastal Region | Total km of Pipelines in the Coastal Region |
|---|---|---|---|
| 1.41 m + $NESE_{100}$ storm | 278 km | 53 km | 7,088 km |
| 1.0 m + $NESE_{100}$ storm | 195 km | 40 km | 7,088 km |
| 0.5 m + $NESE_{100}$ storm | 137 km | 31 km | 7,088 km |
| 0 m + $NESE_{100}$ storm | 56 km | 20 km | 7,088 km |

Results for four SLRx scenarios where x = 0m, 0.5m, 1.0m, and 1.41m.

Spatial scale simply impedes the ability to effectively illustrate in detail the inundated pipeline infrastructure for the coastline in this document. As per the illustration above, the research team limited their maps of the inundated pipeline infrastructure to the Humboldt Bay and the Long Beach regions.

Figures 33, 34, and 35 provide an effective look at the extent of the inundation over the four SLR scenarios for Humboldt Bay, Long Beach and San Diego Bay. At $SLR_{1.41}$, the predicted inundation of pipelines in the region is 278 km (173 miles) is evident. However, of these inundated pipelines, only 53 km (33 miles) are gas pipelines, with the balance of these transmission pipelines essentially transporting liquid fuels.

**Figure 33: Humbolt Bay – Maximum Extent of Pipelines Inundated**

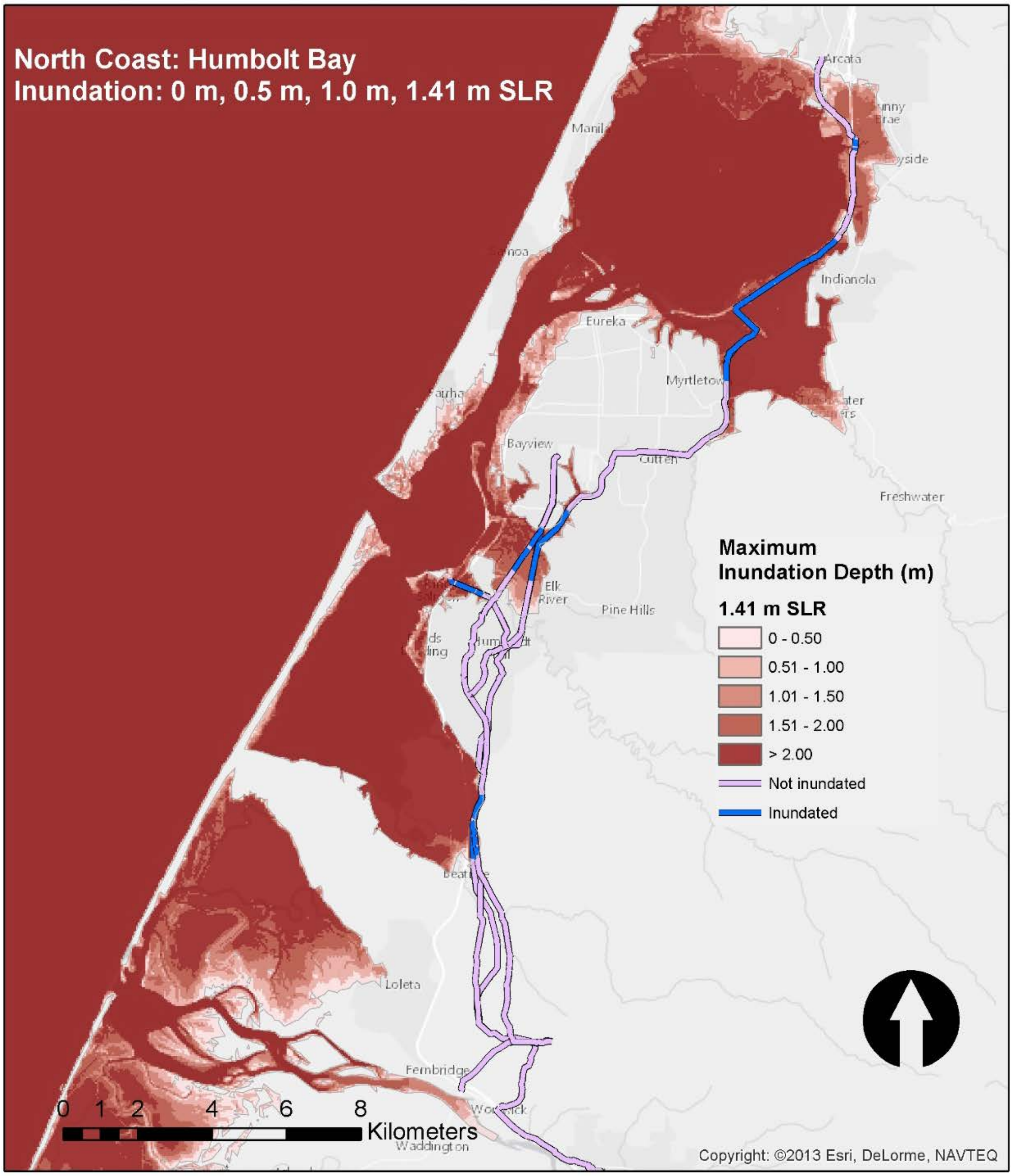


When SLR = 1.41 meters combined with a NESE100

**Figure 34: Long Beach – Maximum Extent of Pipelines Inundated**

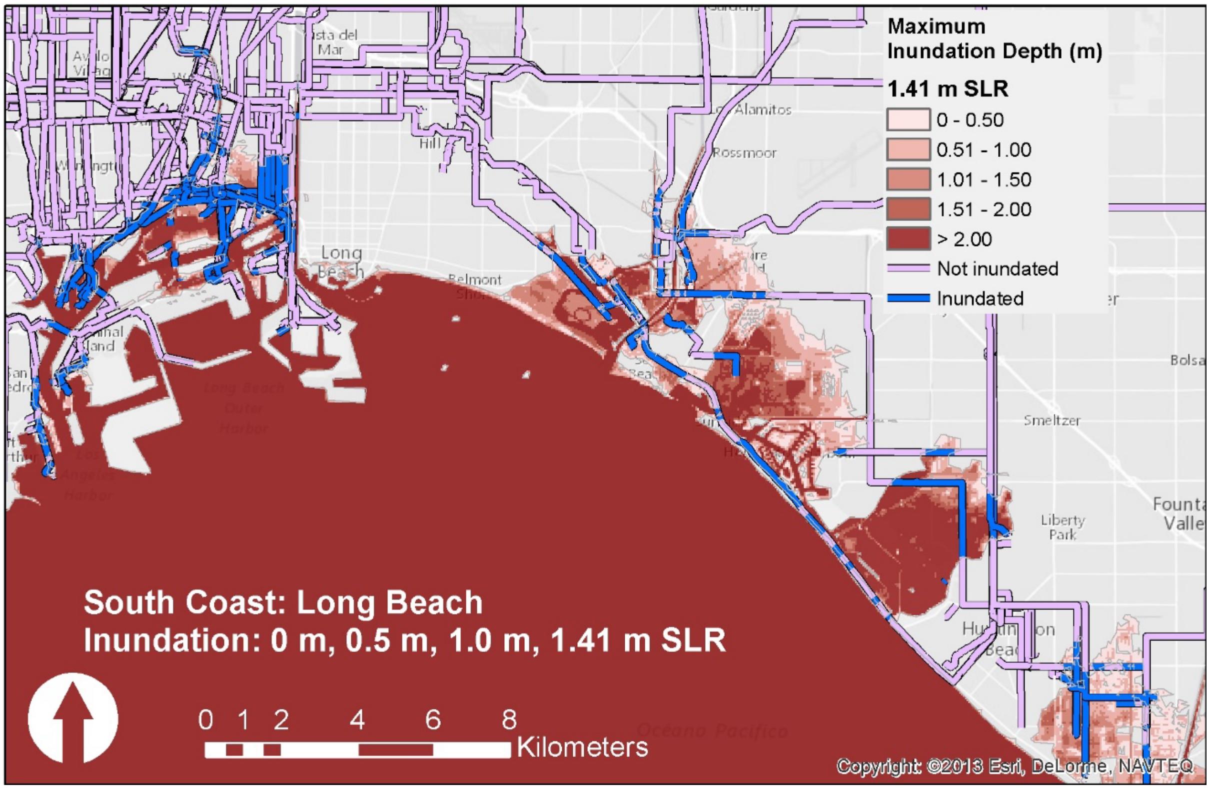


When SLR = 1.41 meters combined with a NESE100.

**Figure 35: San Diego Bay – Maximum Extent of Pipelines Inundated**

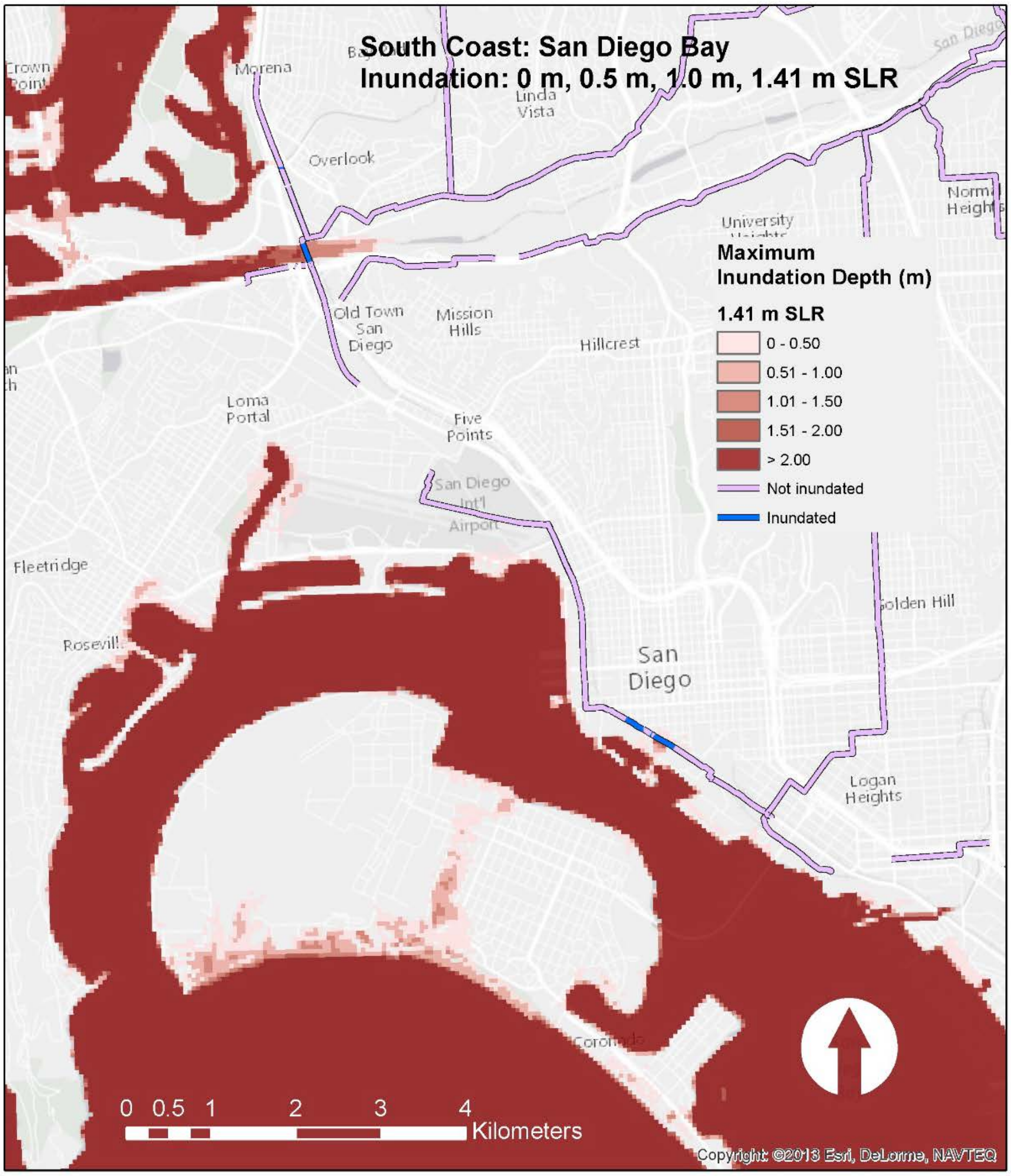


When SLR = 1.41 meters combined with a NESE100.

## 4.2 Preliminary Cost Estimation

### 4.2.1 Summary of PG&E Preliminary Research Results – Bay-Delta Region

As noted in Section 4.1.3, 308 km (191 mi) of PG&E transmission pipeline may be at risk of inundation It should not be assumed that each of those kilometers is of equal criticality to the systemwide operations of PG&E's natural gas transmission. That determination should be made by PG&E's Risk Management groups who analyze the effects of inundated pipeline on their entire pipeline network. Because of the nature of these systems, researchers emphasize the importance of ensuring that any GIS results, with respect to the impact of climate change on the State's energy infrastructure, should be worked on collaboratively with the utilities and companies responsible for the actual operation of that infrastructure.

For example, PG&E's staff responsible for its family of natural gas transmission assets reviewed the worst-case scenario of 1.41m of SLR coupled with a near 100-year storm event. Based on their preliminary interpretation of the model's GIS database and its inundation results, they found that approximately 58 kilometers (36 miles) of transmission pipeline, along with 97 stations and 477 valves, will be at levels of threat requiring specific interventions in the face of projected higher sea level and storm surge.

According to PG&E, this affected pipeline length represents approximately 0.5% of their more than 10,863 km (6,750 mile) natural gas transmission pipeline system (PG&E Corporation 2015 Report on Form 10-K, page 17). Of this length, a small albeit critical part of PG&E's transmission pipeline backbone will be covered (e.g., related to the Western Delta's Sherman Island), with other transmission assets localized to newly inundated segments within the San Francisco, San Jose and Sacramento transmission load areas. PG&E staff estimates the potential annual cost of transmission infrastructure upgrades induced by the worst-case scenario of 1.41m of SLR coupled with a near 100-year storm event would be between $4 and $7 million in 2015 dollars, an amount that includes environmental costs due to new work in wetlands at the upper end of the range. A number of assumptions have been made in order to compute these initial results and are discussed further below.

In light of these considerations and from a reliability (systemwide) perspective, the worst-case scenario appears to pose a long-term threat to the PG&E transmission assets at risk of inundation. Based on the initial analysis and discussions, the scenario does not seem to pose on its own a catastrophic threat to the natural gas transmission system as managed by PG&E, most notably the backbone system running from the north to the south of California and for the most part located inland. The worst-case scenario, however, raises concerns over potential impacts on the distribution and storage assets in PG&E's natural gas system at risk of being inundated late in the century when SLR may reach 1.41m, but that is not the subject of this research.

A major implication to be generalized from this research is the high-quality GIS based model used in the analysis of this worst-case scenario enabled finer-grain distinctions with respect to threats to natural gas transmission assets than is often the case. Most climate change models assume catastrophic impacts on infrastructures generally. Fortunately, the same high-quality GIS model and risk analysis approach could be applied to the other energy assets outside the current research and in need of similar fine‑grained threat assessment in light of projected inundation.

#### 4.2.1.1 Results in Detail

Based on this review of the worst‑case scenario of 1.41m of SLR coupled with a near 100 year storm event, PG&E identified four types of transmission pipeline mitigations that may be undertaken in the future: approximately 37 km (23 mi) of transmission pipeline may need to be replaced and secured with a concrete coating, approximately 19 km (12 mi) may need to be anchored in place with concrete footings, less than 1 km (0.6 mi) of pipeline may need to be deactivated and less than 1 km (0.6 mi) of pipeline may need no action required. Some of the potentially impacted pipeline segments include existing above−ground transmission assets not flooded under the worst−case scenario and below−ground assets already stabilized for negative buoyancy issues or otherwise unaffected by the projected rising water level.

The worst‑case scenario assumes that all soil would be eroded above the pipelines, causing negative buoyancy and the need to stabilize the pipelines. Most of the affected transmission pipe is in the North Bay region of the PG&E service area.

Today's cost of the mitigation efforts would be between $4 and $7 million annually based on a preliminary estimate by PG&E. The upper end of the range assumes a worst case estimate of approximately $20 million per mile of 24" pipe that would have to be replaced and secured through excavation in environmentally sensitive areas, such as wetlands; smaller diameter pipes would entail lower costs. The range of costs also includes a preliminary estimate of approximately $250,000 annually related to mitigations involving valves and stations important for the transmission system in the affected area.

It is important to clarify what this $4 to $7 million figure does not include. It does not include any estimated cost of the worst‑case scenario of 1.41m of SLR coupled with a near 100-year storm event on PG&E natural gas assets other than those of transmission.

The estimated cost also does not include any costs that would be induced by natural gas impacts on other infrastructures interconnected with natural gas transmission, such as electricity. For example, if the 1.41m SLR coupled with a near 100-year storm event were to occur sooner than projected such that SLR in 2100 would exceed 1.41 m, this would impact many other critical infrastructures (transportation, telecommunications, and others not identified in this research), whether interconnected or not with the natural gas infrastructure. The fact that the research team did not report on such potential impacts does not imply any judgment about whether those impacts would be catastrophic or not. Rather the evaluation of impacts induced by regional climate change above and beyond those for the natural gas infrastructure falls outside the terms of the current research.

Finally, the preliminary cost figures do not include any damage of sensitive ecosystems in the inundated areas unrelated to actual PG&E corrective measures. The "damage due to inundation" of interest in this study has two primary parts: the preliminary economic costs that may be incurred by the transmission infrastructure with inundation in the affected area and the environmental costs any mitigation actions may have on sensitive ecosystems. The first part centered on the potential economic costs incurred in mitigations of affected transmission system assets, while the second part included the environmental impact costs that follow from these mitigations. In other words, the key indicator of projected pipeline damage is the economic cost of the projected upgrade, where the upgrade itself might have environmental consequences that entail additional costs. As such, excluded from this analysis are any independent impacts and costs induced by rising sea levels and storm surges on the sensitive ecosystems and non-gas infrastructure such as buildings unrelated to the damage just defined.

The results of this study will inform PG&E's ongoing efforts to better understand, plan for, and respond to climate change risks. PG&E's recent Climate Change Vulnerability Assessment (2016) highlights PG&E's approach to addressing changing climate conditions.

#### *4.2.1.2 Major Assumptions Underlying Research Results*

Just as the research team imposed a number of assumptions in developing the GIS database and scenarios for climate change-induced SLR and storm surge, their research partner, PG&E natural gas transmission operations, made assumptions in undertaking the initial analysis and interpretation of those GIS results.

To increase the usefulness of the research for their own operations, PG&E selected the worst-case scenario from those offered, namely, the 1.41m SLR coupled with a near 100-year storm event. The conservative strategy of focusing on the worst case enable both us and PG&E to assess what would be the maximum potential direct impact on the utility's natural gas transmission system as currently known and at risk of inundation. To ensure the worst-case baseline, it was also assumed that PG&E would have no new resources and improvements above and beyond what they have now and are planned for when it comes to addressing the impacts of climate change such as flooding, erosion and landslides. In particular, PG&E assumed for computation purposes: 1) no change in current operating structure (e.g., operating pressures and flows remain the same and service needs remain the same); 2) no change in pipeline maintenance and inspection requirements; 3) all the soil over inundated segments of pipe would erode (due to tidal flows); 4) cost of materials and labor remain the same; and 5) all facilities can be accessed for maintenance. (When it came to computing costs, it is also assumed that the replaced pipe will be coated with concrete, while the affected pipe segments not replaced would be secured with concrete footings.)

From these high-end assumptions follow important secondary implications for the analysis of the high-end scenario: Current patterns of settlement (residential, commercial, industrial, infrastructural) remain the same; the regulatory regime stays constant; labor and construction costs are at 2015 prices (thereby avoiding discounting of hypothetical infrastructural initiatives over a 100-year "investment period"); and PG&E's current mitigation programs and planning processes in natural gas operations continue to be suitable vehicles for undertaking the new work required by realization of the high-end scenario. In other words, without adding any further layers of complexity, no other major disasters, such as earthquakes, are assumed to occur in the relevant time period.

When it comes to that time period, it is important to note that PG&E's primary planning and investment horizon for its natural gas assets is a five-year cycle with longer-term major infrastructure investments planned out in a few cases 12-15 years ahead. That said, the major impacts of rising sea levels and storm surges—floods, landsides, soil erosion—all have ongoing mitigation programs for PG&E natural gas asset families that can be adjusted to respond to these added impacts induced by longer-term climate change as and when needed.

### 4.2.2 Estimates for the Rest of California

Without knowing how the other natural gas systems with coastal assets are actually operated as systems, any extrapolation of the preceding PG&E figures requires extreme caution and demands skepticism. Gross estimation for the coast could be done by using population density for the Bay Area as approximately 7 million divided by the cost of damage and then estimate based solely on population density along the California Coast. An alternative method could employ the percent of coastal pipeline affected in the Bay-Delta region and apply these rates to coastal pipeline systems. Whatever the case, any such gross extrapolation will have to account for the fact that in the Bay-Delta region, much of the relevant natural gas infrastructure has been built into the Bay or Delta physiographic subregions and not along or adjacent to the Pacific Ocean proper.

Any such back-of-the-envelope extrapolations would produce extremely rough figures that are at best placeholders for further analysis. Additional research would be needed to address, minimally, the degree to which flooding and inundated coastal assets represent chokepoints in their respective system operations. Although the team's California Coast inundation modeling was not at the spatial resolution of that in the Bay and Delta, it is believed the results for the coast provide a valuable estimate of the amount of pipeline at risk to inundation over the four SLR simulations coupled with a near 100-year storm event.

# CHAPTER 5: Conclusion and Discussion

The motivation behind this research came from the flood damage caused by Hurricane Katrina to the natural gas transmission systems in the New Orleans region. Widespread flooding inundated the natural gas pipeline systems with salt-and-brackish water and lead to the pipeline system owner replacing 486 km (302 mi) of pipeline out of concern for damage due to corrosion. With this in mind, researchers set out to model and predict how much gas-pipeline might be at risk to an extreme storm surge today, and how much would be at risk in the future with a rise in sea-level resulting from climate change.

## 5.1 Conclusion

Developing a better natural gas pipeline impact forecast through improved sea-level rise and storm surge modeling will help California produce more realistic mitigation plans and infrastructure management strategies.

- The research team's integrative modeling techniques produced a better and very high-resolution surface model of the San Francisco Bay, Sacramento-San Joaquin Delta, and the coast of California. For the Bay-Delta this model includes objects that might impede or deflect very localized water movements produced in a storm surge.
- The team began the search and assessment of hydrologic models by 1) looking at the current literature and by 2) acquiring access to and testing three credible models in use today.
- After a rigorous testing schedule, researchers eliminated SOBEK[29] and Delft3D[30], as they could not meet the key demands of the study —a very high spatial resolution and a single simulation covering large regions. Researchers adopted and introduced 3Di, a hydrodynamic model that simulates the entire tidal cycle and has the ability to model a very large region at a very high spatial resolution due to its sophisticated quadtree based data compression technology.
- Researchers assembled and processed very high resolution data for vast regions of California. Taking on such a voluminous amount of data and simulations brings its own set of computational challenges. Researchers employed a tiling strategy to reduce the

[29] SOBEK is a powerful modelling suite for flood forecasting, optimization of drainage systems, control of irrigation systems, sewer overflow design, river morphology, salt intrusion and surface water quality. https://www.deltares.nl/en/software/sobek/

[30] Delft3D is Open Source Software and an integrated modelling suite, that simulates two-dimensional (in either the horizontal or a vertical plane) and three-dimensional flow, sediment transport and morphology, waves, water quality and ecology and is capable of handling the interactions between these processes. http://oss.deltares.nl/web/delft3d

total number of high resolution cells in each simulation in order to process the 3D hydrodynamic model and maintain high spatial resolution. In building a more accurate model, researchers incorporated objects on the ground surface that impede and deflect water during a storm surge. To include these objects in the model, a very high horizontal spatial resolution surface with many cells (rasters) is necessary to compute. For example, an average tile contains a total of 194,770,966 1m$^2$ cells, more than it is possible to compute in one simulation. If each cell's horizontal spatial resolution is reduced by a factor of four, and the objects on the surface that impede and deflect water are still included, then the simulation will contain 12,175,746 4m$^2$ cells, which is still more cells than it is possible to compute in one simulation.

- 3Di's quad tree compression technology allows for further reduction of the number of cells to 97,825 4m$^2$ cells in this example, with the remaining 11 million plus cells being much larger than 4m$^2$. It is now possible to compute each tile over a 72-hour period in one simulation. Thus, by retaining high spatial scale only where it is really needed, researchers were able to manage simulating over the entire coastal region of California.
- Rather than model theoretical 100-year storm events, researchers chose real near 100-year storm events so that they could take advantage of gauging station data throughout the event. This strategy allowed for effective calibration of the hydrodynamic model, producing more realistic predictions. These peak water levels measured with gauging stations during the near 100-year storms formed a base upon which to add sea level increments forecast with climate change models.
- Researchers expanded the scope of their research beyond earlier studies to include all coastal regions in California: the San Francisco Bay, the Sacramento - San Joaquin Delta, and the Pacific Coast of California.
- Under a nondisclosure agreement, the research team partnered with a major gas-pipeline operator (PG&E) to obtain direct feedback and preliminary cost estimates based on the flood inundation predictions. From early meetings with PG&E, researchers learned that a concern for them—in the face of the high-end scenario—is less the risk of failure due to corrosion than the risk to pipelines caused by the weight of the water on the landscape during and after a storm surge. With the NDA in place, researchers were able to share the results of the worst-case scenario of 1.41m of SLR coupled with a near 100-year storm event for the Bay and Delta regions with the PG&E staff responsible for its natural gas transmission assets. From this, PGE staffs were able to estimate the amount of transmission gas pipeline that they would have to implement adaptation strategies, and they produced strategies and cost estimates of that adaptation.
- Finally, since decomposing peat soils in the Delta islands are the main cause of subsidence, and since the Delta is mainly comprised of these peat soils, most of the islands in the Delta are currently well below sea level. The inundation modeling of the Delta region shows that when individual island levees are overtopped and breached during an extreme storm event, the islands, being well below sea level, quickly and

completely become flooded. As it will likely take several months to repair and pump dry a flooded island[31], the island-levee phenomenon exacerbates the risk to gas pipelines and their restoration.

### 5.1.1 Length of Pipelines Inundated

The Bay-Delta simulations predict that with a near 100-year storm event and no sea-level rise, approximately 124 km (77 mi) of NPMS documented transmission pipelines are inundated. For the combined 16 pipeline operators in the Bay-Delta region, this inundation almost doubles to approximately 225 km (140 mi) with a $SLR_{0.5}$ and almost doubles again to approximately 413 km (257 mi) at a $SLR_{1.0}$. Finally with a $SLR_{1.41}$ the amount of inundated pipeline increases approximately 1.5 times to approximately 633 km (393 mi).

The California coastal simulations predict that with a near 100-year storm event and no sea-level rise, approximately 56 km (35 mi) of NPMS documented transmission pipelines are inundated. For the combined pipeline operators (between 32-38 different companies) on the California coast, this inundation more than doubles to approximately 137 km (85 mi) with a $SLR_{0.5}$ and increases almost 1.5 times to approximately 195 km (121 mi) at a $SLR_{1.0}$. Finally with a $SLR_{1.41}$ the amount of inundated pipelines again increases 1.5 times to approximately 278 km (173 mi).

### 5.1.2 Recap of PG&E Results

During a near 100-year storm event with no sea-level rise, approximately 41 km (26 miles) of PG&E's transmission pipelines are predicted to be inundated. This more than doubles to approximately 96 km (60 miles) with a $SLR_{0.5}$ and doubles again to approximately 193 km (120 miles) at a $SLR_{1.0}$ .

Finally with a $SLR_{1.41}$ the amount of inundated PG&E pipeline increases 1.6 times to approximately 308 km (191 miles). However, regarding the depth of the inundation, a simulated $SLR_{1.0}$ is found to inundate only approximately 28 km (17 miles) of transmission pipeline to a peak water level (PWL) of more than 2.5 meters and much less, approximately 5 km (3 miles) of more than 3.5 meter PWLs. Therefore, although the extent of pipeline inundated is substantial, the amount experiencing deep PWLs is quite small. A simulated $SLR_{1.41}$ exposes approximately 53 km (33 miles) of pipeline to PWLs of more than 2.5 meters and approximately 30 km (18 miles) to PWLs of more than 3.5 meters.

As a result, even if a near 100-year storm event may be considered catastrophic for some infrastructure, it may not have a catastrophic effect on natural gas pipeline infrastructure. From a reliability (systemwide) perspective, the worst-case scenario of 1.41m sea-level rise with storm surges poses a long-term threat to the PG&E transmission assets. PG&E made a preliminary estimate that the annual cost of natural gas transmission upgrade may be approximately $4 to $7 million and that only about 37 km (23 mi) of transmission pipeline may

---

[31] From personal communication with Sonny Fong (DWR) the pumping dry of an island the size of Sherman Island could take well beyond 6 months.

need to be replaced and secured with a concrete coating. In addition, approximately another additional 19 km (12 mi) may need to be anchored in place with concrete footings, and less than 1 km (0.6 mi) of pipeline may need to be deactivated. Therefore, the $SLR_{1.41} + NESE_{100}$ scenario does not pose a catastrophic threat to the natural gas transmission system as managed by PG&E.

The high-end scenario, however, raises concerns over its potential impacts on the distribution and storage assets in PG&E's natural gas system as well as on infrastructures interconnected with the natural gas system, including but not limited to electricity, transportation and telecommunications. Whether these later impacts would likely be catastrophic or not is beyond the scope of this research.

### 5.1.3 Recap of Value of Research Team's model

Researchers were challenged to build a model that was dynamic, predicting storm surge throughout storm events, while maintaining very high spatial resolution surfaces where details, such as objects[32] would deflect water during a storm surge. This challenge also included building the model for the San Francisco Bay, the Sacramento - San Joaquin Delta, and the coast of California. The team met the challenge to better forecast storm surge inundation by building more accurate surface models as input to a dynamic 3D hydrologic model in which water levels were populated and calibrated using 6-minute interval water level data from numerous gauging stations throughout the study region during real near 100 year storm events.

Researchers built an unprecedented $1m^2$ raster surface model of San Francisco Bay, the Sacramento - San Joaquin Delta, and the coast of California by integrating the best publically available bathymetric data with the latest land surface elevation data from the National Elevation Dataset, and enhancing their output with the latest LiDAR data from numerous coastal projects. Researchers added the footprints of objects on the surface that will impede or deflect the flow of water during a storm surge to this dataset. These include levee structures, building footprints, and other artifacts with considerable size to influence the flow of water.

Similar to other climate changes studies modeling sea level rise, the team chose SLR iterations in 0.5m increments save for the final iteration that stops at 1.41m by 2100 as forecasted by Cayan et al., 2012.

## 5.2 Discussion

This study took a considerable amount of time to compute on no less than 6 very powerful multi processor computers. The resultant very high-resolution surface data model has considerable utility for modeling inundation scenarios into the future. The inundation or flooding results have considerable utility for modeling other infrastructures at risk due to sea level rise and storm surge.

---

[32] For the most part buildings, walls or levees that could deflect or impede water flow.

### 5.2.1 How to Use This Data in the Future

In this study, researchers produced a good baseline that should be informative for quite some time due to the following factors:

- Climate change scenarios can be adjusted, and SLR iterations reassessed.
- Scalability at 3-5m horizontal resolution that is adequate for property leveldecisions (which take into account significant infrastructure [objects on the landscape] that may affect water-flow and inundation impacts).
- A more extensive analysis is possible. If the research team had time and knew how to display a dynamic event on static paper, they could show water movement over the cell and apply this to a specific area of focus (such aswater passing a gauging station).
- For gas-pipeline operators to undertake a modeling effort like this on their own, practically and on a regional basis, they could greatly benefit from mature data acquisition procedures and software systems. To take on a systemwide regional area for analysis, is a major challenge with regard to data acquisition, quality control, analysis and synthesis.

### 5.2.2 How to Prepare for Future Infrastructure Costs

Future costs for infrastructure exist in the redesign, rebuild and repair of the system, all of which have a price tag attached. Strategic Planning often leads to proactive mitigation strategies that almost always lead to more cost effective adjustments or changes to infrastructure. Several issues arise regarding securing funds to address adjustments to the gas-pipeline infrastructure:

- How do we ensure that the funds to cover future infrastructure needs are available?
- What role does the California Energy Commission, the California Public Utilities Commission (CPUC), and operators play in saving capital for future action?
- The research team's estimates are in present day dollars. This means the cost/value will likely change significantly as actual steps are taken at a later dates (10, 20, 50, 100 years from present).

### 5.2.3 In the Future It Would Be Best To

The research team concludes that even with great advances in surface model accuracy, three-dimensional dynamic modeling of water flows, and employing real gauge station data over the duration of an extreme storm event, better data could always be used to obtain better results.

- Even with the many gauging stations used, more information on water monitoring, especially the contribution of river run-off (water flowing from dams, through gates, and being pumped into the central valley and beyond), and run-off from elsewhere in study area, could help produce better results.
- Even with the many gauging stations used, more gauging stations could be used to better calibrate the model and to reduce the number of pseudo or virtual station data needed to populate the individual tile simulations.

Better information on the current Delta water management system, more information on the projected changes to the system, and a better risk assessment of the Delta island levee stability could help determine if some islands would fail before overtopping occurs.

Integrating the results of other climate change studies could change inundation prediction scenarios. For example, the islands of the Delta are protected by a system of earthen levees and the susceptibility of these levees to failure due to high-water overtopping is related to rates of vertical land motion and SLR combined. Brooks and Manjunath (2012) calculate Delta-wide vertical land motion rates using satellite-based synthetic aperture radar interferometry (InSAR) and global positioning system (GPS) data. They find general subsidence rates in the Delta of approximately 1-2 millimeters per year (mm/yr) and use twenty-first century sea-level rise predictions to project when, assuming subsidence continues at this rate, Delta levees will fall below high-water design thresholds.[33]

Brooks and Manjunath (2012) assume that SLR in the Delta will not significantly differ from global estimates, and follow the Vermeer and Rahmstorf's semi-empirical methodology relating sea level to global temperature change (Vermeer and Rahmstorf 2009) to project twenty-first century SLR. They use Vermeer and Rahmstorf's (2009) projection of a 1–1.9 m SLR by 2100 as a maximum SLR scenario and Vermeer and Rahmstorf's (2007) projection of a 0.5–1.4 m SLR by 2100 as a minimum SLR scenario. They conclude that under the minimum SLR scenario, by approximately 2050 the first levees will have subsided below design thresholds and by approximately 2075 more than 90 percent of the levees will have done so (Brooks and Manjunath 2012). Under their maximum SLR scenario they find that the first levees will have subsided below design thresholds by approximately 2035 and more than 90 percent will have done so by approximately 2065.

Thus, overtopping of Delta levees resulting from levee subsidence combined with future sea-level rise may begin to pose a substantial and increasing threat to levee integrity sooner than current results indicate (i.e. sooner than the year 2050).

[33]Although levee design standards in the Delta are variable, Brooks and Manjunath (2012) use as a consistent high-water design standard the Federal target requirement that levees have approximately 0.5 m (1.5 ft.) freeboard above the 100-year flood stage.

# GLOSSARY

| Term | Definition |
|---|---|
| BGE | Baltimore Gas and Electric Company |
| CCLP | California Costal LiDAR Project |
| CDFW | California Department of Fish and Wildlife |
| CEC | California Energy Commission |
| CLICK | Center for LIDAR Information Coordination and Knowledge |
| CPUC | California Public Utilities Commission |
| DEM | Digital elevation model |
| DSM | Digital surface model |
| DWR | California Department of Water Resources |
| EEZ | Exclusive Economic Zone |
| ESRI | Environmental Systems Research Institute |
| GCMs | Global Climate Models |
| GIS | Geographic information systems |
| GMT | Greenwich Mean Time |
| GPS | Global Positioning System |
| IDW | Inverse distance weighting |
| InSAR | Synthetic Aperture Radar Interferometry |
| IPCC | Intergovernmental Panel on Climate Change |
| LiDAR | Light Detection and Ranging |
| MHHW | Mean higher high water |
| MLLW | Mean lower low water |
| MLW | Mean low water |
| MSL | Mean sealevel |
| MWLx | Mean water level |
| NASA | National Aeronautics and Space Administration's |

| | |
|---|---|
| NAVD 88 | North American Vertical Datum of 1988 |
| NDA | Non-disclosure agreement |
| NED | National Elevation Dataset |
| $NESE_{100}$ | Near 100-year storm event |
| NGVD29 | National Geodetic Vertical Datum 29 |
| NOAA | National Oceanic and Atmospheric Adminsitration |
| NOI | Oceanic Niño Index |
| NPMS | National Pipeline Mapping System |
| NTGS | NOAA Tide Gauging Stations |
| PG&E | Pacific Gas and Electric Company |
| PHMSA | Pipeline and Hazardous Materials Safety Administration |
| PST | Pacific Standard Time |
| PWL | Peak Water Level |
| QA/QC | quality assurance / quality control |
| $R^2$ | Coefficient of determination |
| SLR | Sea-level rise |
| TNO/DUT | Defence, Security and Safety/Delft University of Technology |
| U.S.E.D. | United States Engineering Datum |
| US GAO | United States Government Accountability Office |
| USACE | US Army Corps of Engineers |
| USGS | United States Geologic Survey |
| UTM | Universal Transverse Mercator |
| WDL | Water Data Library |
| WSEs | Water surface elevations |

# REFERENCES

After Katrina, New Orleans Gas Rebuild Ahead of Pace. (2009). *Pipeline & Gas Journal*, *236*(12). Retrieved from http://www.pipelineandgasjournal.com/after-katrina-new-orleans-gas-rebuild-ahead-pace

Bahr, E. (2007). Pipeline purge: Entergy New Orleans to replace 844 corroding gas conduits. *New Orleans CityBusiness*. Retrieved from http://www.highbeam.com/doc/1P2-9649283.html

Barnard, P.L., van Ormondt, M., Erikson, L.H., Eshleman, J., Hapke, C., Ruggiero, P., Adams, P. N., and Foxgrover, A. (2014). Development of the Coastal Storm Modeling System (CoSMoS) for predicting the impact of storms on high-energy, active-margin coasts *Natural Hazards* 74(2) 1095-1125. Retrieved fromhttp://link.springer.com/article/10.1007%2Fs11069-014-1236-y

BGE. (2015). Storms, Floods and Natural Gas Outages. Retrieved from http://www.bge.com/safetyreliability/reliability/stormsoutages/currentoutages/pages/gas-outages.aspx

Biging, G., Radke, J. D., & Lee, J. H. (2012). *Impacts of Predicted Sea-Level Rise and Extreme Storm Events on the Transportation Infrastructure in the San Francisco Bay Region* (No. CEC-500-2012-040). California Energy Commission. Retrieved from http://www.energy.ca.gov/2012publications/CEC-500-2012-040/CEC-500-2012-040.pdf

Bromirski, P. D., Cayan, D. R., Graham, N., Flick, R. E., Tyree, M., & Scripps Institution of Oceanography. (2012). *Coastal Flooding Potential Projections: 2000–2100* (No. CEC-500-2012-011). California Energy Commission. Retrieved from http://www.energy.ca.gov/2012publications/CEC-500-2012-011/CEC-500-2012-011.pdf

Bromirski, P. D., & Flick, R. E. (2008). Storm surge in the San Francisco Bay/Delta and nearby coastal locations. *Shore & Beach*, *76*(3), 29–37.

Brooks, B. A., and Manjunath, D. (2012). *Twenty-First Century Levee Overtopping Projections from InSAR-Derived Subsidence Rates in the Sacramento-San Joaquin Delta, California: 2006–2010.* California Energy Commission. No. CEC-500-2012-018. Retrieved from http://www.energy.ca.gov/2012publications/CEC-500-2012-018/CEC-500-2012-018.pdf

California Coastal Conservancy. (2009 - 2011) Coastal Lidar Project

http://coast.noaa.gov/dataservices/Metadata/TransformMetadata?u=http://coast.noaa.gov/htdata/lidar1_z/geoid12a/data/1124/2010_California_Coastal_metadata.xml&f=html

California Department of Fish and Wildlife. (2007). Marine Region GIS Unit: Downloads. Retrieved from ftp://ftp.dfg.ca.gov/R7_MR/BATHYMETRY/

California Energy Commission. (2014). California Natural Gas Data and Statistics. Retrieved from http://energyalmanac.ca.gov/naturalgas/

Casulli, V. and Stelling, G. S. (2011), Semi-implicit subgrid modelling of three-dimensional free-surface flows. Int. J. Numer. Meth. Fluids, 67: 441–449

Casulli, V. and Stelling, G. S. (2013), A semi-implicit numerical model for urban drainage systems. Int. J. Numer. Meth. Fluids, 73: 600–61

Cayan, D. R., Bromirski, P. D., Hayhoe, K., Tyree, M., Dettinger, M. D., & Flick, R. E. (2008). Climate change projections of sea level extremes along the California coast. *Climatic Change*, *87*(S1), 57–73. http://doi.org/10.1007/s10584-007-9376-7

Cayan, D., Tyree, M., Pierce, D., & Das, T. (2012). *Climate Change and Sea-level rise Scenarios for California Vulnerability and Adaptation Assessment* (No. CEC-500-2012-008). Scripps Institiution of Oceanography: California Energy Commission. Retrieved from http://www.energy.ca.gov/2012publications/CEC-500-2012-008/CEC-500-2012-008.pdf

California Department of Fish and Wildlife. "Marine Region GIS Unit: Downloads," 2007. ftp://ftp.dfg.ca.gov/R7_MR/BATHYMETRY/.

California Department of Water Resources. (2008). *Delta Risk Management Strategy (DRMS) Phase 1 Technical Memorandum: Topical Area: Flood Hazard Final.* Prepared by URS Corporation / Jack R. Benjamin and Associates, Inc. p.28

Cheng F., and Venetsanopoulos, A.N. (1991). "Adaptive Morphological Operators, Fast Algorithms and their Applications" *Pattem Recognition* 33 (2000) 917-933

Climate Prediction Center - Monitoring & Data: ENSO Impacts on the U.S. - Previous Events. (n.d.). Retrieved September 28, 2014, from http://www.cpc.ncep.noaa.gov/products/analysis_monitoring/ensostuff/ensoyears.shtml

Coastal Lidar Project Metadata for "2009 - 2011 CA Coastal Conservancy Coastal Lidar Project: Hydro-flattened Bare Earth DEM"

http://coast.noaa.gov/dataservices/Metadata/TransformMetadata?u=http://coast.noaa.gov/data/Documents/Metadata/Imagery/harvest/ca2010_coastal_dem.xml&f=html

California Climate Action Team (CO-CAT). (2013). *State of California Sea-Level Rise Guidance Document*. Retrieved from http://www.opc.ca.gov/webmaster/ftp/pdf/docs/2013_SLR_Guidance_Update_FINAL1.pdf

Clark, E.B., Battelle, B.N.L. & Eiber, R.J. (2004). *Integrity Characteristics of Vintage Pipelines*. F-2002--50435 Copyright ® 2005 by The INGAA Foundation, Inc. Retrieved from

http://primis.phmsa.dot.gov/gasimp/docs/integritycharacteristicsofvintagepipelineslbcover.pdf

Dahm, R., Hsu, C.-T., Lien, H.-C., Chang, C.-H., & Prinsen, G. (2014). Next Generation Flood Modelling using 3Di: A Case Study in Taiwan. Presented at the DSD International Conference, Hong Kong. Retrieved from http://www.dsdic2014.hk/abstract/Paper (A5-3).pdf

DRMS. (2008). *Technical Memorandum: Delta Risk Management Strategy (DRMS) Phase 1 Topical Area: Levee Vulnerability Final*. Prepared by URS Corporation / Jack R. Benjamin and Associates, Inc.

DWR. (2010). "DWR LiDAR (1m, 2007)." *Dudas, 2010*

http://baydeltaoffice.water.ca.gov/modeling/deltamodeling/modelingdata/DEM.cfm

Eldredge, T. J. (2011). *Local Vertical Datum Conversion, NAVD vs. NGVD*. Eldredge Surveying & Engineering. Retrieved from http://proceedings.esri.com/library/userconf/survey11/papers/pap_3235.pdf

Entergy. (2015). Rebuild Project Status Map. Retrieved from http://www.entergy-neworleans.com/content/gas_rebuild/Gas_Rebuild.pdf

ESRI, DigitalGlobe, GeoEye, i-cubed, USDA, USGS, … GIS User Community. (2014). *ESRI World Imagery (MapServer)*. Retrieved from http://www.arcgis.com/home/item.html?id=c1c2090ed8594e0193194b750d0d5f83

Federal Code: 49 CFR Part 192.327. Retrieved from https://www.law.cornell.edu/cfr/text/49/192.327

Fessler, R.R. (2008). *Pipeline Corrosion: Final Report* (No.DTRS56-02-D-70036). United States Department of Transportation Pipeline and Hazardous Materials Saftey Administration. Retrieved from http://primis.phmsa.dot.gov/iim/docstr/finalreport_pipelinecorrosion.pdf.

Flick, R. E., Chadwick, D. B., Briscoe, J., & Harper, K. C. (2012) "Flooding" versus "inundation." *Eos Trans.* AGU 93(38) 365.

Folga, S. M. (2007). *Natural Gas Pipeline Technology Overview* (No. ANL/EVS/TM/08-5). Argonne National Laboratory. Retrieved from http://corridoreis.anl.gov/documents/docs/technical/APT_61034_EVS_TM_08_5.pdf

Foxgrover, A., Smith, R. E., and Jaffe, B. E. (2003) " Suisun Bay and Delta Bathymetry (10m, 2005)", United States Geological Survey

http://sfbay.wr.usgs.gov/sediment/delta/downloads.html

Fugro Earthdata, Inc., "Task Order 014 Final Report: Sacramento-San Joaquin Delta Lidar" November 2009.

Fugro EarthData, Inc. "Coastal California LiDAR; Classified LiDAR Point Cloud Data," October 20, 2011. http://coast.noaa.gov/dataviewer/webfiles/metadata/ca2010_coastal_dem.html?redirect=301ocm - 2.

Gokhale, S., & Rahman, S. (2008). *Pipelines 2008: Pipeline Asset Management, Maximizing Performance of Our Pipeline*. ASCE Publications.

Harris, S. P. & Wilson, D. O. (2008). Mitigating Hurricane storm surge perils at the DeLisle Plant. *Proc. Safety Prog.* 27: 177–184.

Heberger, M., Cooley, H., Herrera, P., Gleick, P., & Moore, E. (2009). *The impacts of sea-level rise on the California coast* (No. CEC-500-2009-024-F). Retrieved from http://mtcweb1.mtc.ca.gov/planning/climate/sea_level_report.pdf

Hug, C., Krzystek, P., and Fuchs, W. (2004). "Advanced Lidar Data Processing With Lastools". *IAPRS*, 35, Part B, pp. 832

Isenburg, M. (2013). *LASTOOLS: Software for rapid converting, filtering, viewing, gridding, and compressing of LiDAR*. Retrieved from http://www.cs.unc.edu/~isenburg/lastools/

Kennedy, R., Bauer, S., Brathwaite, L., Puglia, P., Gonzales, J., & Anderson, K. (2014). *2013 Natural Gas Issues, Trends, and Outlook Final Staff Report* (No. CEC-200-2014-001-SF). California Energy Commission. Retrieved from http://www.energy.ca.gov/2014publications/CEC-200-2014-001/CEC-200-2014-001-SF.pdf

Kiefner, J.F, & Rosenfeld, M.J. (2012). *The Role of Pipeline Age in Pipeline Safety.* Final Report No. 2012.04, INGAA Foundation, Inc. Retrieved from http://www.ingaa.org/file.aspx?id=19307

Knowles, N. (2009). *Potential inundation due to rising sea levels in the San Francisco Bay region* (No. CEC-500-2009-023-F). California Energy Commission. Retrieved from http://www.energy.ca.gov/2009publications/CEC-500-2009-023/CEC-500-2009-023-D.PDF

Leiss, W. (2014). "Keynote: Identifying and Portraying Risk for the Public", *Conference on Calculating Risk and Its Influence on Public Policy*, University of Calgary (June 23-24), Calgary, Alberta

Luiijf, E., Nieuwenhuijs, A. H., Klaver, M. H. A., van Eeten, M. J. G., & Cruz, E. (2008). *Empirical findings on critical infrastructure dependencies in Europe*. Retrieved from http://critis08.dia.uniroma3.it/pdf/CRITIS_08_40.pdf

Luiijf, E., Nieuwenhuijs, A. H., Klaver, M. H. A., van Eeten, M. J. G., & Cruz, E. (2010). Empirical findings on European critical infrastructure dependencies. *International Journal of Systems Engineering*, *2*(1), 3–18.

Mcleod, E., Poulter, B., Hinkel, J., Reyes, E., & Salm, R. (2010). Sea-level rise impact models and environmental conservation: A review of models and their applications. *Ocean & Coastal Management*, *53*(9), 507–517. http://doi.org/10.1016/j.ocecoaman.2010.06.009

Nakicenovic, N., & Swart, R. (2000). Special Report on Emissions Scenarios. *Special Report on Emissions Scenarios, Edited by Nebojsa Nakicenovic and Robert Swart, Pp. 612. ISBN 0521804930. Cambridge, UK: Cambridge University Press, July 2000.*, *-1*. Retrieved from http://adsabs.harvard.edu/abs/2000sres.book.....N

National Research Council (NRC). (2012). *Sea-Level Rise for the Coasts of California, Oregon, and Washington: Past, Present, and Future*. Retrieved from http://www.nap.edu/catalog.php?record_id=13389

National Transportation Saftey Board. (2014). *Marine Accident Brief: Fire on Board Towing Vessel Shanon E. Settoon*. Retrieved from http://www.ntsb.gov/investigations/AccidentReports/Reports/MAB1422.pdf

Needham, H., Brown, D., & Carter, L. (2012). *Impacts and Adaptation Options in the Gulf Coast*. Louisiana State University: Center for Climate and Energy Solutions. Retrieved from http://www.c2es.org/docUploads/gulf-coast-impacts-adaptation.pdf.

Pacific Gas and Electric Company (PG&E). (2015). *2015 Corporate Responsibility and Sustainability Report*. Retrieved from

http://www.pgecorp.com/corp_responsibility/reports/2015/business.jsp

Pacific Gas and Electric Company (PG&E). (2015) Corporation's and the Utility's Annual Reports on Form 10-K. Retrieved from

http://d1lge852tjjqow.cloudfront.net/CIK-0001004980/f370dc51-3268-435d-b586-349d583be76b.pdf?noexit=true

Pacific Gas and Electric Company (PG&E). (2016). *Climate Change Vulnerability Assessment*. Retrieved from

http://www.pgecurrents.com/wp-content/uploads/2016/02/PGE_climate_resilience.pdf

PHMSA. (2011a, December). Fact Sheet: Selective Seam Corrosion (SSC). Retrieved from http://primis.phmsa.dot.gov/comm/FactSheets/FSSelectiveSeamCorrosion.htm?nocache=717

PHMSA. (2011b, December). Fact Sheet: Transmission Pipelines. Retrieved from http://primis.phmsa.dot.gov/comm/FactSheets/FSTransmissionPipelines.htm?nocache=5866

PHMSA. (2012, October). Fact Sheet: ExxonMobil Silvertip Pipeline Crude Oil Release into the

Yellowstone River in Laurel, MT on 7/1/2011. Retrieved from

http://www.phmsa.dot.gov/staticfiles/PHMSA/DownloadableFiles/Files/Other files/ExxonMobil_HL_MT_10-2012.pdf

PHMSA. (2013). National Pipeline Mapping System. Retrieved from https://www.npms.phmsa.dot.gov/About.aspx

PHMSA. (2015a). 2013 Gas Transmission & Gathering Annual Data (ZIP). Retrieved January 15, 2015, from http://phmsa.dot.gov/staticfiles/PHMSA/DownloadableFiles/Pipeline2data/annual_gas_transmission_gathering_2013.zip

PHMSA. (2015b). Significant Incident 20 year Trend. Retrieved from http://opsweb.phmsa.dot.gov/primis_pdm/significant_inc_trend.asp

Roe, E., & Schulman, P. R. (Forthcoming). *Reliability and Risk: The Challenge of Managing Interconnected Infrastructures*. Stanford, CA: Stanford University Press.

Roe, E., & Schulman, P. R. (2008). *High Reliability Management*. Stanford, CA: Stanford University Press.

Sathaye, J., Dale, L., Fitts, G., Larsen, P., Koy, K., Lewis, S., & Lucena, A. (2011). *Estimating Risk to California Energy Infrastructure from Projected Climate Change* (No. CEC-500-2011-XXX). California Energy Commission. Retrieved from http://emp.lbl.gov/sites/all/files/lbnl-4967e.pdf

Soininen, *A.* (2012), *TerraScan* User's Guide; The National Mapping Agency of Great Britain: Southampton, UK.

Stelling, G. S. (2012). Quadtree flood simulations with sub-grid digital elevation models. *Proceedings of the ICE - Water Management*, *165*(10), 567–580. http://doi.org/10.1680/wama.12.00018

Stoms, D., Franco, G., Raitt, H., Wilhelm, S., & Grant, S. (2013). *Climate Change and the California Energy Sector* (No. CEC-100-2013-002). California Energy Commission. Retrieved from http://www.energy.ca.gov/2013publications/CEC-100-2013-002/CEC-100-2013-002.pdf

Tachikawa, Tetsushi, Manabu Kaku, Akira Iwasaki, Dean Gesch, Michael Oimoen, Zheng Zhang, Jeffery Danielson, et al. "ASTER Global Digital Elevation Model Version 2-Summary of Validation Results." NASA Land Processes Distributed Active Archive Center and the Joint Japan-US ASTER Science Team, August 31, 2011. https://lpdaacaster.cr.usgs.gov/GDEM/Summary_GDEM2_validation_report_final.pdf.

Thompson, R. (2010, September 20). Threat of gas line explosion is unlikely in Louisiana. Retrieved June 15, 2015, from http://www.nola.com/business/index.ssf/2010/09/threat_of_gas_line_explosion_i.html

Tcheslavski, G. V. (2010) *Morphological Image Processing: Gray-scale morphology.* Lamar University, Texas. Retrieved June 15, 2015, from http://www.ee.lamar.edu/gleb/dip/10-3 - Morphological Image Processing.pdf

US GAO. (2014). *Climate Change: Energy Infrastructure Risks and Adaptation Efforts* (Report to Congressionhttp://www.gao.gov/assets/670/660558.pdfal Requesters). Retrieved from http://www.gao.gov/assets/670/660558.pdf

US Army Corps of Engineers. (2011). *CalFed/Delta Islands & Levees Feasibility Study of the Sacramento - San Joaquin Delta Sea-Level Rise Analysis Using the Extended Delta EFDC Hydrodynamic Model*. Prepared by Dynamic Solutions Inc.

Van Eeten, M. J. G., Nieuwenhuijs, A. H., Luiijf, E., Klaver, M. H. A., & Cruz, E. (2011). The state and the threat of cascading failure across critical infrastructures: The implications of empirical evidence from media incident reports. *Public Administration*, *89*(2), 381–400.

Van Leeuwen, E. (2012). 10 questions to professor Guus Stelling about 3Di water managment. *Hydrolink*, *3*, 80–82.

Wang, R. & Ateljevich, E. (2012). A Continuous Surface Elevation Map for Modeling (Chapter 6).In Methodology for Flow and Salinity Estimates in the Sacramento-San Joaquin Delta and Suisun Mars, 23rd Annual Progress Report to the State Water Resources Control Board.California Department of Water Resources, Bay-Delta Office, Delta Modeling Section

Wilbanks, T. J. (2009). *Effects of Climate Change on Energy Production and Use in the United State*. DIANE Publishing. Retrieved from http://www.google.com/books?hl=en&lr=&id=KW4nl88YErcC&oi=fnd&pg=PR13&dq=related:LLTD0nWoXpvFVM:scholar.google.com/&ots=jcTmXYxoGX&sig=bg0py_TOj8EstAC8WGbizhAaKsc

Zervas, C. (2013). *Extreme water levels of the United States 1893-2010* (NOAA Technical Report No. NOS CO-OPS 067). National Oceanic and Atmospheric Administration. Retrieved from http://tidesandcurrents.noaa.gov/publications/NOAA_Technical_Report_NOS_COOPS_067a.pdf

Zimmerman, R. (2004). "Decision-making and vulnerability of critical infrastructure". Proceedings of IEEE International Conference on Systems, Man and Cybernetics, 2004: pp. 4059-4063.

# APPENDIX A:
# Elevation Surface Models

## San Francisco Bay

### *Ground Elevation Data (DEM)*

For the San Francisco Bay, we incorporate a DEM produced by Biging et al. (2012). Biging et al. (2012) obtained and processed two, high spatial resolution LiDAR data sets covering areas of the San Francisco, San Pablo, and Suisun Bays that fall north of the Bay Bridge (NOAA LiDAR) and south of the Bay Bridge (USGS LiDAR), respectively. Both data sets are collected as a part of the California Costal LiDAR Project (CCLP) and are obtained by Biging et al. (2012) from the USGS Center for LIDAR Information Coordination and Knowledge (CLICK) in LAS 1.2 point cloud format and a 1.5 km square tiled structure. The data sets are highly accurate and their vertical and horizontal projections and accuracy are presented in Table A1.

| Name | Projection | | Accuracy | |
|---|---|---|---|---|
| | vertical | Horizontal | Fundamental vertical | Horizontal |
| NOAA California Coastal LiDAR Project | NAVD88 | NAD83, UTM Zone 10N | 0.05 meters at 95% confidence level | 2.0 meters at 95% confidence level |
| USGS California Coastal LiDAR Project | NAVD88 | NAD83, UTM Zone 10N | 0.12 meters at 95% confidence level | 2.0 meters at 95% confidence level |

Table A1. Projection and Accuracy information for LiDAR Datasets used by Biging et al. (2012).

Biging et al. (2012) process the LiDAR data sets into a DEM for the San Francisco Bay Region. For the North Bay (NOAA region), they obtained 649 DEM tiles ($1m^2$ resolution) generated by NOAA from the original LiDAR point cloud dataset, along with the original LiDAR point cloud. Processing involved merging those Lidar tiles into a single DEM with $1m^2$ horizontal resolution for the entire northern region. For the South Bay (USGS region), they obtained 712 tiles of LiDAR point cloud data with a resolution of 1 point per 0.7 $m^2$ but did not receive any existing DEM tiles. Biging et al. (2012) processed the LiDAR data into a $1m^2$ horizontal resolution DEM on a tile-by-tile basis using a linear interpolation method on points representing the ground surface (those classified as Class 2 = Ground Class or Class 9 = Water Class).[34] It should be noted that in order to produce a seamless DEM from the LiDAR data,

[34] LiDAR points classified as both ground and water were used as most of the water points were mudflats (Biging et al. (2012). For the interpolation method used, a tile area is divided into 1m x 1m pixels and if a single LiDAR point is found in a pixel, its height is assigned to the pixel (Biging et al. (2012). If multiple LiDAR points exist in a pixel, then the pixel is assigned the highest height observed in that pixel, and if a

Biging et al. (2012) resampled the LiDAR points into tiles with 100m overlap on each side (1.7 $km^2$ tiles) then clipped the resulting DEM tiles back down to the original 1.5 $km^2$ tile size to prevent any edge discrepancies when merging the DEM tiles together. Biging et al. (2012) compare the techniques used to derive the DEMs for the two regions of the Bay by using the technique described for the South Bay to reproduce three tiles in the North Bay from the NOAA point cloud data, and comparing the difference between the obtained DEM and derived DEM pixel heights for those three tiles. More than 63% of the elevations are within 1.5 inches of each other and more than 90% were within 5.5. inches demonstrating a high correspondence between the two methods (Biging et al., 2012)

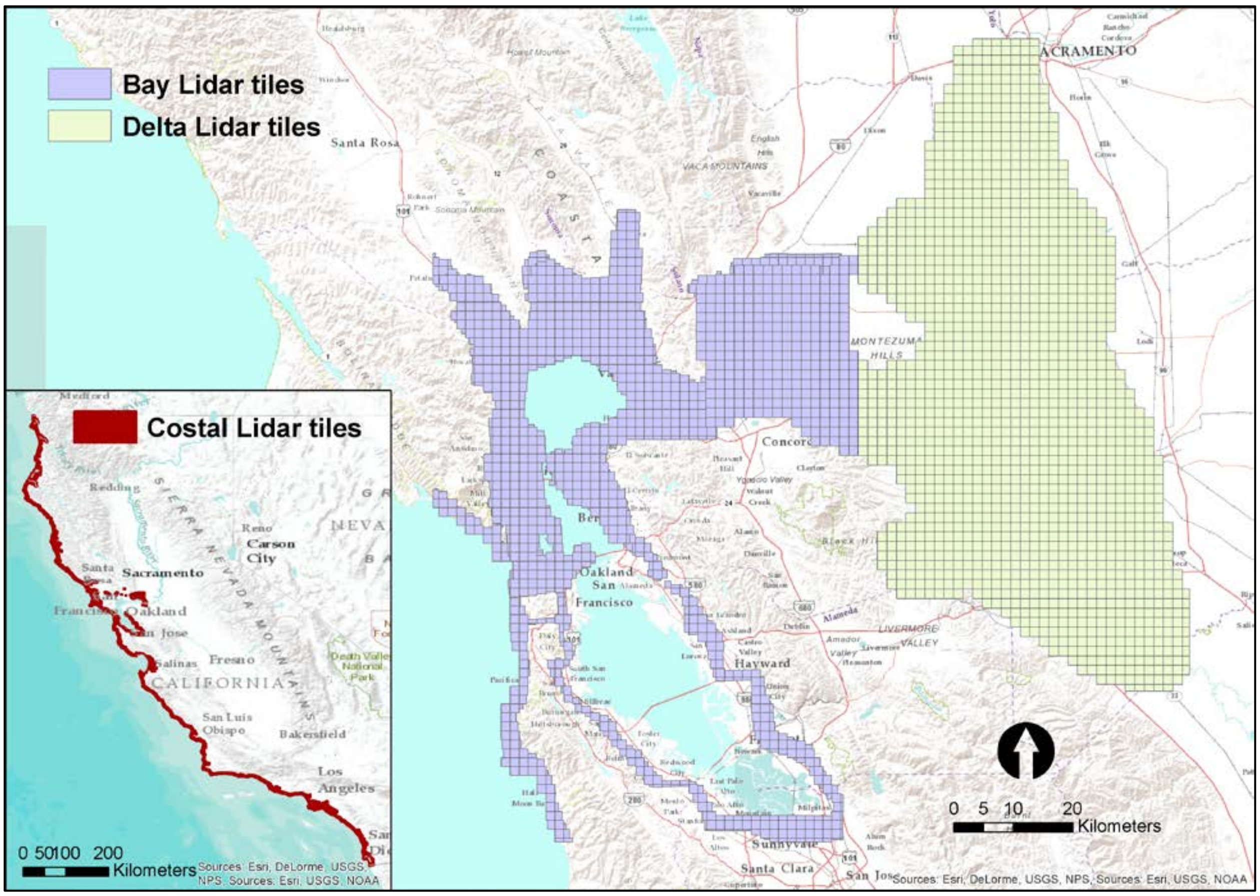


Figure A1. The Lidar tiles used in this research study containing more than 8 billion data points (x,y,z coordinates)

### *Digital Surface Model (DSM)*

Like the DEM, we use a DSM produced by Biging et al. (2012) to extract the heights of surface objects (buildings) for the San Francisco Bay region. The method used by Biging et al. (2012) to

---

pixel height is missing, it is interpolated from the heights of surrounding pixels (Biging et al. (2012).

create the DSM is similar to that used to create the DEM for the South Bay (USGS LiDAR) region, including the interpolation method and process of creating overlapping 1.7 km$^2$ LiDAR tiles then clipping the resulting DSM back down to the original 1.5 km$^2$ tile size to prevent edge discrepancies. The only difference in creating the DSM was that in order to accurately model all surface objects (not just the ground), Biging et al. (2012) use all classes of LiDAR points other than Class 7 (= noise class) when creating the DSM as opposed to only the classes representing ground and water for the DEM. Using this method, they produce a DSM with 1m$^2$ horizontal resolution for the entire Bay region, but exluding the Delta. We incorporate the DSM from Biging et al. (2012) directly into this analysis.

### *Surface Feature Height Extraction*

In order to create a land model containing features or objects assumed likely to play a significant role in diverting inundation, such as buildings, we use vector-based object (building) footprints to extract object heights from the DSM and later merge these with the DEM and bathymetry to form the final land surface model to be inundated by our 3Di hydrodynamic model. Object footprints are polygons representing the area on the Earth's surface covered by an object (such as a building). Object footprints alone do not usually contain data indicating the elevation of the features they represent. Figure A2 provides an example of object footprints overlain on an aerial photograph of the objects they represent. One source of uncertainty in using object footprints is that they often represent the rooftop outline as opposed to the outline of the base of the object that is likely to be encountered by flooding. However, for most objects this difference is negligible and we assume the discrepancy adds little error to our analysis.

Figure A2. An example of object (building) footprints overlaid on an aerial photograph of the buildings they represent (left) and the DSM which they are used to extract heights from (right)

An enormous number of object (building) footprints would need to be obtained or derived in order to represent every object in the study region. However, for the purposes of this analysis, we do not need to represent objects well outside likely regions of flooding since the purpose of including them in the land surface model is to take into account any effects they may have on the flow of water in flooding zones. Thus, we limit the object footprints included in our analysis to areas clearly falling within either the extent of flooding modeled by Biging et al. (2012) or the extent of inundation from a run of the 3Di model with only the DEM surface buffered by 100m in the horizontal extent.

Figure A3. Extent of inundation from Biging et al. (2012) and DEM only 3Di run with 100m buffer, object (building) footprints included for this land surface model are limited to those in these extents.

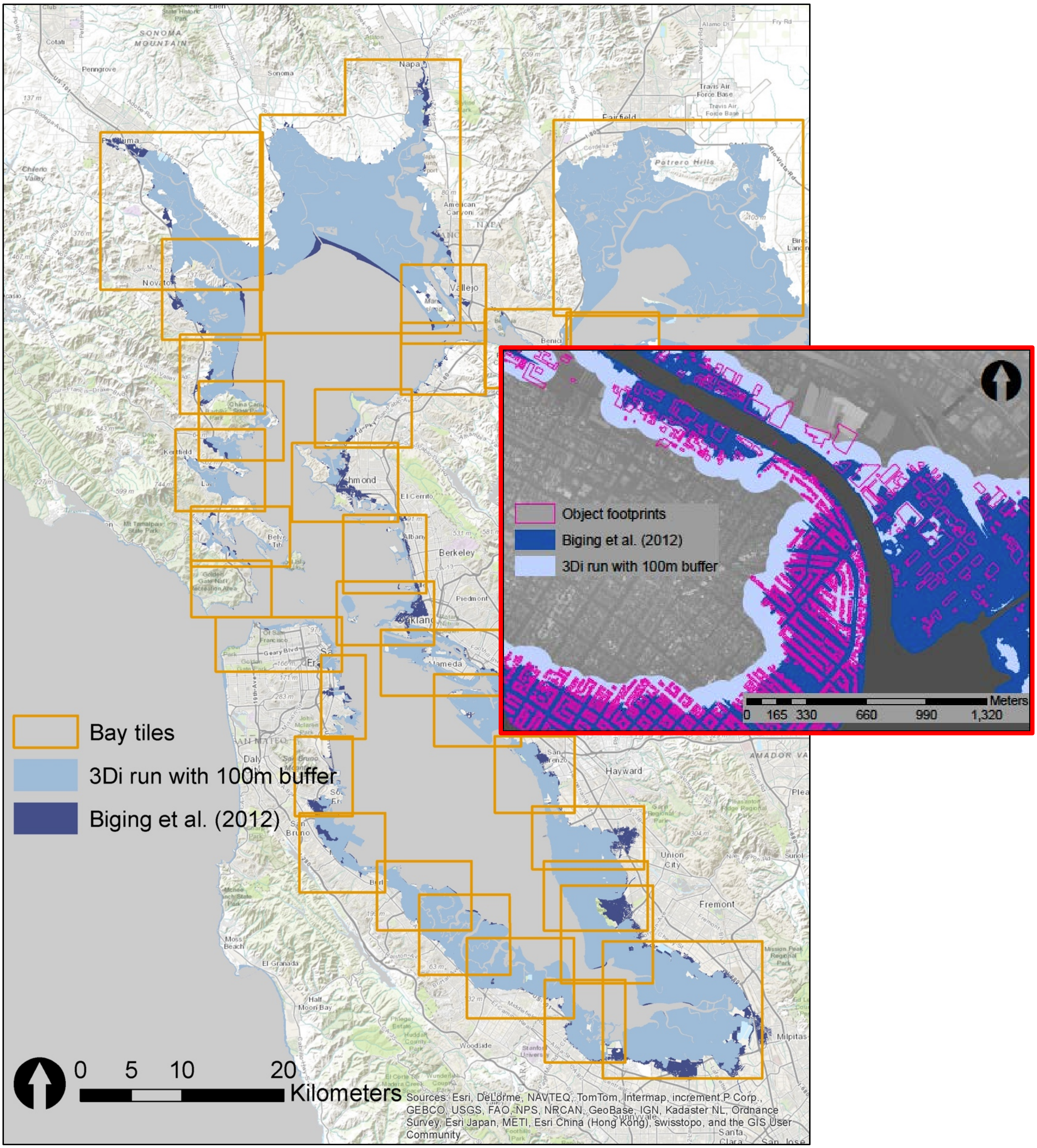

Object (building) footprints for the areas falling within the inundation extents are either obtained from existing city or county datasets, derived by automated feature extraction, or hand-digitized from orthoimagery and using the DSM for quality control purposes. Since the use of GIS by local governments has become a common practice, many city and county planning or engineering departments have datasets containing the footprints of buildings within their limits. We collected existing footprint datasets online or directly from departmental staff for all or portions of four counties (Marin, Napa, San Francisco, Sonoma) and fifteen cities (Milpitas, Oakland, Palo Alto, Menlo Park, Redwood City, San Mateo, Burlingame, Mountain View, San Jose, San Leandro, Vallejo, Belmont, Fremont, Hayward, Sunnyvale) as shown in Figure A4. We perform quality assurance / quality control (QA/QC) on the collected datasets by spot checking to evaluate if the provided footprints lined up with buildings in the DSM and an imagery base map. We keep the majority of the data, removing only the objects (buildings) corresponding to one neighborhood that no longer exists.

Figure A4. Existing object (building) footprint datasets from cities and counties in the San Francisco region.

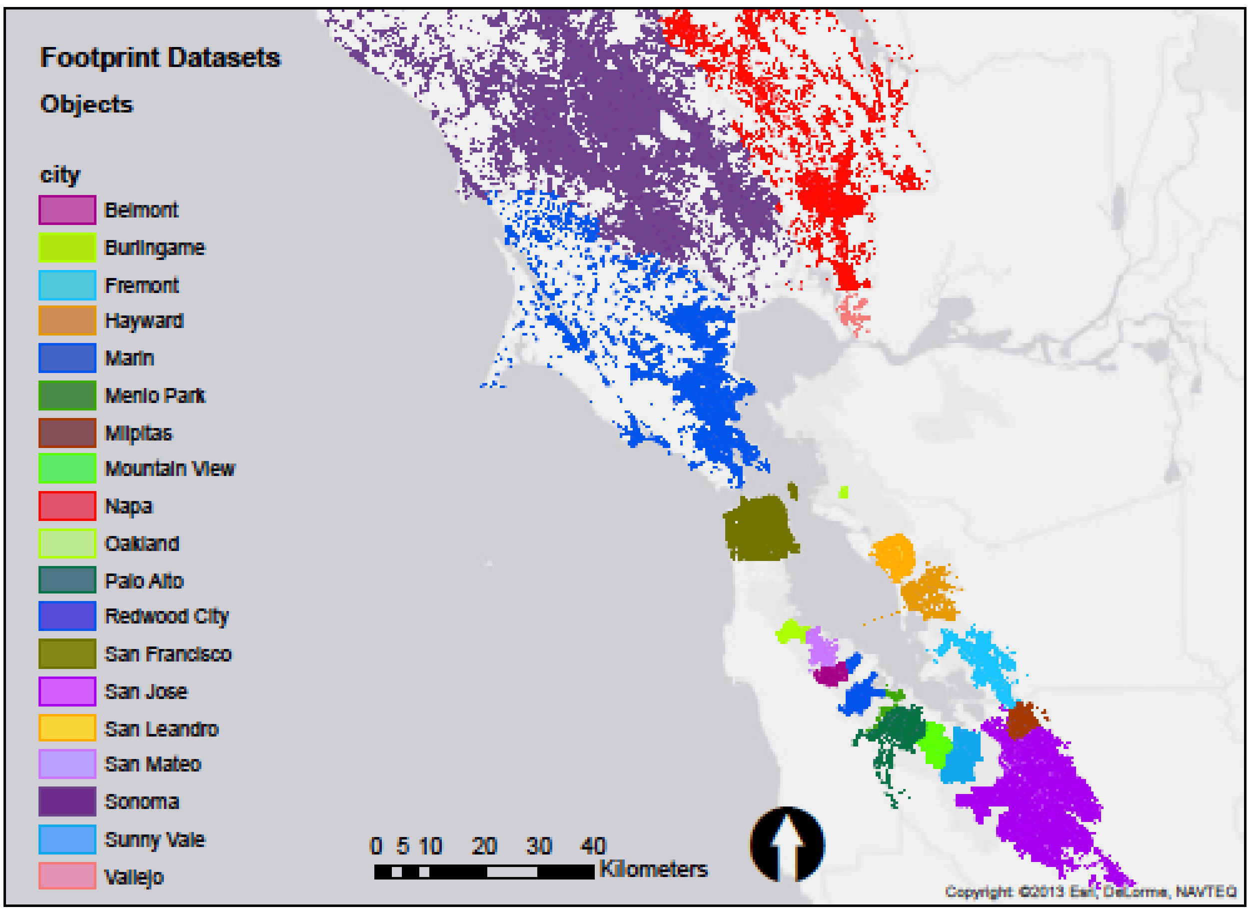

For objects (buildings) falling in the inundation extent limits that are not included in datasets obtained from outside sources, we derive footprints by automated feature extraction or hand digitizing. A majority of these data gaps are filled with footprints delineated by human interpreters of orthoimagery from Environmental Systems Research Institute (ESRI; ESRI et al., 2014). Given the large geographic extent of this study, hand-digitizing of individual objects (mostly buildings) is performed at multiple imagery resolutions depending on the size of the objects, the "closeness" of objects to each other, and the degree to which the sight line between the target object and the camera is obstructed. Hand-digitization is challenging within some portions of the inundation extent's reach, particularly in residential areas where objects tend to be small, tightly spaced, architecturally complex, masked or shaded by tree canopies, and diverse in their orientations.

We also attempted to extract object footprints directly from the LiDAR data used to construct the DSM with two tools: a trial version of Overwatch System's LIDAR Analyst for ArcGIS (vers. 5.1.2.1) and LASTools (Isenburg, 2013). In general, both tools produced inadequate results for our purposes and their outputs are used to obtain a limited number of object heights for areas that surrounded the San Francisco Bay.

Finally, we use the resulting dataset of object footprints within the inundation extent in ArcGIS as a mask to extract from the DSM produced by Biging et al. (2012) 1m$^2$ resolution raster data containing the elevation values within each object's footprint (Figure A5a). This creates a new DSM of only the object surface features (Figure A5b).

Figure A5a:

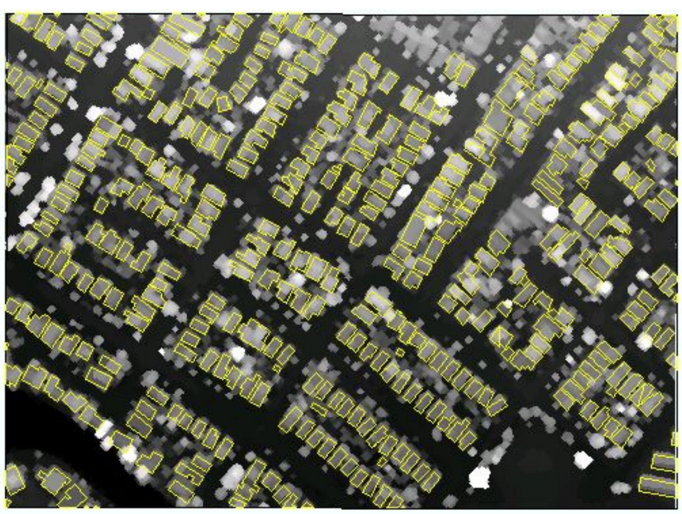

Figure A5b:

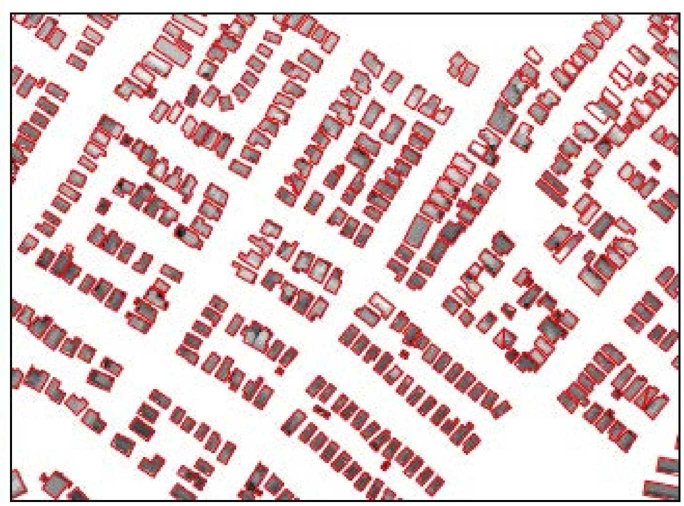

Image showing the extraction of object (building) heights from the DSM produced by Biging et al. (2012) (black to white background) using vectorized object footprint dataset (yellow outlines) for the Alameda Island region of California.

Figure A5c: DSM surface heights. This illustration is from the Alameda Island region of California.

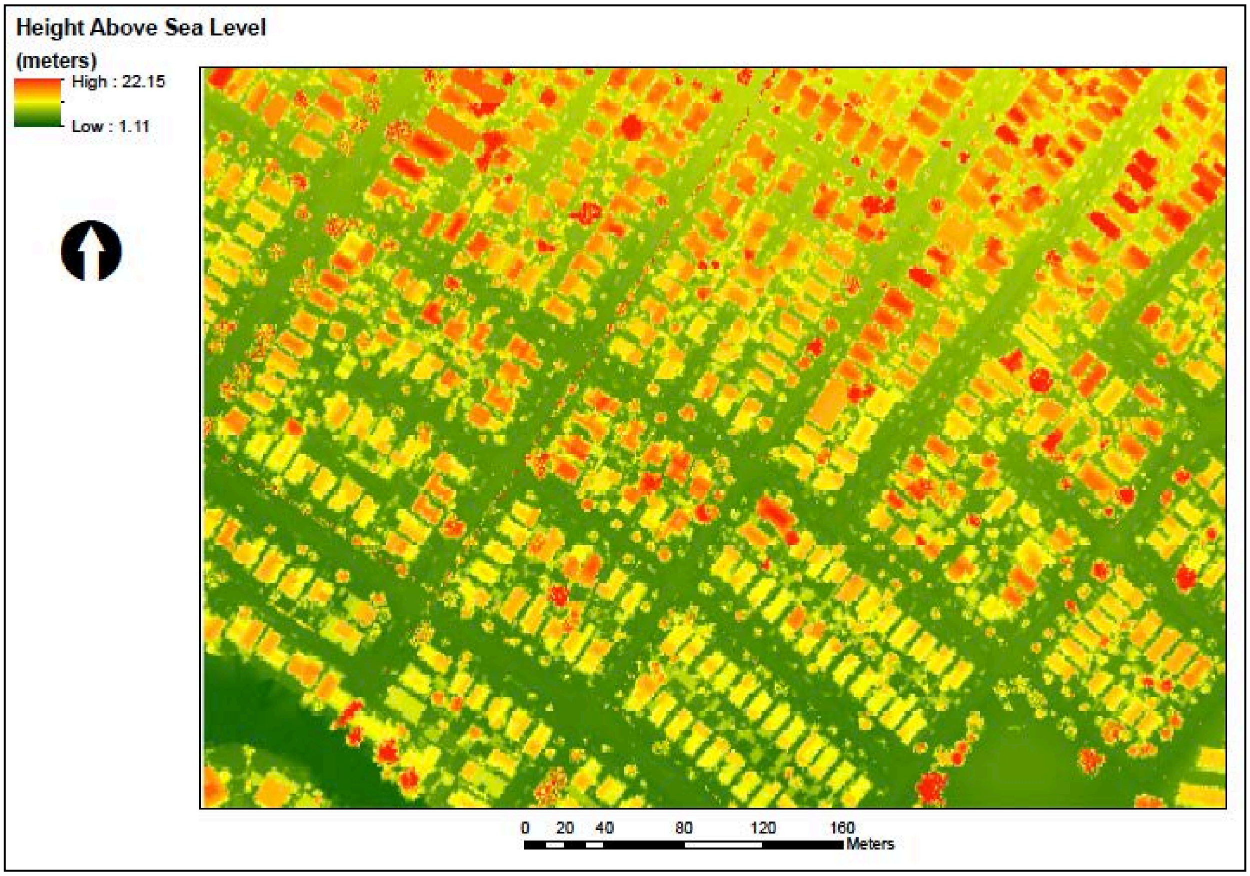


### *Final Land Surface Model*

The final land surface model for the San Francisco Bay combines the bare ground DEM, bathymetry data, and surface objects (including levees, building footprints, and other water blocking features) to represent the inundation environment.

In order to create the final land-side element of the 3Di input surface, we mosaic together in ArcGIS the object elevation raster and DEM. The resulting land-side surface is illustrated in Figure A5d with small objects such as trees removed.

Figure A5d. Combined DEM ground surface with extracted object heights to create the land-side element for the 3Di input surface. This illustration is from the Alameda Island region of California.

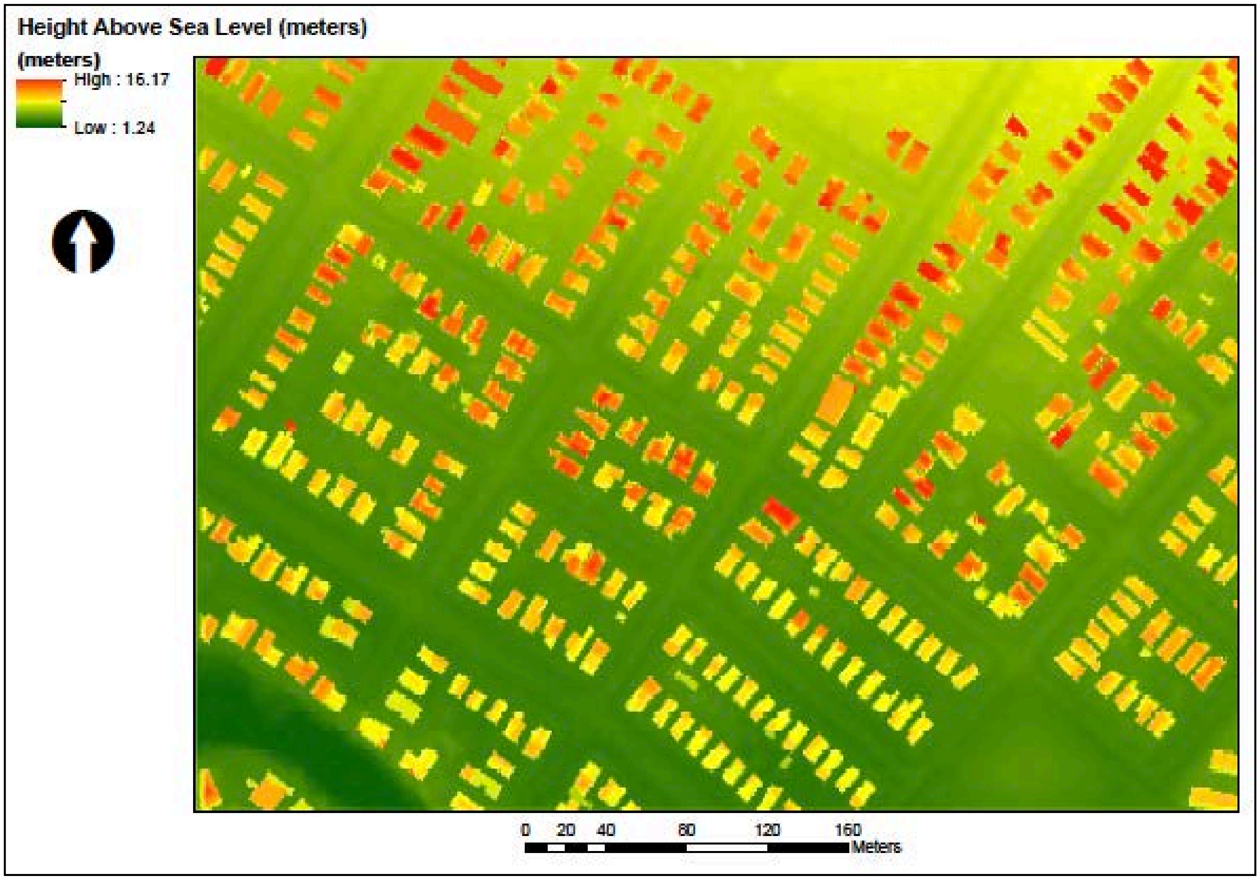


Figure A5e. 3D model of combined DEM ground surface with extracted object heights (no trees).

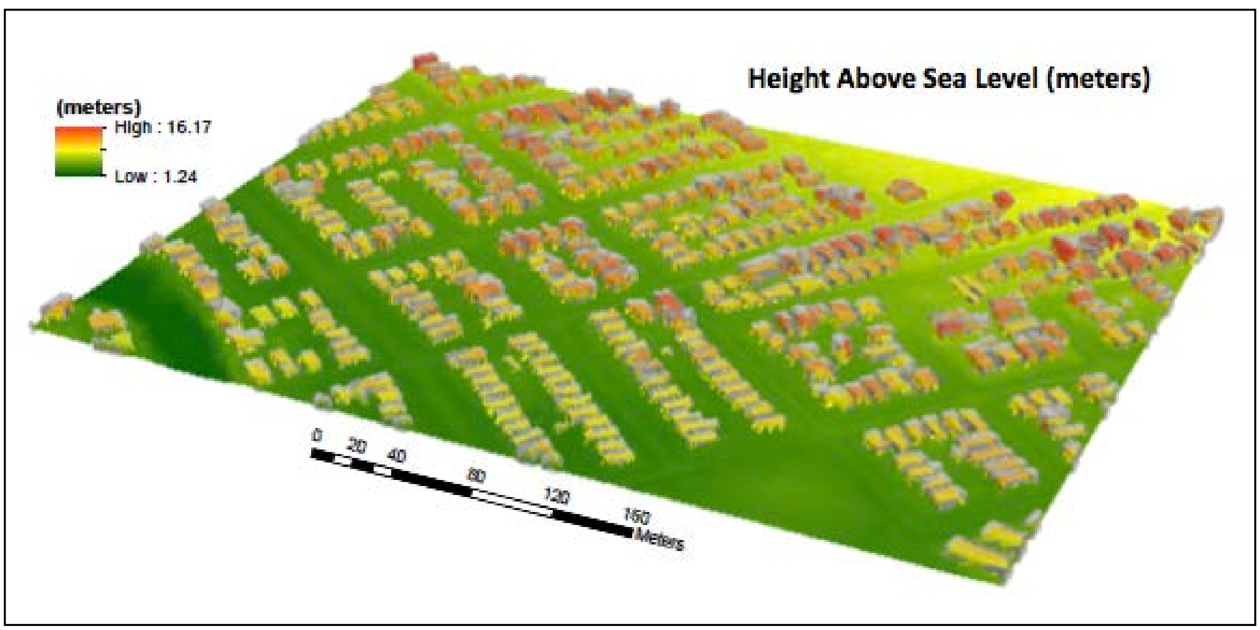

## Sacramento - San Joaquin Delta

### *Digital Elevation Model*

For the Sacramento-San Joaquin Delta (the Delta) ground surface model we downloaded and processed high spatial resolution LiDAR ground elevation data from the California Department of Water Resources (DWR). The DWR, Delta-Suisun Marsh office, commissioned the Delta LiDAR Acquisition and the Airborne 1 Corporation (CA) collected the data via aerial survey between late January and February 2007 (DWR 2010). Some areas were re-flown in February and March of 2008 to correct issues with the original flights (DWR 2010). EarthData International (later Fugro EarthData) was responsible for processing the data and Spectrum Mapping LLC was subcontracted to do QA/QC.

The derived products include raw, bare earth and first return point data clouds (in LAS format); bare earth DEMs with a horizontal resolution of $1m^2$ (in Arc interchange (e00) format); and break lines indicating areas underwater at the time of acquisition (in Esri geodatabase format). All data are registered to UTM Zone 10N, NAD83, with vertical datum NAVD88. Elevation values for the point cloud data are in meters while the grid files have elevations in decimeters. The fundamental vertical accuracy of the data was assessed as 95% at 0.6 feet (ft) and 90% at 0.5 ft, and the horizontal accuracy of the data was assessed to be within one foot (DWR 2010). However, DWR (2010) reported three known issues with the quality of the data:

1. Swath edge errors occur throughout the study area, and are sometimes as much as 3-4 inches. These are most pronounced in tiles west of Antioch.
2. Bare earth editing is inadequate in some ponded areas so LiDAR pulses hitting water are not properly excluded. Two very prominent examples are Prospect Island and Van Sickle Island.
3. There are good breaklines for the entire study area for the areas underwater at the time of data acquisition. This means that any land areas with ponding or inundated by high river flows or tides at the time of data acquisition, are assigned no data values in the dataset.

We use $1m^2$ resolution bare earth DEM tiles provided by DWR to derive the Delta region DEM for our analysis. Fugro EarthData (Fugro) generated the bare earth DEM tiles from the original LiDAR point cloud data by classifying ground points from the raw (unclassified) LiDAR data and using an interpolation method to generate DEMs from those points. They classified bare earth points using a combination of automated filtering[35] (for 90% of points) and manual

[35] Furgo EarthData (2009, p. 25) states that automated filtering was conducted using “Fugro EarthData-developed algorithms.” Presumably this refers to using the “classify ground” tools in TerraScan. This tool classifies ground points by building a triangulated irregular network (TIN) above known ground points and requires the user to set an iteration angle (maximum angle between ground points) and iteration distance (maximum distance between point and TIN surface) (Soininen, 2012). However, Fugro EarthData (2009) does not specify the value used for these parameters in classifying the Delta LiDAR data.

processing based on ancillary aerial imagery provided by DWR (for 10% of points; Fugro EarthData 2009). Fugro then used the export lattice tool in TerraScan, the LiDAR processing software used for their project, to create DEMs from the bare earth points (Fugro EarthData, 2009). This tool can generate DEMs with pixel values representing maximum, minimum, average, or triangulated heights (z values) (Soininen, 2012), however Fugro does not document the z-value method used in producing the Delta bare earth DEMs. The classified bare-earth points Figure A6 (left) and resulting DEM Figure A6 (right) from Fugro for a small region in the Delta are shown in Figure A6 color coded by elevation range.

Figure A6. Bare-earth points (Left) and resulting DEM from Fugro for a region in the Delta.


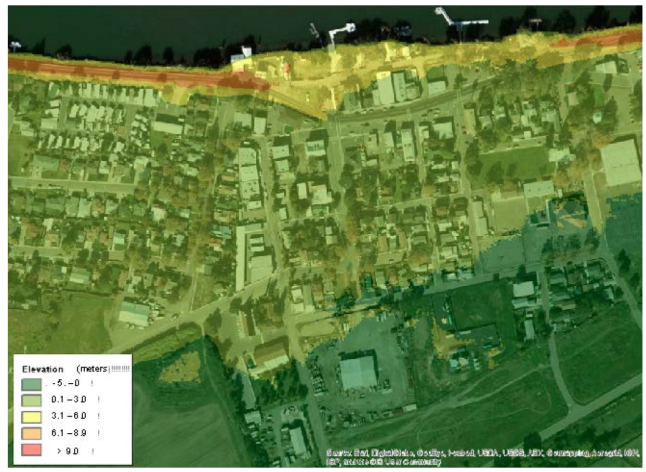


We analyze the accuracy of the bare earth classification conducted by Fugro EarthData, by classifying ground and non-ground points from the raw LiDAR data provided by DWR using the "lasground" python script (Isenburg, 2012) from the open-source LASTools. This tool uses a contour-based object detection method to parse out objects from the point cloud (Hug, Krzystek, and Fuchs 2004). Figure A7 (left) presents classified ground points from Fugro, and using the LASTools method, Figure A7 (right) for the same region. From our comparison it appears that the undocumented bare earth classification from Fugro EarthData produces reasonable results. As shown in Figure A7, the Fugro bare earth classification is more accurate and complete in classifying the levee in the upper left corner of the image as bare earth, that is important for our modeling purposes. Moreover, a visual assessment of the Fugro classified bare earth points did not reveal significant inaccuracies or misclassified points.

Figure A7. Comparison of bare earth (ground) points classified by Fugro (left) and using LASTools (right). Object heights are in meters in both images.


Fugro (DWR) Bare Earth Lidar Points


Bare Earth Lidar Points Classified with LASTools

In addition to testing the accuracy of the classification of ground points, we attempt to determine the z-value method used by Fugro to derive DEMs from the bare earth points. We create DEMs for a specific region from the classified bare earth point cloud products provided by DWR using five z-value methods in ESRI's ArcGIS similar to the potential methods Fugro could have used in TerraScan: minimum, maximum, average, interpolated value using inverse distance weighting (IDW), and interpolated values using a triangulation method. We compared the results to the bare earth DEM created by Fugro for the same region by subtracting the Fugro DEM from each of the DEMs we created and analyzing the differences. The DEM built using the triangulation method is essentially identical to the Fugro DEM with only 0.12% of cells off by more than 1cm (Figure A8) and visual inspection showed these are concentrated in ground areas under buildings. Thus, we presume Fugro used a method with high correspondence to the triangulation method in TerraScan's export lattice tool to derive Z-values for the pixels in their DEM products.

Figure A8: Histogram of the count (y-axis) of Lidar ground points by differences (in cm) between our DEM created using triangulation and the DEM from Fugro (x-axis). A total of 2,761 cells (0.12 percent) are more than 1 cm off. From inspecting the surfaces, we can determine that all of these areas are underneath buildings.

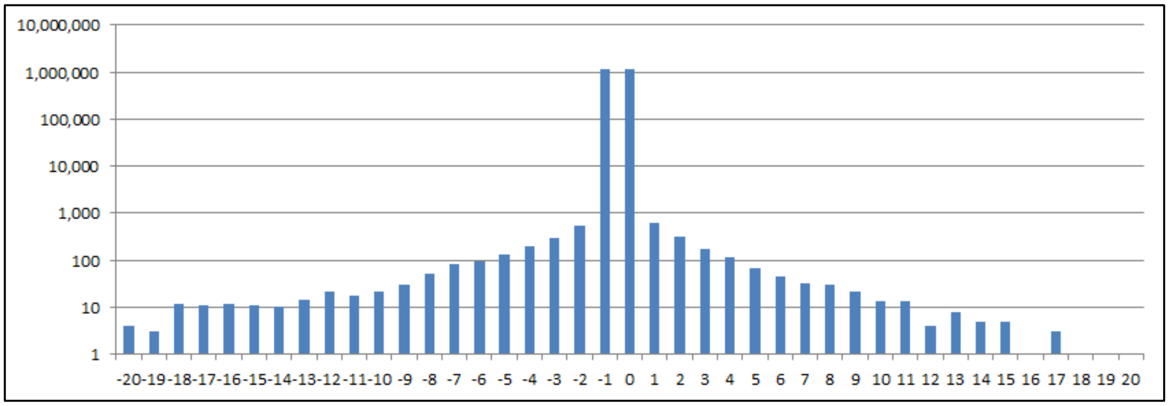


We use the DWR 1m$^2$ DEM and use an Inverse Distance Weight (IDW) interpolation algorithm to fill in the holes where Lidar was missing, likely due to water being present during scanning. In areas well above the potential flood inundation zones, where data was missing from the DWR DEM, we sampled and integrated 1/3 arc second NED data to complete the DEM surface.

### *Bathymetry Model*

We integrated bathymetry data compiled by DWR with our DEM for the Delta region. The DWR bathymetry dataset includes 10m$^2$ resolution DEM/bathymetry grids and more local 2m$^2$ resolution grids that together cover the entire San Francisco Bay/Delta region. DWR has compiled these data from a variety of sources, including the Foxgrover 10m$^2$ bathymetry (Foxgrover, Smith, & Jaffe 2003) and 1m$^2$ DWR LiDAR data (DWR 2010) in the Delta. DWR fixed errors in the transition zones between these two datasets by hand using local kernel averages over a 100m transition zone (Wang and Ateljevich 2012). Additionally, DWR reinforced some low spots in the levees that are an artifact of resampling data. This reinforcement is completed by drawing (vector) lines around levees, and taking the maximum value of the underlying 2m$^2$ resolution data for each 10m$^2$ cell (Wang and Ateljevich 2012).

In many cases, the regional and local bathymetry grids overlap one another, and we use the higher-resolution 2m$^2$ grids wherever possible. Two 10m$^2$ regional grids are used where local 2m$^2$ grids are not available. We combine all the 2m$^2$ grids together using the “Mosaic to New Raster” tool in ESRI’s ArcGIS with any overlapping cells being assigned the value of the raster that is loaded earlier into the tool (“First” mosaic operator), insuring the highest resolution data is preserved in the dataset. We resample the combined raster to a 1m$^2$ resolution using the cubic convolution resampling method to insure an accurate interpolation as specified in the ESRI documentation. We separately apply the same combination and resampling methodology to the two 10m$^2$ grids that are used and then combine the two resampled, 1m$^2$ bathymetry raster products together into one single bathymetry surface. The bathymetry values in the resulting product, originally in centimeters, are converted to meters for consistency with our elevation surfaces.

### *Digital Surface Model*

We produced a DSM for the Delta region using point cloud data from the same California Department of Water Resources' (DWR) LiDAR dataset that was used to generate the Delta DEM for this analysis. The collection, primary characteristics, and accuracy of the LiDAR dataset are described in the DEM section for the Delta region, above. While the DEM tiles are generated by Fugro using points classified as bare earth (ground surface), we use the point set of "first returns" to generate the DSM. First returns represent the first reflected signal from each laser pulse emitted during a LiDAR survey to return to the LiDAR sensor equipment and are generally associated with the highest features in a landscape such as vegetation or objects (buildings). They are appropriate for generating digital surface models of features above the ground surface. The products provided by DWR include point cloud datasets in LAS format containing only the first return points. We use this data along with ESRI's ArcGIS "LAS Dataset to Raster" tool to generate DSM rasters for the Delta region.

In order to maintain consistency across the regions modeled in this analysis, we sought to generate a DSM using methods as similar as possible to that created for the San Francisco Bay region by Biging et al. (2012). We build the DSM using the binning interpolation method, maximum cell assignment type, natural neighbor void fill method, and single-cell sampling in the "LAS Dataset to Raster" tool, followed by filtering with the "Focal Statistics" tool first using a closed filter with a circular neighborhood of 1-cell then by an *open* filter with a circular neighborhood of 2 cells.

Using this method we closely approximate the DSMs for the San Francisco region and the DWR first return LiDAR point cloud datasets for the Delta region; we generate Delta DSM grids with a horizontal resolution of $1m^2$. In general, each cell in a DSM grid represents the elevation of the LiDAR point falling within that cell. If multiple points fall within a cell, the cell represents the point with the highest elevation, and if no points fall within a cell, the cell value is interpolated from neighboring cell elevations using the nearest neighbor algorithm. In some cases, the resulting DSM rasters have gaps in areas where there are not enough elevation points to assign cell values based on the nearest neighbor algorithm (Figure A9a). We attempt to fill these voids using the linear void filling method, however the result was unsatisfactory (Figure A9b). We fill the gaps using elevation values from the Delta DEM products provided by DWR that were used to derive the DEM for this analysis (Figure A9c).

Figure A9a,b,c. Example of gaps in the original DSM (a); the same DSM with gaps filled using linear void filling (b); the same DSM with gaps filled using DEM elevation values (c).

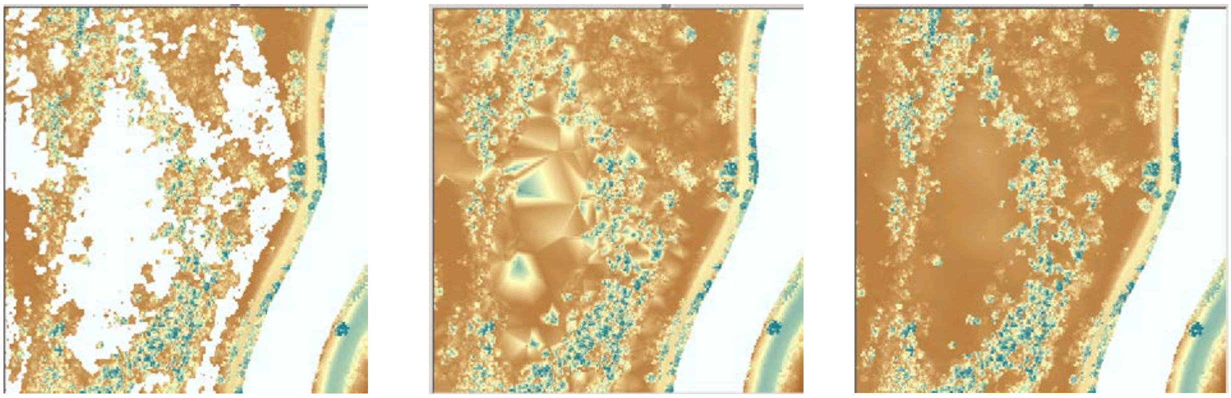

*Gaps in marshy areas with insufficient pulse density to use the natural neighbor algorithm*

*A DSM built from the same tile using the linear void filling method*

*The gaps from the first image filled using values from the DEM*

Finally, we apply morphological filtering techniques to smooth the surface of the DSMs to better approximate those created by Biging et al. (2012). We apply two separate filtering procedures. Initially, all DSM tiles are run through an original LiDAR filtering program. The program implements the open and closed filter described in Tcheslavski (2010) to highlight features of the 3D terrain. We further filter the resulting DSM outputs using ESRI's "Focal Statistics" tool with a closed filter with circular neighborhood of 1-cell followed by an open filter with circular neighborhood of 2 cells. In order to accomplish smoothing, this process combines an open filter that takes the minimum value within the neighborhood (erosion) with a closed filter that takes the maximum value within the neighborhood (dilation) (Cheng and Venetsanopoulos 1991).

### *Surface Feature Height Extraction*

Following the technique used for the San Francisco region, we use vector-based object footprints to extract object heights from the Delta DSM and later merge these with the Delta DEM and bathymetry to form the final land surface model. Similar to the object (building) extent limiting methodology, we limit the object footprints in the Delta region to areas falling within the inundation extent from a 3DI model simulation using only the DEM buffered by an additional 100 meters in the horizontal extent. The resulting buffered polygon that delineates the area of object footprint inclusion is illustrated in Figure A10.

Object footprints for the areas falling within the inundation extents are either obtained from existing datasets or hand-digitized from orthoimagery. We obtain one set of existing building footprints from the City of Stockton. As in the San Francisco region, we initially attempt to use LiDAR data and automate feature extraction with LAStools (Isenburg, 2013) to derive the remaining object footprints, but we determine that the error associated with the automated process is too great and we opt to manually digitize the remaining object footprints for the Delta's rural residential landscape.

Figure A10. The blue polygon represents the output of the 3DI simulation buffered by 100m. The red outline is the LiDAR data acquisition boundary.

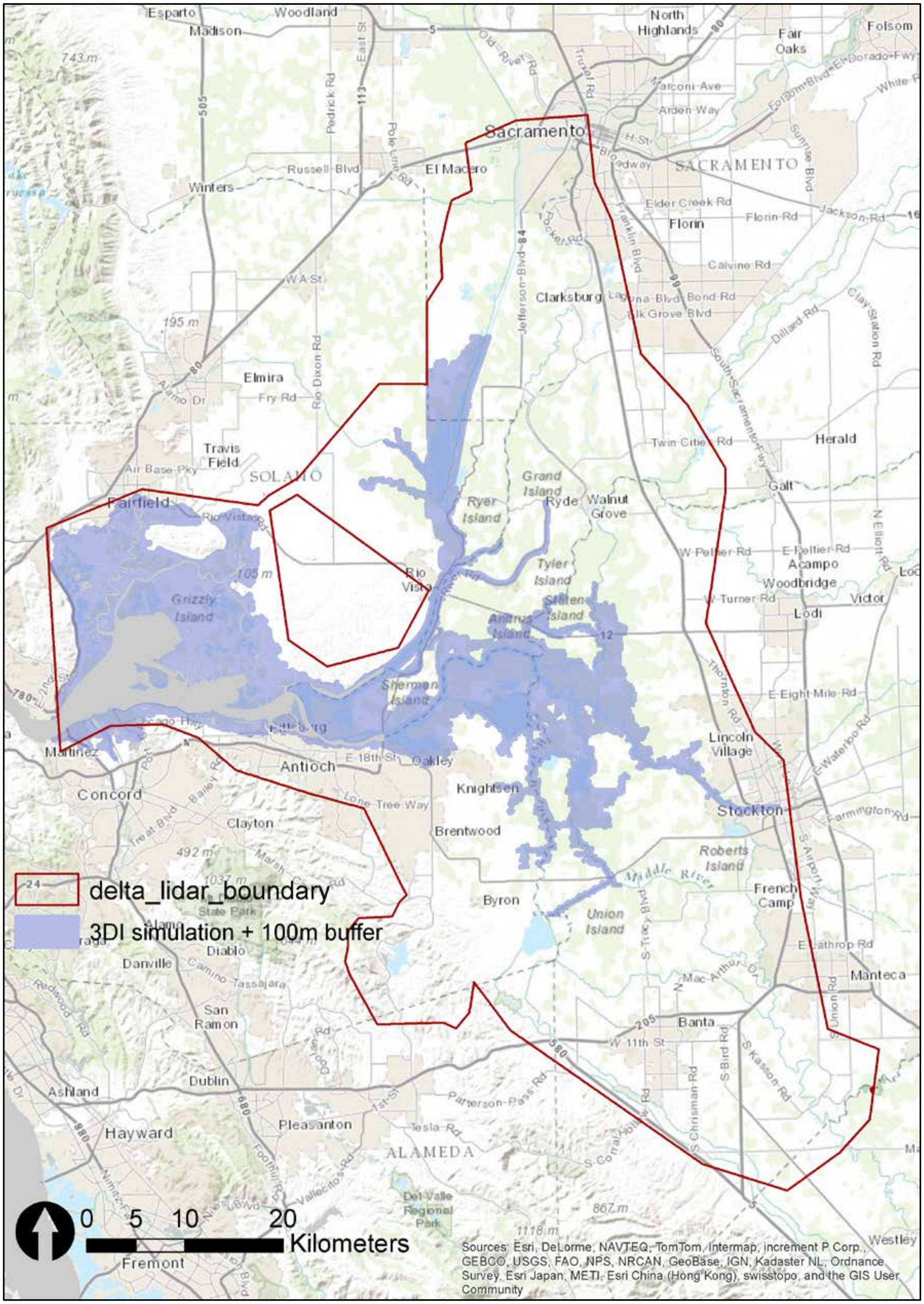

We digitize applicable object footprints within the inundation extent using ESRI orthoimagery at a scale of 1:1,500. We do not include details of the footprint, but rather draw a rectangle that best approximates the shape of the object. We draw only permanent structures (not including mobile homes and vehicles) and structures that will clearly impede the flow of water (not including canopies, or permeable structures such as electrical towers; and not including floating or cantilevered structures such as boats and docks). Figure A11 provides an example of the digitized object footprints for the Delta region.

Figure A11. An example of digitized object (building) footprints for the Delta region.

Once the object footprint vector dataset for areas within the limiting inundation extent is complete, we combine the DSM and object footprints to extract the object feature heights. We calculate the average elevation of the DSM cells within each object footprint and generate a raster representing these values using the "Zonal Statistics" tool in ArcGIS. The final object heights are generated with a cell size of $1m^2$ to facilitate combining them with the DEM and bathymetry.

### *Final Land Surface Model*

We combine (mosaic) the bare ground DEM, bathymetry data, and surface object height raster dataset to create a final land surface model representing the environment to be inundated in the Delta. Figure A12 shows the results of combining the bathymetry, bare earth DEM, and object height products.

Figure A12. The bathymetry and DEM (left), the average elevations of the DSM within each object footprint (middle), and the mosaic of the three (right).


## California Coast

The scope of our proposal and study treats the massive Coast of California at a different resolution ($50m^2$) for modeling inundation. We create surface models for the California Coast by combining two sets of ground surface elevation data (DEM) and bathymetry data. In contrast to the elevation surfaces generated for the Bay and Delta regions, we do not incorporate DSM data (i.e. extracted surface objects) along the coast given the coarse resolution at which we process it. We divide the State's coast into two zones based on the projection applicable to data for that zone: the UTM10 Zone (the northern coast) and the UTM11 Zone (the southern coast). In order to compute the entire coastline at $50m^2$, we further divide the coastline into tiles: 9 tiles in the UTM11 Zone and 24 tiles in the UTM10 zone. We use the same data processing procedure (described below) for creating the coastal elevation surface model for each tile.

### *Ground Elevation Data (DEM)*

To derive ground surface elevations for the California Coast we obtain 30m horizontal resolution DEM data in GeoTiff format and 1-degree squared tile-structure from the United States Geological Survey's (USGS) EarthExplorer database. The data was originally collected by National Aeronautics and Space Administration's (NASA) ASTER satellite in November 2011 with a horizontal projection of WGS 1984 and mean absolute vertical accuracy of 0.20m (Tachikawa et al., 2011). We merge the tiles and produce a surface for the land area along the coast.

In addition to the 30 m DEM data, we incorporate fine resolution 1-m DEM data at the immediate edge of the Coast for improved detail in areas of expected inundation. We obtained the 1m-DEM data directly from the California Coastal Conservancy (Claire O'Reilly, California Coastal Conservancy, Personal Communication, 2014) and the vertical and horizontal accuracy were reported as 18 cm and 50cm, respectively (Fugro EarthData, Inc., 2011). The DEM was derived from LiDAR collected via aerial survey between 2009 and 2011. The LiDAR dataset was processed by Fugro EarthData Inc. (2011) and NOAA performed further filtering to remove outliers from the dataset. We obtained the data in tiled format with UTM Zones 10 and 11 horizontal coordinate systems (depending on the location along the coast) and NAVD88 vertical datum.

The remotely sensed high-resolution elevation data was collected by an airborne platform (Piper Navajo twin engine aircraft) using a Light Detection and Ranging (LiDAR) sensor (a

Leica ALS60 MPiA). This LiDAR dataset is a survey that covered approximately 2616 square miles of the California Coast. The project design of the LiDAR data acquisition was developed to support a nominal post process spacing of 1 meter. Fugro EarthData, Inc. acquired 1546 flight lines in 108 lifts between October 2009 and August 2011.

### *Bathymetry Data*

We obtain 200 m bathymetry data for the entire California coast from the California Department of Fish and Wildlife (CDFW) Marine GIS Unit (2007). The bathymetry data extends from the coast to slightly beyond the 200-nautical mile exclusive economic zone and was derived from a combination of the following data sources (CDFG, 2007):

- Hydrographic Survey Data version 4.0, National Ocean Service (NOS), National Oceanic and Atmospheric Administration, U.S. Department of Commerce. Dataset name = hydsura (ESRI coverage format).
- U.S. Geological Survey bathymetric contours for the California Exclusive Economic Zone EEZ - 100m contours from 200m to maximum depth. Dataset name = eezbata (ESRI coverage format).
- 30 meter terrestrial DEM based on the National Elevation Dataset (NED), U.S. Geological Survey, U.S. Department of the Interior. Dataset name = dema (ESRI grid format).
- 1:24,000-scale State of California Coastline, State Lands Commission, State of California. Dataset name =rawclipa (ESRI coverage format).

### *Final Surface Model*

In order to create a final elevation surface model for tiles along the coast, the three data products (50 m DEM, 1 m DEM, and 200 m bathymetry were mosaicked together using the blend operator to combine overlapping cells and using the mean as the aggregation technique to a final 50m cell size using the mean operator. The resulting tiles were exported to ASCII format for processing in 3Di.

Figure A13a. An illustration of the bathymetry, the DEM and the average elevations of the DSM within each object footprint.

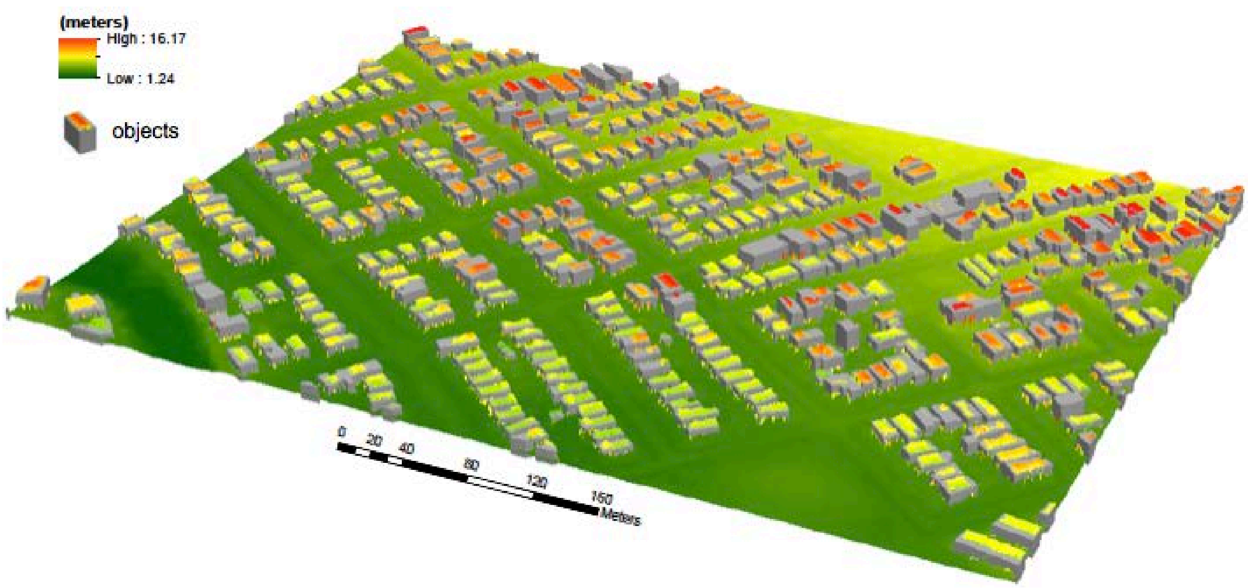


Figure A13b. 3Di simulation output $SLR_{1.41}$ + $NESE_{100}$

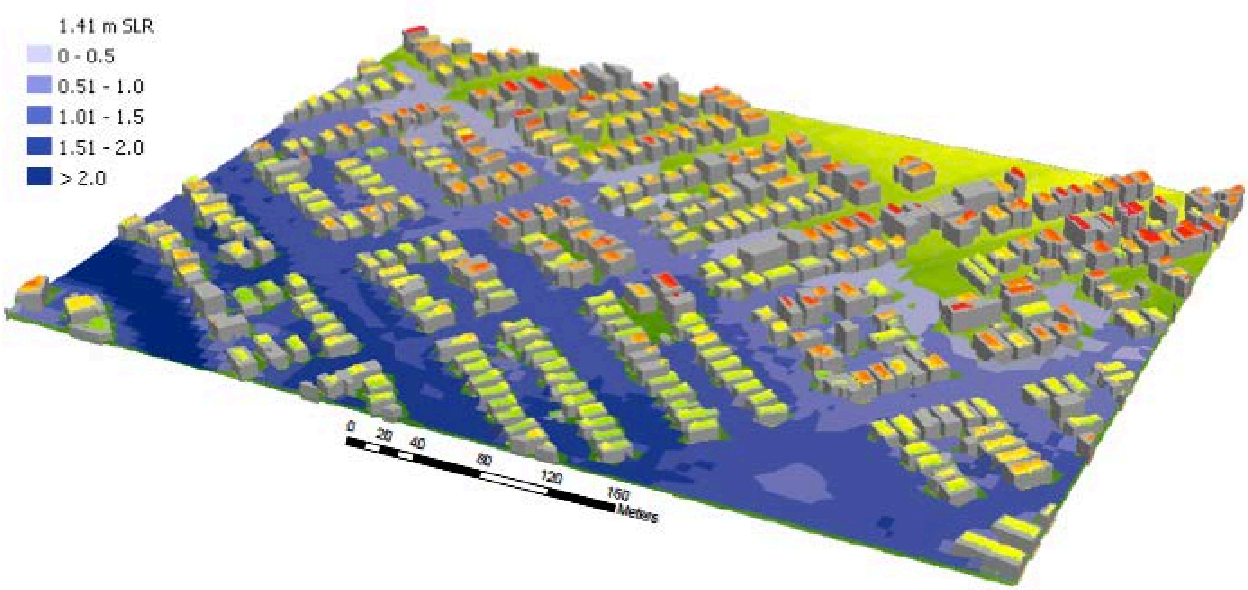

# APPENDIX B:
# Analysis and selection of Storm Event Data

### *Analysis and Selection of Storm Event Data for the Bay and Delta Regions*

Before selecting the 1998 "near 100-year" storm event, we analyzed water level data for the region to identify extreme storm events with frequent and complete water level data. A National Oceanic and Atmospheric Administration (NOAA) study of extreme water levels at 112 National Water Level Observation Network gauging stations between 1893-2010 (Zervas, 2013), noted that during that time period the network's San Francisco Station experienced two storms in 1983 where measured water levels exceeded 2.64m NAVD 88, the water level associated with a 100-year storm event. In addition, the NOAA study included one storm in 1998 where water levels measured close to 2.64m NAVD 88 (Table B1). All three events occurred during strong EI Nino years (Figure B2). Sub-hourly water level fluctuations have been recorded at numerous gauging stations within the San Francisco Bay-Delta region for long periods of time (Bromirski & Flick, 2008) and we examine all available water-level data at those gauging stations for each of the three extreme storm events identified in the NOAA report. We found the January and December 1983 events had useable data at a total of only 11 and 14 stations respectively, while the February 1998 event had useable data at 21 stations. Given the greater availability of water level data for the 1998 event and the fact that it is very close to a 100-year storm event, we select it as the basis for our modeling in this study. We refer to this storm as a near 100-year storm event ($NESE_{100}$).

| Station Number | Station Name | Date of Event | Measured Water Level (in NAVD 88) | Comparison to 100-year storm water level (2.64m NAVD 88) |
|---|---|---|---|---|
| 9414290 | San Francisco | 1/27/1983 | 2.707m | Exceeded 100-year level |
| | | 12/3/1983 | 2.674m | Exceeded100-year level |
| | | 2/6/1998 | 2.587m | Close to 100-year level |

Table B1. Events exceeding or close to the 100-year storm probability level at the National Water Level Observation Network's San Francisco station from 1893-2010 (Data Source: Zervas, 2013)

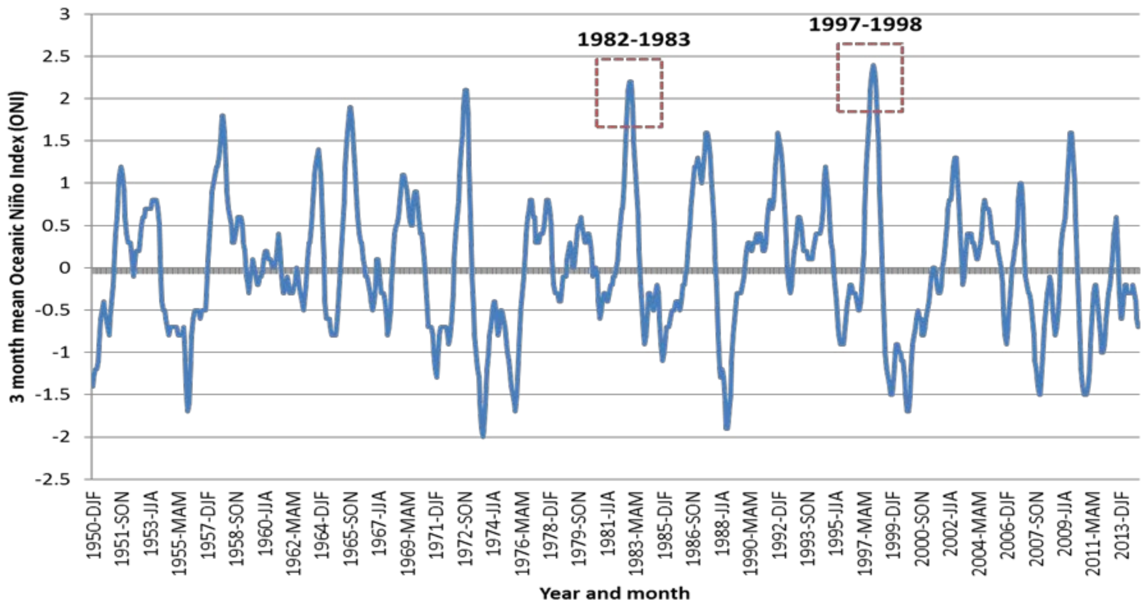


Figure B2. Change in the Oceanic Niño Index (NOAA/National Weather Service) through time. An index value above +0.5 indicates an El Niño event and an index value below -0.5 indicates a La Niña event. The dashed boxes highlight the index measurements corresponding to the events in Table B1. The NOI is calculated by averaging sea surface temperature anomalies in an area in the east-central Pacific Ocean. El Nino episodes are indicated by sea surface temperature increases of more than 0.5 °C for at least five successive overlapping three-month seasons.

## Collection and Processing of Water Level Data from Storm Events

In order to simulate overland water flow, the 3Di model requires water level data in addition to digital ground surface data. Given that 3Di is a hydrodynamic model that simulates the entire tidal cycle, it requires time series water level data for the duration of the event being simulated. To estimate the impact of sea-level rise coupled with an extreme storm event, we incorporate water level data from a February 5-8, a 1998 near 100-year storm event for the Bay and Delta regions and for the California coastal regions. These storm event water level data are used to generate our baseflow profile, and we add 0.0, 0.5, 1.0, and 1.41-meter SLR increments to derive peak water levels for input into different scenarios.

### *Bay and Delta Water level Data*

Currently water level data are available through multiple agencies and archived in different online databases for the San Francisco Bay and Sacramento San Joaquin Delta areas. No single agency or database provides good spatial coverage of water level data in both the Bay and Delta regions. Thus, to obtain a good spatial coverage to model inundation throughout the entire study region, we obtained water level data from different sources including the National Oceanic and Atmospheric Administration (NOAA), the Department of Water Resource's (DWR) Water Data Library (WDL) database, and the U.S. Geological Survey (USGS). However, these different databases often utilize different data conventions and units of measurement. To ensure the accuracy of the water level data, we use several criteria to evaluate data quality and then process the data to ensure compatibility across sources.

The criteria we evaluate in determining data quality includes: data availability, station information, and vertical datum information. In terms of availability, we require water level data with a consistent time interval of 6-minutes, 15-minutes, or 1-hour. The water level data also has to be verified or contains data quality information to ensure its accuracy. Finally, vertical datum and station information has to be provided as this information is essential in order to convert water level data from different vertical datums into the reference NAVD88 datum used for our analysis. For the Bay region, we determine the NOAA Tides and Current tidal stations have the most reliable data based on our above criteria. For the Delta region we determine the DWR's WDL has the most reliable data (Robert Crane, Personal Communication, 2013).

For our 3Di analysis, we collect water level data from a total of 21 tide or river stage stations, including 4 NOAA stations, 14 WDL stations, and 3 USGS stations illustrated in Figure B3.

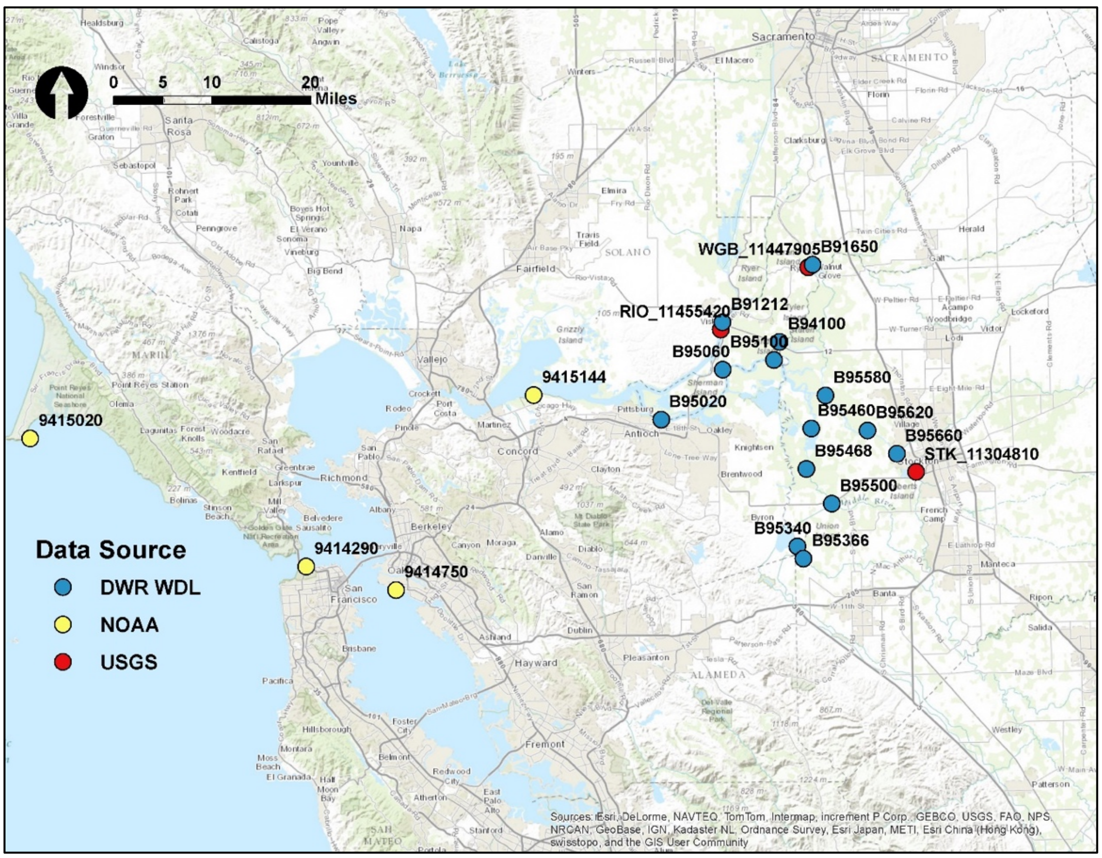


Figure B3. Location of gauge stations from which the February 5-8, 1998 near 100-year storm event data is collected. The gauge stations are colored according to data source.

### *NOAA Tides and Current Tide Station Data*

Water level height data from the NOAA Tides and Current tide stations can be downloaded relative to different vertical datums: mean sea-level (MSL), mean higher high water (MHHW), mean low water (MLW), mean lower low water (MLLW), or the standard (NAVD88). However, the NAVD 88 datum is not available for all of the NOAA stations since NOAA did not create a NAVD 88 bench mark for some. Because our analysis is performed using the NAVD 88 vertical datum, we choose to use data from the NOAA tide stations that do have water level data relative to NAVD 88. These stations included the San Francisco Presidio, Alameda, Point Reyes and Port Chicago stations. We download 6-minute interval data for the 1998 near 100-year storm event from these online NOAA stations[36]. It should be noted that water level measurements from NOAA stations are recorded in the Greenwich Mean Time (GMT) time zone, so data are downloaded for the 72-hour period from 2/5/1998 at 0:00 to 2/8/1998 at 0:00 GMT to reflect the period of the 100-year storm event.

### DWR Water Data Library (WDL) Data

Water level data from DWR's WDL is available from 1983-2013 or 2000-2013 depending on the station. Stage data are available in 15-Minute (ft), Daily Mean (ft), Daily Minimum (ft), and Daily Maximum (ft) format. We identify 14 WDL stations in the Delta region with available data for the period during the 1998 near 100-year storm event. We download water level data for these stations during the storm event as continuous, 15-minute interval data (in feet). We confirm time zone information for this continuous data with DWR staff as Pacific Standard Time (PST) with no daylight saving time or time changes included. We obtained water level data for these stations between 2/4/1998 @ 16:00 PST and 2/7/1998 @ 16:00 PST, the equivalent to the 72-hour period from 2/5/1998 @ 0:00 to 2/8/1998 @ 0:00 GMT used for the NOAA data.

### U.S. Geological Survey (USGS) Data

Water level data from USGS is available in 15-Minute (ft) format from the 1990s or 2000s to 2013 depending on the station. Stage data is available from USGS' Water Resources Department, Estuarine Hydrodynamics and Sediment Transport Group, that maintains the agency's continuous flow stage and water quality monitoring stations. We identify a total of 3 USGS stations in the Delta region with available data during the period of the1998 near 100-year storm event. We obtain the water level data and vertical datum conversion information directly from USGS staff (Brad Sullivan, Personal Communication, September 20, 2013). The Time zone information for these stations is recorded in Pacific Standard Time (PST). We obtain water level data between 2/4/1998 at 16:00 PST and 2/7/1998 at 16:00 PST, that is the equivalent to the 72-hour period from 2/5/1998 at 0:00 to 2/8/1998 at 0:00 GMT we use for the NOAA data.

## California Coast Water level Data

For the California coast, we used water level values from a total of eight NOAA tide-gauging stations located along the coast with data referenced to the NAVD88 vertical datum (Table B2). We download 72-hours of water level data at 1-hour intervals for each near 100-year storm event considered. In total, data is collected for three temporally separate events that began on the following dates: February 5, 1998; January 9, 2005; and December 30, 2005. These water

[36] http://tidesandcurrents.noaa.gov/est/northpacific.html

levels are then assigned to the tiles in which they fell. Tiles that did not house a NOAA tidal gauging station take on water-level values from the station to which they are nearest.

| NOAA Tidal Gauging Station | NOAA Station ID | UTM Zone | Storm Start Date | Storm End Date | Storm Zone | Tiles |
|---|---|---|---|---|---|---|
| La Jolla | 9410230 | 11 North | 1/9/2005 | 1/11/2005 | South | 1, 12 |
| Los Angeles | 9410660 | 11 North | 1/9/2005 | 1/11/2005 | South | 2, 3, 4 |
| Pt. San Luis | 9412110 | 10/11 North | 1/9/2005 | 1/11/2005 | South | 5, 6, 7, 8, mid 1a, mid1b |
| Monterey | 9413450 | 10 North | 1/9/2005 | 1/11/2005 | South | mid2, mid3, 2a, 2c,2d,2e |
| Pt. Reyes | 9415020 | 10 North | 2/5/1998 | 2/8/1998 | Central | 2b, 3a, 3b, 4a, 4b, 4c |
| Arena Cove | 9416841 | 10 North | 2/5/1998 | 2/8/1998 | Central | 5a, 5b, 5c, 6a |
| North Spit | 9418767 | 10 North | 12/30/2005 | 1/1/2006 | North | 7a, 8a, 8b |
| Crescent City | 9419750 | 10 North | 12/30/2005 | 1/1/2006 | North | 8c, 9a |

Table B2. NOAA Tidal Gauging Station Information and the Tiles to which the data is applied.

### *Datum Issues*

A vertical datum is a fixed reference used to determine elevation (height) or depth. The datum is an established zero and is used for surveying, engineering, mapping and other applications (Eldredge, 2011). Agencies such as DWR often use water level data to detect relative water level changes and gauge stations are originally installed at low water mark or an arbitrary height that is used as the "Gauge 0.00" elevation (Robert Crane of DWR, Personal Communication, 2013). By 1988 most gauge stations in California and across the U.S. were switched to the National Geodetic Vertical Datum 29 (NGVD29) as a standard reference datum. In October 2006, the standard vertical datum was updated and set to NAVD88. We use the NAVD88 vertical datum for water level data in our analysis and in some cases employ vertical datum conversion values to convert long-term monitoring station water level data to the NAVD88 standard.

While the data obtained from the NOAA tidal stations is benchmarked against the NAVD88 vertical datum used in our analysis, much of the data collected from the WDL and USGS requires processing to derive a consistent NAVD88 vertical datum and unit of measurement. The WDL and USGS water level data use different vertical datums depending on the year and gauging station. In general, data prior to the 1980's is either in United States Engineering Datum (U.S.E.D.) or NGVD29. Data from 1980's to 2005, are for the most part, in NGVD29, and require a conversion factor to convert from NGVD29 to NAVD88, while data after 2006 are all recorded in NAVD88. In addition to datum conversion factors, DWR WDL stations have a 3-foot adjustment added to station measurements while USGS stations have a 10-foot adjustment added (Robert Crane of DWR, Personal Communication, 2013; Brad Sullivan of USGS, Personal

Communication, September 20, 2013). Thus, a 3 ft or 10 ft subtraction is necessary to calculate the actual NGVD29 water level.

We perform manual vertical datum conversions to convert applicable measurements from the WDL and USGS stations into the NAVD88 datum after obtaining specific vertical datum adjustment information for each gauging station from DWR and USGS staff (Robert Crane, Personal Communication, 2013; Brad Sullivan, Personal Communication, September 20, 2013). To adjust the vertical datum for a station's measurements, we follow the below procedure:

1. Determine the vertical datum for the water level data at a station using a conversion factor spreadsheet or station documentation provided by staff from DWR or USGS. We also check the adjustment value used by DWR or USGS historically to prevent water measurements from being negative. For WDL stations this value is usually -3ft, and for USGS the value is usually -10ft, with some exceptions.
2. Use information provided by DWR and USGS staff to verify NGVD29 to NAVD88 difference value and gauge height correction factors. We correct the water level data using the following equation:

   [NGVD29 value] + [G.H. Corr.] = [New NAVD88 value]

   (where [G.H. Corr.] is the difference between NAVD29 + adjustment value and NAVD88)

3. We convert feet to meters using 1 foot = 0.3048 meter

Once the WDL and USGS water level data is converted to NAVD88, we use them, along with the NOAA tide station water level data, to calculate peak water levels for input into the 3Di hydrodynamic simulation.

### *Peak Water Levels*

To capture the effects of SLR and storm surge, our simulations are based on peak water levels. Peak water levels have two components: a sea-level rise component and a 100-year flood event component (Biging et al., 2012). The 100-year flood is a flood that has a 1/100 (1%) chance of occurring in any given year. It can be shown that there is a 63% chance that a 100-year flood will occur over the next 100 years and a 9.5% chance that it will occur over the next 10 years (Biging et al., 2012). We often refer to the 100-year flood event as a 100-year extreme storm event ($ESE_{100}$). In this analysis we use data from a number of near 100-year extreme storm events depending on the region analyzed. Conceptually, in order to derive peak water levels (PWLx) for this analysis, we individually add the four sea-level rise ($SLR_x$) increments {x: 0 m, 0.5 m, 1.0 m or 1.4 m} to the near 100-year extreme storm event ($NESE_{100}$) water levels ($PWL_x = SLR_x + NESE_{100}$). As described in detail in Section 3.3.2 (Modeling Strategy), this calculation becomes slightly more complex for the Delta region where peak water levels have a distance decay increment as well.

# APPENDIX C:
# 3Di Hydrodynamic Model

3Di is a new software package to build models to simulate the movement of water. The following common hydrological processes are included:

1. Interception of rainfall
2. Infiltration from surface to the unsaturated zone
3. Evaporation and transpiration from interception layer, surface water and unsaturated zone
4. Percolation and capillary rise between unsaturated zone and groundwater
5. Infiltration and seepage between groundwater and deeper groundwater
6. Horizontal flow between groundwater and surface water

Precipitation, evaporation and seepage between groundwater and deeper groundwater are external forces that can be defined by the modeler. Flows through drainage systems and sewer systems are computed in a separate 1D- module, which can fully interact with the overland and groundwater flows. This enables the computation of the overland flow on the course grid, which minimizes the computation time and still takes all the geometrical details of canals, weirs, culvers and pumps into account.

The water movement in the model is based on the continuity equation, which describes the conservation of mass and momentum and solved with a converging nested Newton-type algorithm. For shallow water this is mathematically described in the Saint Venant equations:

$$\frac{\partial \eta}{\partial t} + \frac{\partial (\eta u)}{\partial x} + \frac{\partial (\eta v)}{\partial y} = 0$$

$$\frac{\partial (\eta u)}{\partial t} + \frac{\partial}{\partial x}\left(\eta u^2 + \frac{1}{2} g \eta^2\right) + \frac{\partial (\eta u v)}{\partial y} = 0$$

$$\frac{\partial (\eta v)}{\partial t} + \frac{\partial (\eta u v)}{\partial x} + \frac{\partial}{\partial y}\left(\eta v^2 + \frac{1}{2} g \eta^2\right) = 0$$

Here η is the total fluid column height. The 2D vector (μ,υ) is the fluid's horizontal velocity, averaged across the vertical column. g is acceleration due to gravity. The first equation is derived from mass conservation, the second and third from momentum conservation in two dimensions.

The numerical method to quickly solve these equations, under the condition that a high resolution of model output be maintained, is based on four novel principles. By doing so the model accuracy can be substantially improved with just a moderate increase of the corresponding computational effort (See Casulli and Stelling (2011), Stelling (2012) and Casulli and Stelling (2013):

- The sub-grid method. In this method a distinction is made between a detailed grid and a course grid. In the detailed grid (i.e. the sub-grid) all details can be taken into account at a high resolution (e.g. 1 by 1 meter). This includes elevation, surface roughness and parameters for groundwater flow, such as interception capacity, infiltration rate and seepage rate. In the course grid the pixels are clustered for the computation of water levels and velocities (see Figure C4).
- Quadtrees to detail the course grid, in which the water levels and velocities are calculated on places were the elevation grid has a high variation, such as along high and low line elements such as embankments and canals.
- Bottom friction based on the concept of roughness depth, in which the spatial variation of the roughness in the sub-grid is taken into account in calculating the water levels and velocities in the course grid.
- The finite-volume staggered grid method for shallow water equations with rapidly varying flows, including semi-implicit time integration. This method ensures that the continuity equations are always solved strictly.

In the current version 3Di can do a lot already, but 3Di is still under development. Since 2011 several Dutch parties (mainly regional Water Authorities and the municipalities of Amsterdam, The Hague and Rotterdam) have invested 6 million euros in it. At the moment they are working on an in-the-cloud version, which utilizes the computation power of several servers instead of just using one desktop PC without even the need of installing the software. Furthermore, they are working on a dynamic breach growth module, a library of precipitation radar images as input for the simulations and an integrated damage module.

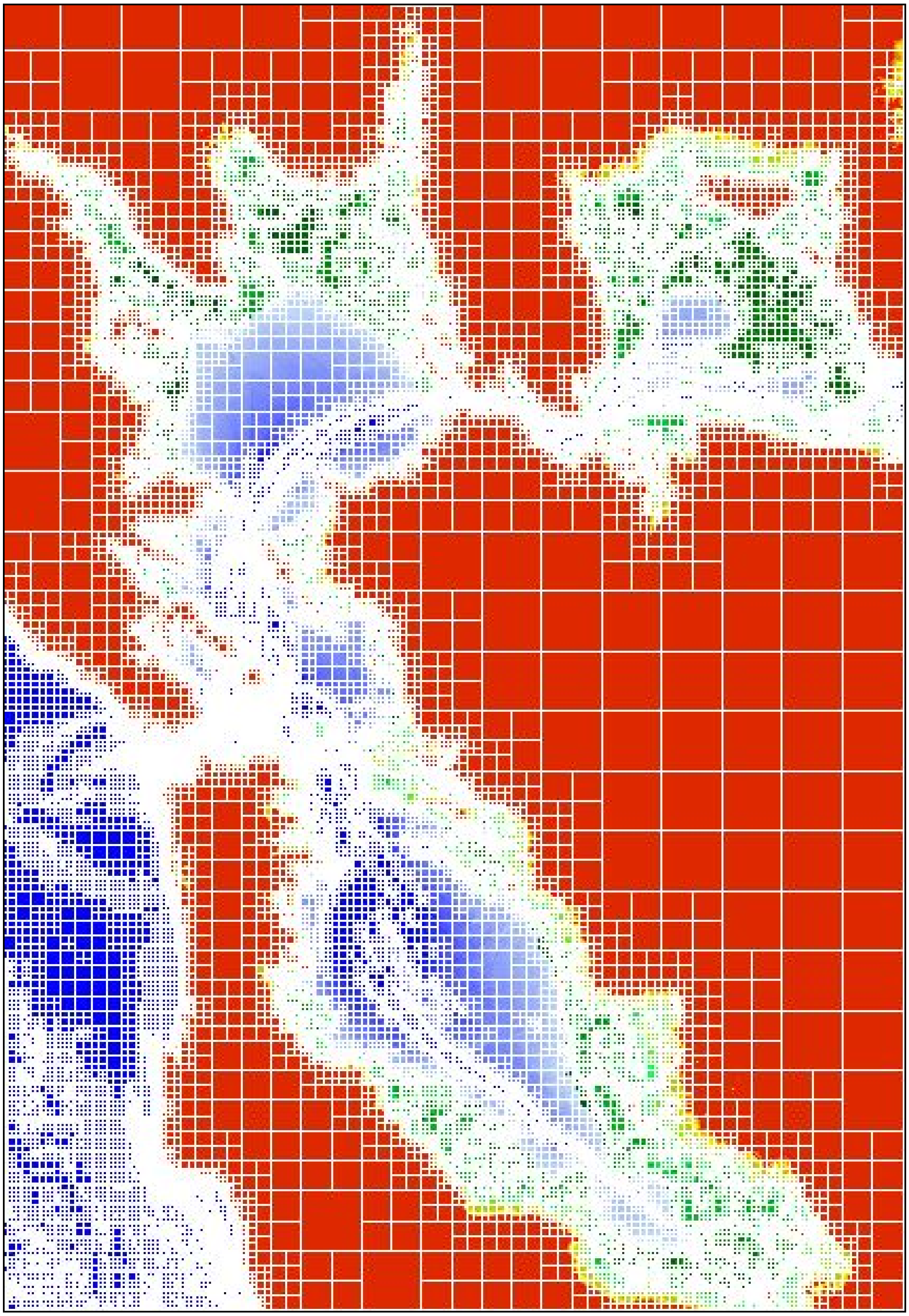

Figure C1. Quadtree sub-grid showing both detailed and course grids.

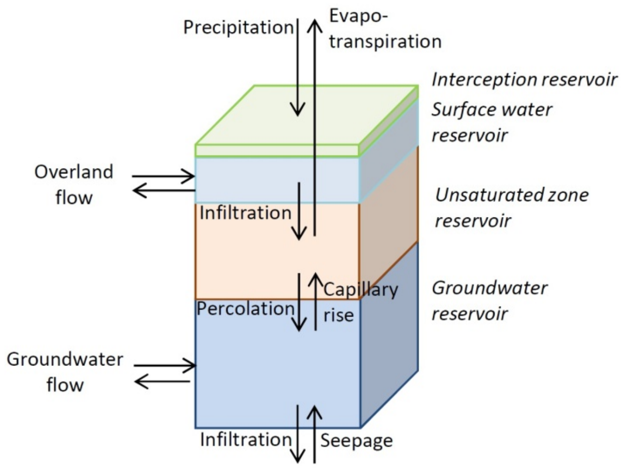


Figure C2: Groundwater flows

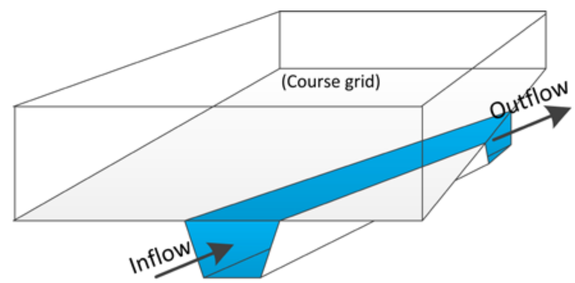


Figure C3: 1D-module, coupled with the sub-grids

Source: Olivier Hoes (original drawing) TU Delft

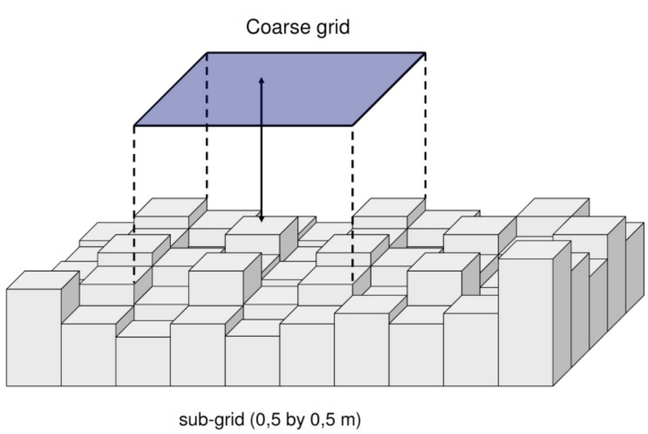


Figure C4: Sub-grid method

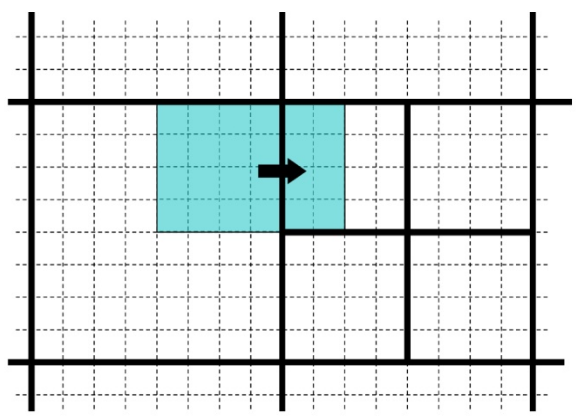

Figure C5: Quadtrees method

Source: Stelling, G. S. (2012). http://doi.org/10.1680/wama.12.00018

# APPENDIX D:
# Initial Water Level Data for tiles

### *A. Initial water level data for the Bay tiles*

For the Bay, initial water level data are directly obtained from Bay-wide simulations of the different SLR scenarios. Since we divide the study area into tiles, we must provide water level input data for each tile. We obtain the water level input for all the tiles in an Xm SLR scenario (where X is 0.0, 0.5, 1.0, or 1.4m of SLR) by:

1. Adding a virtual water level gauging station to each tile located at the mid-point of the initial water boundary (Figure D1).

2. Running a Bay-wide simulation at 50 $m^2$ resolution, with the initial water boundary set close to NOAA's Point Reyes gauge and the initial water level data set as the peak water level at the NOAA Point Reyes gauge: the water level from the 1998 storm event recorded at that gauge with Xm of SLR added, and then using the peak water levels at the Bay-wide Actual stations to calibrate the model.

3. Recording water levels at virtual gauging stations during the Bay-wide simulation. The water level recorded by a tile's virtual gauging station during this simulation is considered to be the initial water level for that tile in the X m SLR scenario.

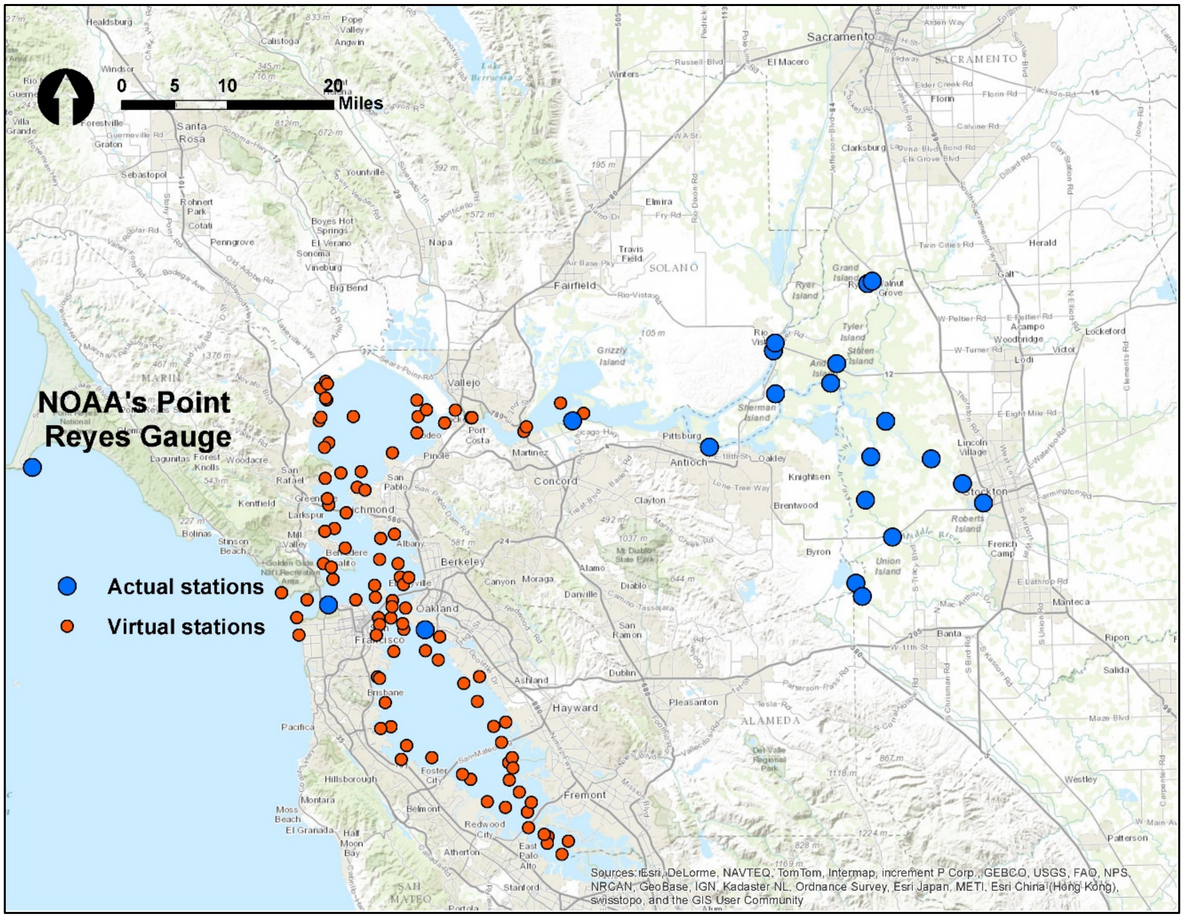


Figure D1. Actual (blue) and Virtual (red) gauging stations in the San Francisco Bay and Delta regions

### *B. Initial water level data for the Delta tiles*

Obtaining water level data for the Delta tiles is more difficult than for the Bay. Since the Delta is a complex hydrologic system that contains several narrow channels (width < 50m), those narrower channels would be indistinguishable in an entire Delta simulation at a spatial resolution of $50m^2$. The elimination of narrower channels would lead to underestimation of inundation extents as the simulated waves would not be able to travel as far into the Delta as they can in reality. Therefore, instead of using water level data from virtual gauging stations, we use water level data from actual gauging stations in the Delta and a "drape line" strategy to calculate the SLR increments for each tile in each Xm SLR scenario.

The "drape line" strategy assumes there is a distance decay in SLR increments from the Bay to the Delta. We used the following steps to formulate regression equations to estimate the SLR increments for each Delta tile:

1. Delineate four drape lines from the Bay to the Delta with each drape line representing a major channel in the Delta.
2. Create a series of virtual gauging stations along each drape lines spaced 1000 m apart (Figure D2).

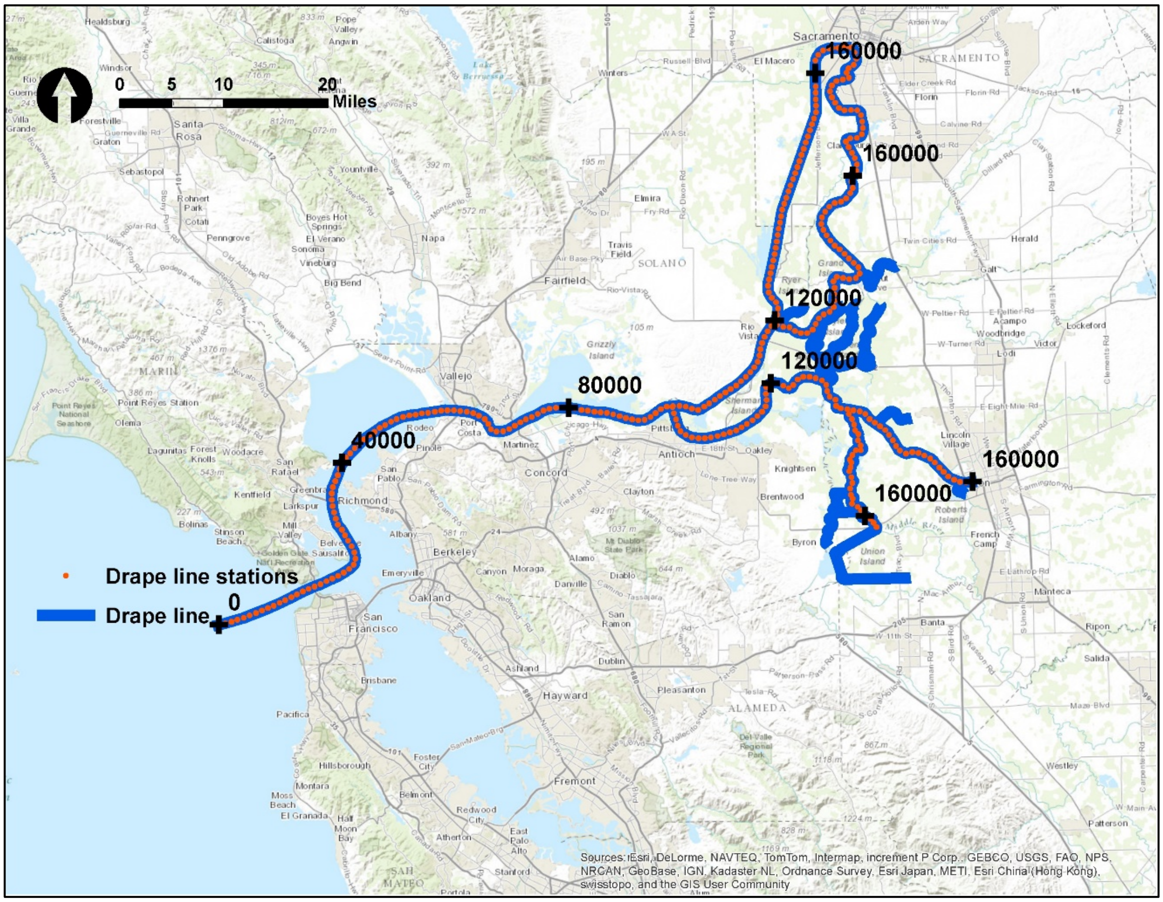


Figure D2. Drape line and drape line gauging stations

3. Simulate the 1998 storm with X m SLR over the entire study area (the Bay and the Delta) at 70m[2] resolution. The simulation process begins with the westmost gauging station and passes on the predicted mean water level to the adjacent real or virtual gauging station (mapped in Figure D1) for simulation. Have the virtual gauging stations we record simulated water levels and calculate the mean water level ($MWL_{X\ m\ SLR}$) for each virtual station as:

$$MWL_{x\ mSLR,gauge\ i} = \frac{\sum_{n=1}^{m} WSE_{x\ m\ SLR,gauge\ i,n}}{m}$$

Where x is the water surface elevation at record *n*, under *x* m SLR scenario, y is the total number of records calculated in the storm event per 15 minute interval, z is the mean sea level of under *x* m SLR scenario.

Iterate this process for 0, 0.5, 1.0, 1.41 m SLR to get $MWL_{0\ m\ SLR}$, $MWL_{0.5\ m\ SLR}$, $MWL_{1.0\ m\ SLR}$, $MWL_{1.41\ m\ SLR}$ at each station.

4. Compute the MWL difference (SLR increment) for X m SLR scenario at each station by subtracting MWL under 0 m SLR scenario from MWL under X m SLR scenario (where X is 0.5, 1.0, or 1.41m).

$$SLR_{gauge\ i} = MWL_{Xm\ SLR.gauge\ i} - MWL_{0m\ SLR.gauge\ i}$$

Where $SLR_{gauge\ i}$ is the SLR increment at *gauge i*.

Iterate this process for 0.5, 1.0, 1.41 m SLR to get $\Delta MWL_{0.5\ m\ SLR}$, $\Delta MWL_{1.0\ m\ SLR}$, $\Delta MWL_{1.41\ m\ SLR}$ at each station.

5. For each X m SLR scenario, form a regression using $\Delta MWL_{X\ m\ SLR}$ at each station and the stations' distances to the ocean. Run this regression analysis for each drape line.
6. For each Delta tile, measure the distance from the initial boundary designated to the Ocean along the drape line. Then, use the measured distance and the regression equation to calculate the SLR increments for the boundaries (Figure D3).

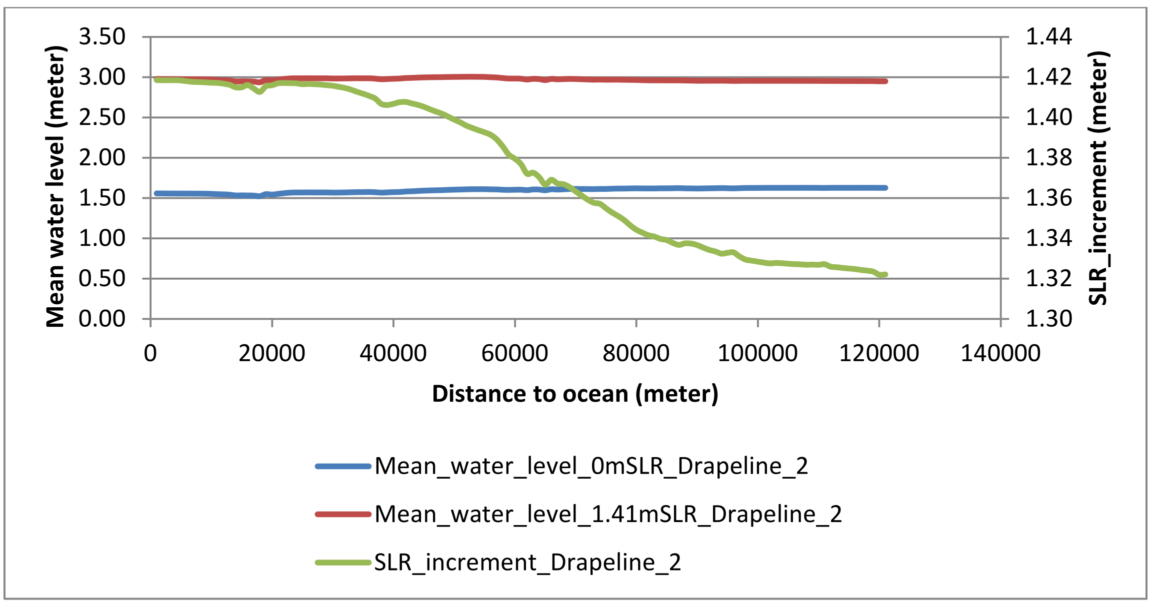


Figure D3. 3Di calculation of the SLR 1.41 increment values (green line, right axis) is a subtraction of the 0 mean sea level water surface elevation profile (blue line, left axis) from the 1.41 mean sea level water surface elevation profile (red line, left axis). Note the use of different Y axis value ranges in the graph.

7. Assume the 1998 storm event water level at an initial boundary for a tile equals the water level measured at the closest real or virtual gauging station (mapped in Figure D1) during that event. Add the SLR increment of water level of this initial boundary during a 100-year storm with SLR. that initial boundary to the 1998 storm water level from the closest gauging station to get the future

### *C. Influence of model choice in predicting sea-level rise in the Sacramento/San Joaquin Delta*

As described by URS Inc. in the Delta Risk Management Strategy (see below), accurate assessment of sea-level rise in the Delta requires a more sophisticated analysis than applying simple bathtub models. To account for bathymetry, tidal interactions and the influence of river discharge, we looked at hydrodynamic models that predict water surface elevations (WSEs) based upon these factors, plus a sea-level rise value at coastal location such as the Golden Gate. The sea level rise parameter is exogenous to modeling WSEs and is taken from various global climate change assessments. The models use the sea level rise value as one of its inputs and then predict WSE values at various points along a river profile starting from the Bay and extending up into the Delta, taking into account existing water surface gradients, bathymetry and river flows, and complex interactions of flows and channel surfaces; all of which can raise or lower water levels at various points along the Bay / Delta watercourse. How these factors are considered is described in more detail in the discussions of the various models.[37]

The WSE models we examined start with a two dimensional graph—a profile or “drapeline”—of existing water surface elevations taken along a centerline from the Bay up one of the various Delta watercourses (e.g., the Sacramento or San Joaquin Rivers) (see figure D3). Input baseline or baseflow WSE values are derived from historic observational data from gauges maintained by the California Department of Water Resources, US Geological Survey and other maintainers and it should be noted that there are significant datum-conversion and idiosyncratic processing issues associated with these data that are described elsewhere in this study report. The contribution of sea level rise (SLR) to the new, predicted WSE profile can be derived by subtracting the baseline WSE values from the new, SLR-influenced WSE values, or, as follows:

> Modeled SLR increment $_{[\text{location xy}]}$ = modeled SLR-influenced WSE$_{[\text{location xy}]}$ – baseline WSE$_{[\text{location xy}]}$

In our discussions with California Department of Water Resources and US Army Corps of Engineers (USACE) personnel we became aware of two modeling efforts aimed at estimating new maximum water surfaces in the Delta from sea level rise. These are (1) URS’s Inc. Delta Risk Management Strategy/Technical Memorandum Topical Area: Flood Hazard, “Future Delta Water Surface Elevations” (Sec. 6.5), (2006); (2) Dynamic Solutions’ Inc., “Sea-Level Rise Analysis Using the Extended Delta EFDC Hydrodynamic Model”, (2011), a study performed for the USACE Sacramento District. In addition, (3) we applied 3Di software, made available to us from Deltares Systems (described elsewhere in this report) to model higher water surface elevations throughout the Delta. For the following discussion we abbreviate these approaches as “URS”, “Dynamic Solutions/USACE”, and “3Di”.[38]

---

[37] The Delta is a managed water system. All of these methods are processed under the current-day condition, where the channel width and depth do not change in the future SLR scenarios. In addition, they assume the management of the Delta remains unchanged over the simulation period.

[38] See the D Appendix References section.

### Modeling changes in sea-level rise for San Francisco Bay and the Sacramento River

1. The URS approach

Some quotes best describe their approach and the factors considered (URS: Section 6.5, page 28)

> *"The increases in sea level cannot simply be added to the water-surface elevations…the sea-level rise will change the hydraulic characteristics of flows through the Delta and its impact should decrease the farther inland a location is and the larger the storm event."…"A rise in sea level increases the tailwater that inflows must overcome to pass through the Delta and enter San Francisco Bay. For any given inflow magnitude and pattern flow, depths in the Delta channels will be larger, thereby reducing flow velocities and hydraulic head losses. The reduction in hydraulic headloss must be accounted for in estimating water-surface elevations under future increased sea-level conditions."*

URS: From page 28:

*"1. Manning's Equation can be used to describe the flow in the Delta channels during storm events."*

*"2. The channels are much wider than they are deep; therefore, the hydraulic radius can be approximated as the channel depth."*

*"3. The slope of the channel can be approximated as the water-surface slope between the station of interest and the next downstream station."*

*"4. The water-surface elevation at any station can be approximated using the relationships developed in Section 5."*

*"Using the above assumptions, the sea-level rise at any location in the Delta can be estimated using Section 5."*

*"Using the above assumptions, the sea-level rise at any location in the Delta can be estimated using Equation 6-1."*

$$\left(\frac{hb}{hb+db}\right)^{5/3} = 1 + \frac{db-da}{fb(Q_1) - fa(Q_1)} \qquad \text{(Equation 6.1)}$$

where

hb = water depth at location of interest
db = sea-level rise (SLR) at point of interest
da = known sea-level rise at downstream point
$fb(Q_1)$ = water surface elevation at point of interest
$fa(Q_1)$ = water surface elevation at point downstream

A python script was developed to apply this model to various baseflow water surface elevation (WSE) values. For the Sacramento River a sample data table and resultant SLR values as calculated by the URS model are as follows:

| Station | Baseflow WSE *(m) | Average channel depth (m) | Station information |
|---|---|---|---|
| PC | 1.870 | - (dummy value) | Port Chicago |
| MAL | 1.942 | 12.08 | Sacramento R. at Mallard Island |
| RVB | 2.426 | 6.41 | Sacramento R. at Rio Vista Bridge |
| SWG | 4.018 | 7.20 | Sacramento R. at Walnut Grove |
| SSS | 5.495 | 4.59 | Sacramento R. at Snodgrass Slough |

Table D1. Input data for the 1998 storm, Sacramento River drapeline

* Gauge data sources and the derivation of average WSE values for 1998 storm and Summer/lowflow conditions are described earlier is this document.

| Station | Baseline WSE (m) | SLR increment (m) | WSE+SLR (m) | Average channel depth (m) |
|---|---|---|---|---|
| PC | 1.870 | 1.41 | 3.280 | - |
| MAL | 1.942 | 1.398 | 3.340 | 12.08 |
| RVB | 2.426 | 1.272 | 3.698 | 6.41 |
| SWG | 4.018 | 0.97 | 4.988 | 7.20 |
| SSS | 5.495 | 0.67 | 6.165 | 4.59 |

Table D2. URS calculated total WSE elevations and SLR increment values for the 1998 storm, Sacramento River drapeline

| Station | Baseline WSE (m) | SLR increment (m) | WSE+SLR (m) | Average channel depth (m) |
|---|---|---|---|---|
| PC | 1.161 | 1.41 | 2.571 | - |
| MAL | 1.192 | 1.4 | 2.592 | 12.08 |
| RVB | 1.547 | 1.35 | 2.713 | 6.41 |
| swg | 1.547 | 1.31 | 2.857 | 7.20 |
| sss | 1.952 | 1.18 | 3.132 | 4.59 |

Table D3. URS calculated total WSE elevations and SLR increment values for summer (low) flows, Sacramento River drapeline

Modeled sea-level rise increment using the URS model under two base flow conditions are presented in figure D4. Note the sea-level rise increment decreases (decays) as one goes up the Sacramento River; in addition, high levels of river discharge reduces the SLR increment relative to low-flow conditions.

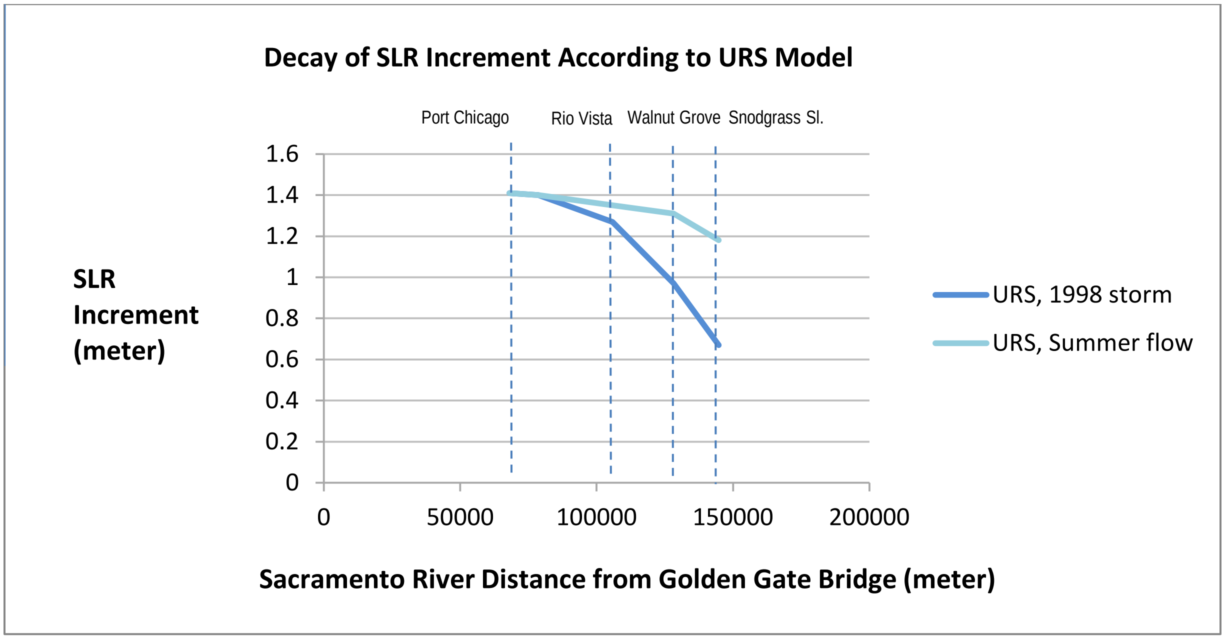


Figure D4. URS sea-level rise increments under two baseflow conditions (1998 storm, average summer low-flow runoff).

2. Dynamic Solutions/USACE

To quote from the report:

> *"The modeling effort utilized the Extended-Delta EFDC Hydrodynamic Model [p3: EFDC is a general-purpose modeling package for simulating three-dimensional (3-D) flow, transport, and biogeochemical processes in surface water systems including rivers, lakes, estuaries, reservoirs, wetlands, and near-shore to shelf-scale coastal regions.]… which includes the Delta proper extending up the Sacramento River to Verona and the San Joaquin River to Vernalis, westward through Suisun, San Pablo, and San Francisco Bays into the Pacific Ocean 26 miles to the Farallon Islands.*
>
> *Low, intermediate, and high sea-level rise rates of the Pacific Ocean taken from USACE guidance documents were tested along with an estimated subsidence rate for the Delta for 50 and 100 years in the future to evaluate the potential effects of sea-level rise. A total of eight scenarios were simulated and compared with the conditions in 2004. Among them, two scenarios, 100-year scenarios under low and high sea-level rise rates, incorporated channel subsidence. Sea-level rise values of between 0.10 and 1.7m and subsidence values between 0 and 0.15m were tested. Water level and depth-averaged salinity concentration results for each scenario were compared to those of the base case of the 2004."*

We did not employ the EFDC model independently of this study but, rather, used the study findings from the maps and graphics to derive a set of SLR increment values for comparison to other model output.[39] The 1.7m ocean SLR models / 100 year timespan were closest to our 1.41 input (100 year) value and we made some slight adjustments to this value for our numerical comparison.

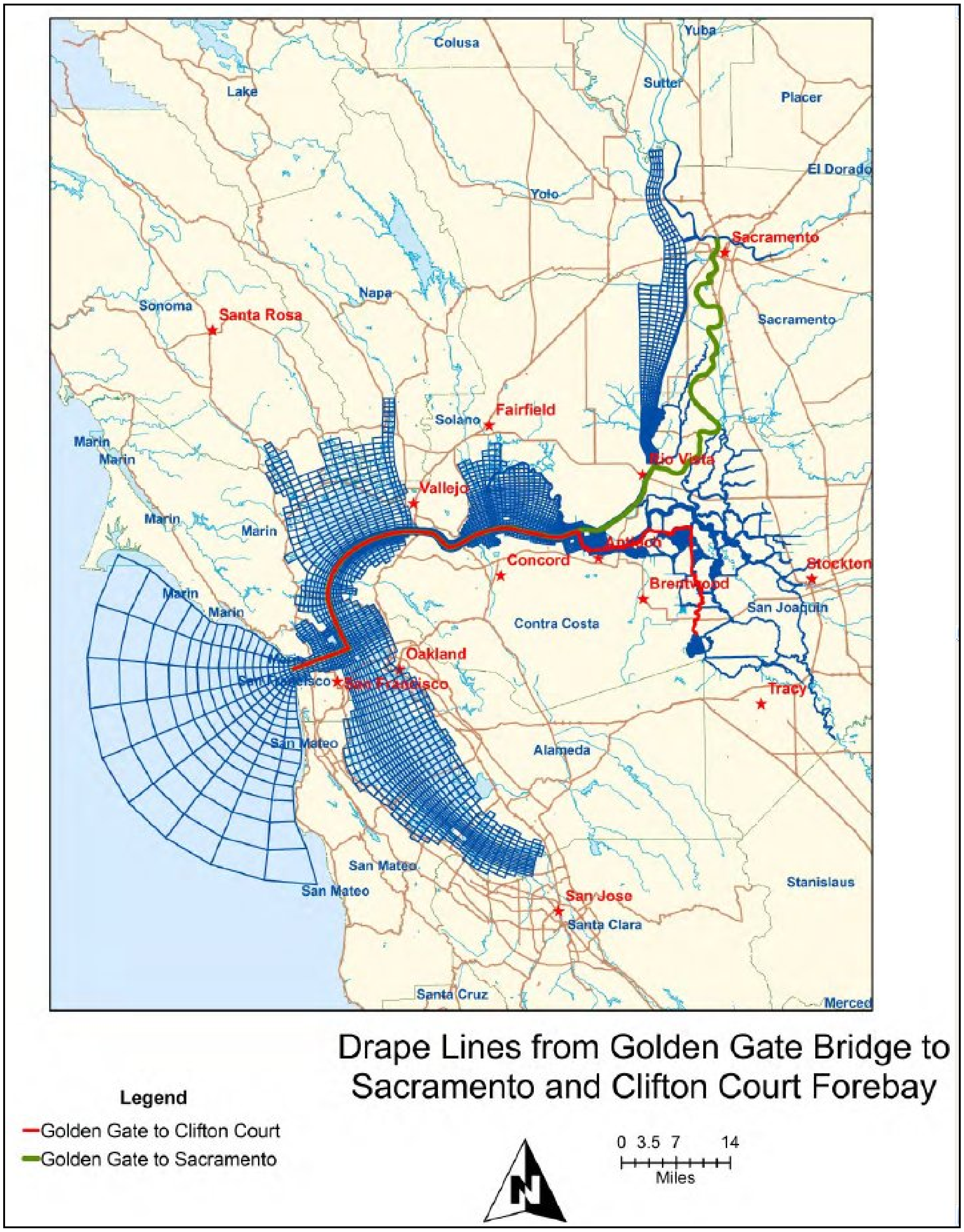


[39] see Appendix D References, p. D-16.

Figure D5. Drapelines used in the Dynamic Solutions/USACE study. We used these same drapelines throughout our comparison of sea-level rise studies.

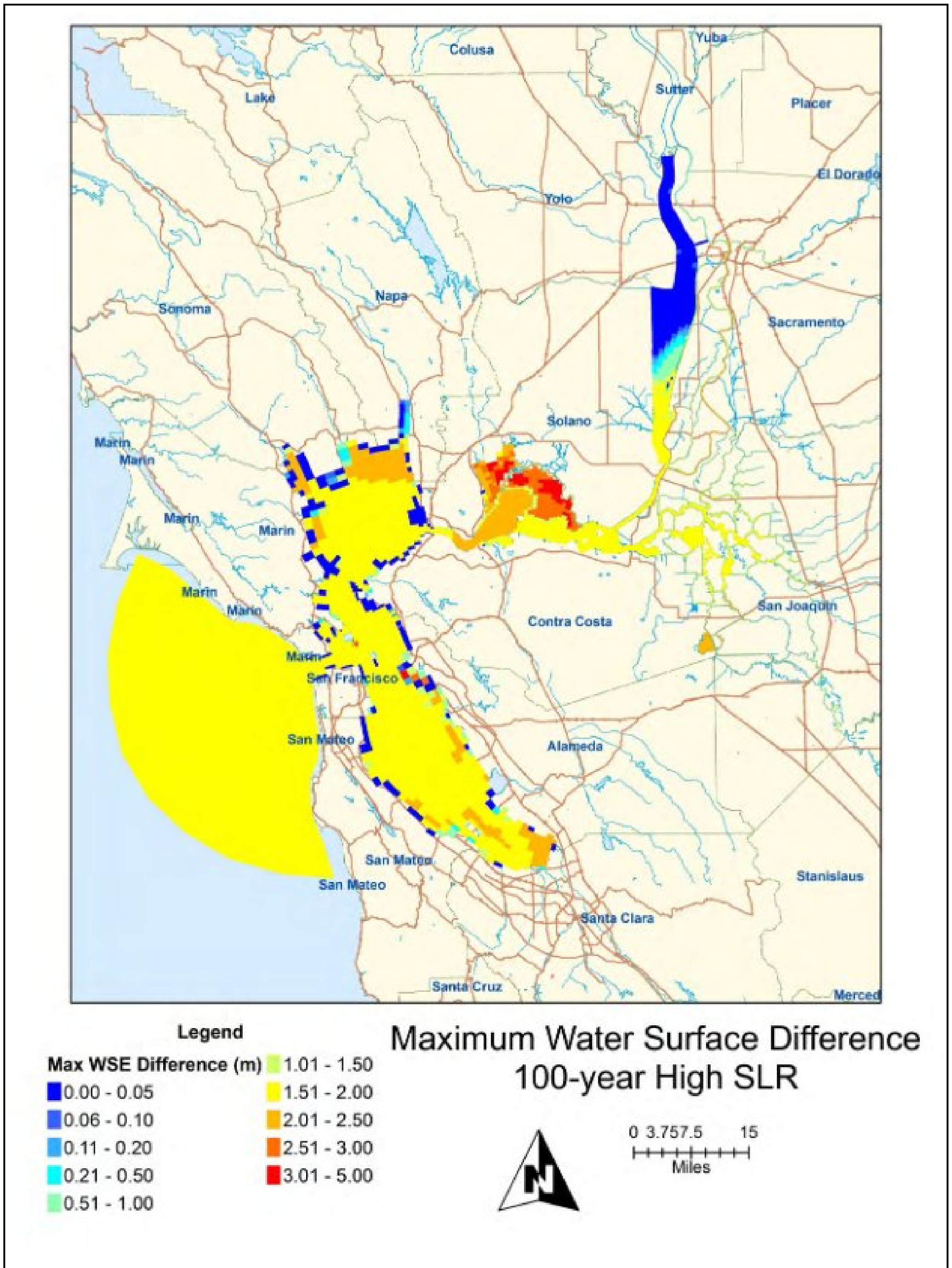


Figure 8 Maximum Water Level Increases (High 100 –Base Case) for the High 100 Scenario

Figure D6. (Dynamic Solutions/USACE, figure 8) sea-level rise increments in San Francisco Bay and the Delta for the high input SLR value of 1.71m. Note that in some areas, e.g., Suisun Bay, the increments is actually higher than the input value at the Golden Gate.

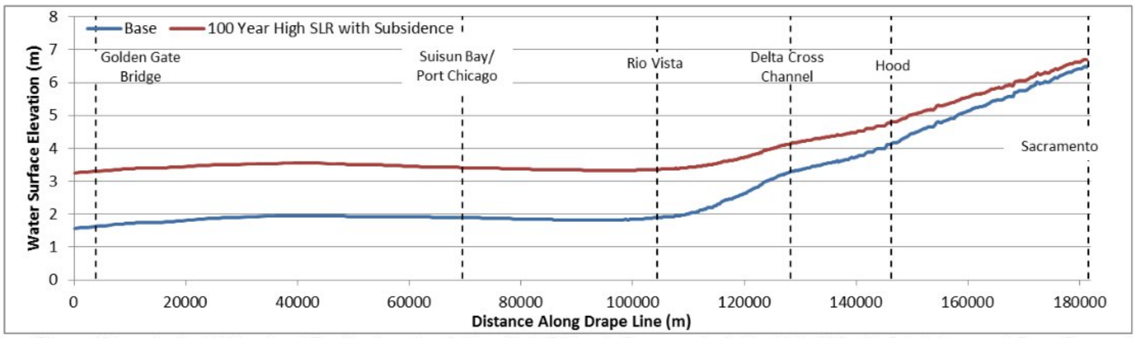


Figure 12 Longitudinal Water Level Profiles from the Golden Gate Bridge to Sacramento for the High 100 with Subsidence and Base Case Scenarios during Flood Tide (Higher High Water) at Golden Gate for Spring of 2004

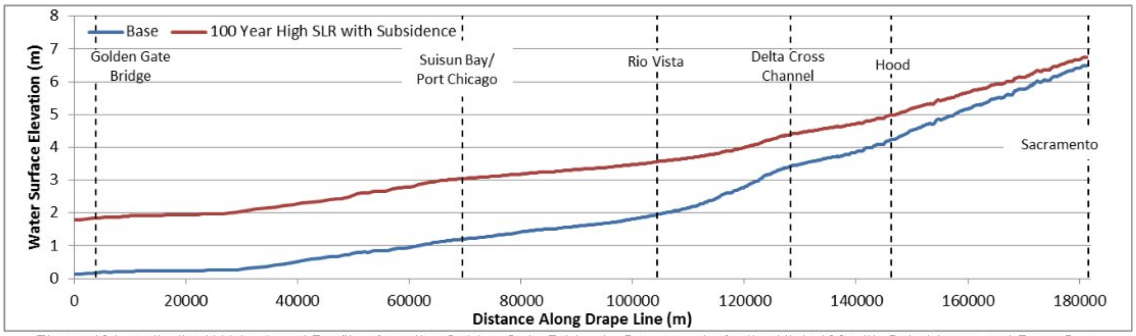


Figure 13 Longitudinal Water Level Profiles from the Golden Gate Bridge to Sacramento for the High 100 with Subsidence and Base Case Scenarios during Ebb Tide (Lower Low Water) at Golden Gate for Summer of 2004

22

Sacramento District, US Army Corps of Engineers
Extended Delta EFDC Hydrodynamic Model Sea Level Rise Analysis (Task 21)

Figure D7. Water surface profiles for the Sacramento River generated from the high-SLR-input value of 1.71 under higher high water and lower low water observed on the same day, 3-04-04. Note that the only area affected is from the Golden Gate to Rio Vista and that upstream of Rio Vista the profiles are essentially the same. (Figure 12 and Figure 13 in the original Dynamic Solutions/USACE study).

## 3. 3DI

The 3Di model is described in more detail in section 3.3.1 of this report. This model was developed by TU-Delft Netherlands to simulate flood inundation time sequence and flood depths over low-lying land surfaces for modeled flood events. The model is similar to other hydrodynamic models as it preserves fluid mass and momentum and incorporates detailed land surface and bathymetry information. 3Di can incorporate the influence of river discharge and tidal inputs. 3Di output can be combined to make movies of flood simulations, a facility particularly useful for infrastructure hardening and emergency service planning as the vivid representation of the sequence of infrastructure loss -- transportation system, emergency services and loss of critical infrastructure—gives a much more detailed and clearer understanding of the impact of flooding.

In this application, we used 3Di to predict the maximum of the tidal-influenced water surface elevations, over a 72 hour period, along the major river courses of the Delta, with 0, 0.5, 1.0 and 1.41m input SLR values starting at the Golden Gate. For the following model comparison, 3Di's

SLR increment was developed under average high runoff conditions –the average WSEs influenced by tides and runoff over a 72 hour period for the 1998 storm.

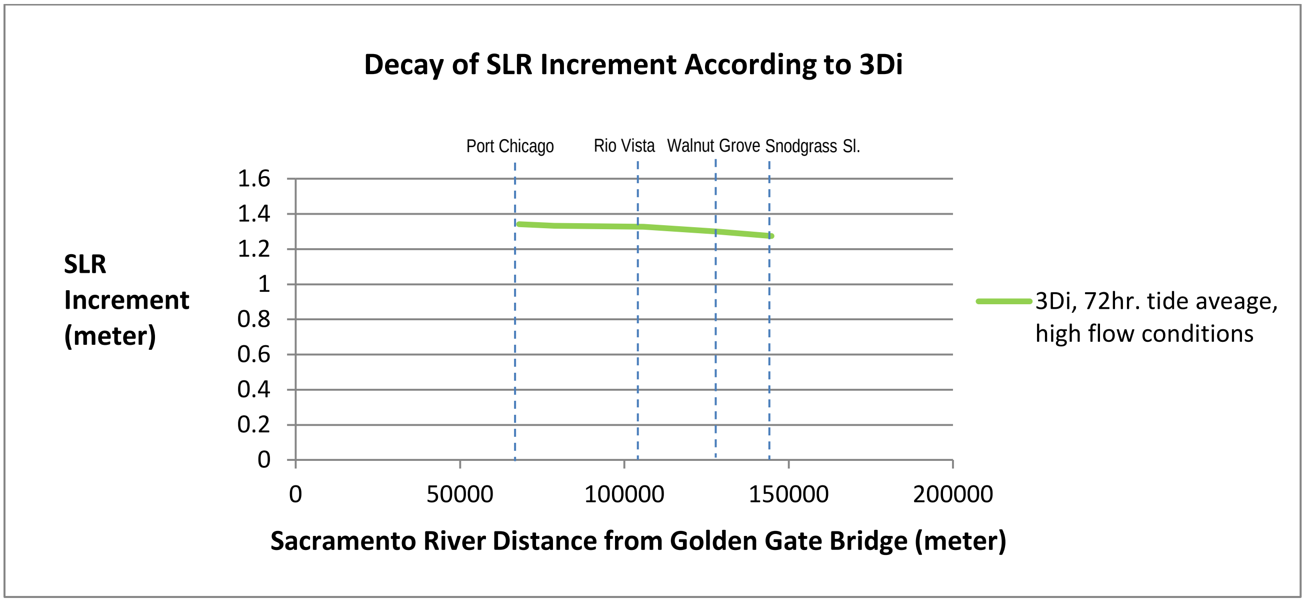


Figure D8. SLR increment decay as modeled by 3Di software. Note the gradual reduction of the SLR. However, this result is a composite of 72 separate 3Di runs in which there are a number of tide and runoff interactions.

### *D. Analysis and discussion: comparison of SLR models for the San Francisco Bay and Sacramento/San Joaquin Delta, variations in baseline conditions*

**Comparing SLR models: influence of different baseline tide and river discharge conditions**

A numerical comparison of modeled SLR values is tempered by the different tide and river discharge conditions under which the various models were run. For the URS model, we used a real, high-discharge event, the 1998 storm, which is close to a 100 year storm for California. As we used maximum WSE values experienced over a 72 hour period, our baseline WSE values represent the maximum of tide and high runoff conditions. In contrast, the baseline water surface elevations used in the USACE model occur on a single day where river discharge is a fixed value for both model runs -- a relatively high value typical of Spring conditions. Therefore, for the USACE model, the only variation in baseline WSE values between the two USACE model runs is due to tides, a low and high tide event for the day. As noted in figure D9, (below), baseline WSE values for the USACE analysis are only significantly different downstream of Rio Vista--upstream, WSE values are very similar. For 3Di, baseline WSEs tide data are taken under summer average low-flow conditions.

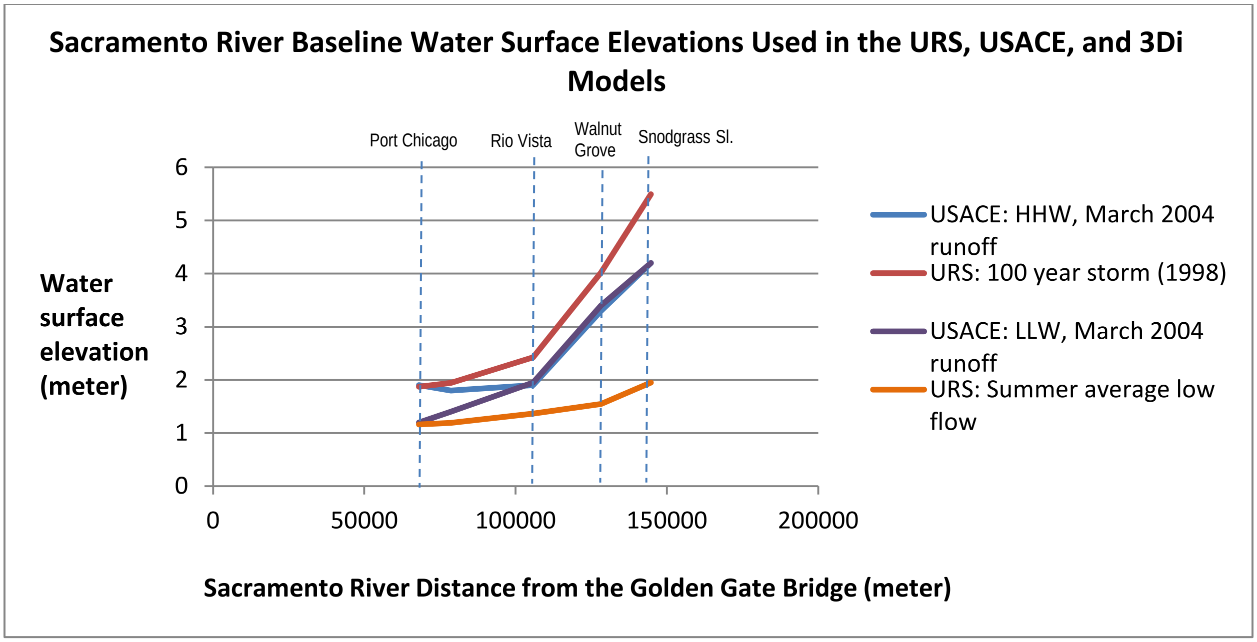


Figure D9. Baseline water surface elevations (WSEs) used in the various models. These differences significantly contribute to the differences in predicted SLR-influenced WSEs in the Delta. Note: the river data terminate at Snodgrass Slough.

**Comparison of WSEs and SLR increments by model**

**1.** ***Comparison of URS and Dynamic Solutions/USACE models.***

<u>Similar high baseflow conditions</u>

In this comparison (Figure 4), we look at the USACE and URS models under somewhat similar baseflow conditions: for the USACE model, a high tide event is selected with a moderately high runoff (Spring 2004) condition; for the URS model, the maximum of tide and runoff influenced WSEs is used from a very high runoff event (1998 storm). The USACE model shows the influence of a particular high tide that dominates WSEs up to Rio Vista (circa 105,000 m from the Golden Gate Bridge), but not much further. The URS model shows a more even decline in the influence of sea level rise. Otherwise, the two models show a similar SLR decay function overall, but are shifted relative to each other by about 0.2 m, perhaps explainable by the difference in input SLR elevation conditions at Port Chicago.

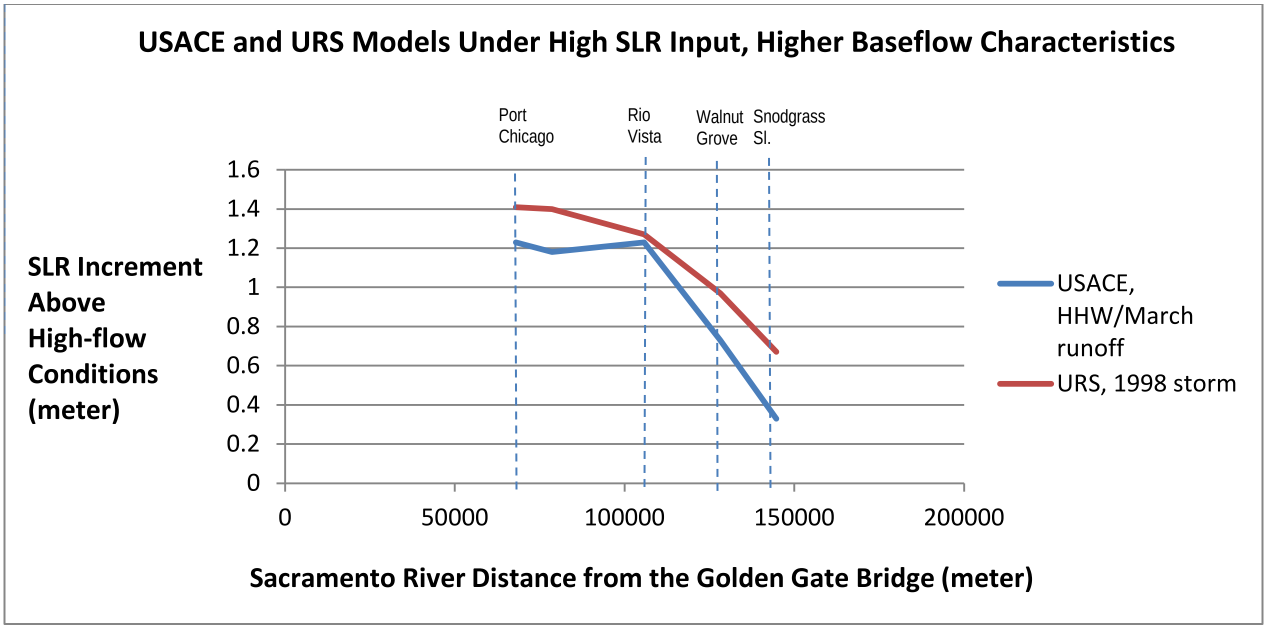


Figure D10. USACE and URS models under moderate to high baseflow / high to average tide conditions.

Mixed tide and baseflow conditions

These two models only agree in the river portions that are not dominated by runoff. In the upper reaches (up from Rio Vista), the Dynamic Solutions/USACE model is particularly influenced by the moderate to high March 2004 Spring runoff, whereas this URS model was run under low runoff, summer conditions. The SLR decay function of the URS model is particularly sensitive to baseflow gradient conditions.

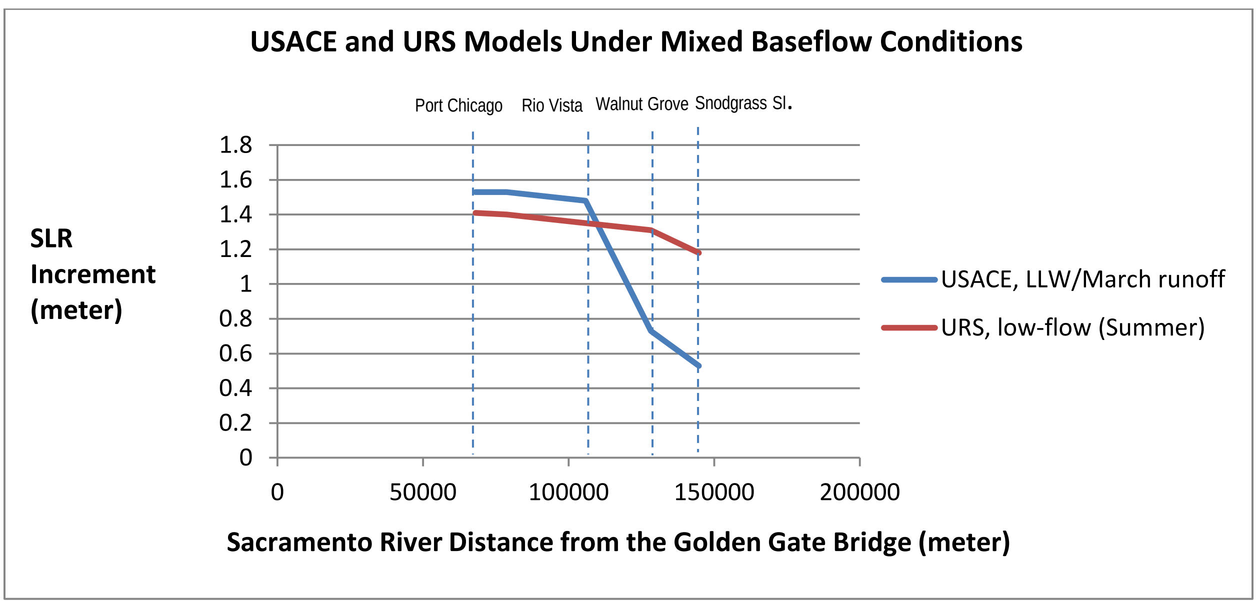


Figure D11. USACE and URS models under low tide/low and moderate flow conditions.

URS and USACE model comparison using the same input data

In this comparison, we adjusted initial WSEs at Mallard Island to be identical between the two models. In the USACE model there is actually an increase of WSEs at Mallard Island (1.8m) over the base input value of 1.63m at the Golden Gate, due to bathymetry and flow interaction effects (our Figure D6 above and figure 8 in the original URS report). We set the URS input value 1.8m and used the low-runoff WSE input values. The difference between the two models shows an approximately 0.2m difference in SLR on the upper portions of the Sacramento River.

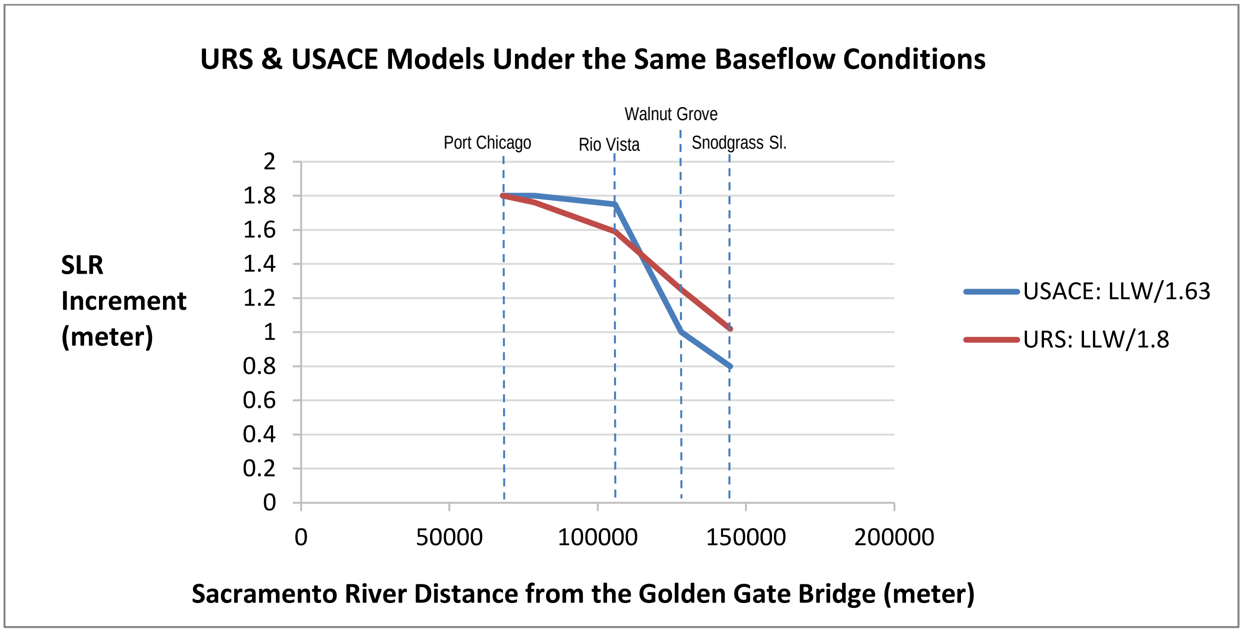


Figure D12. URS and Dynamic Solutions/USACE model comparison using identical baseflow (Dynamic Solutions/USACE) data.

**2.** ***Comparison of SLR decay characteristic of all models under all tide and flow conditions.***

In this comparison of SLR increment decay functions, virtually all tide and runoff conditions are represented. The absolute difference between the models is approximately 1 meter at Snodgrass Slough (~ 150,000m from the Golden Gate Bridge) between the 3Di and USACE models. The 3Di model shows the least SLR decay that is closely matched by the URS model under low flow conditions. The two USACE models are essentially identical above Rio Vista, accountable by the reduced influence of tides at upstream locations.

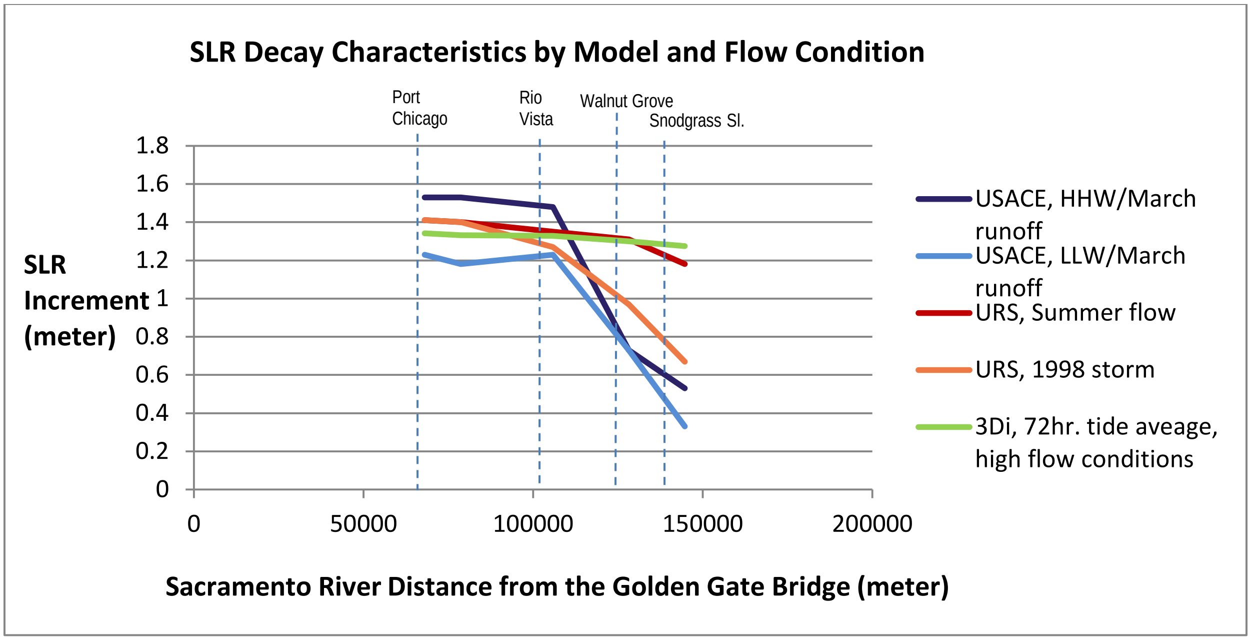


Figure D13. Differences (m) in the sea-level rise increment according to model and tide and runoff conditions.

**3.** ***Comparison of predicted Water Surface Elevation values for all models under all tide and flow conditions.***

This chart is a comparison of total predicted WSE values from the models under all conditions. We consider this comparison to be an indicator of the uncertainty of sea-level rise influenced water surface elevations in the Delta. At Snodgrass Slough (just north of Walnut Grove), the upper reach of the Sacramento River in our analysis (right-hand edge of the data graphics), river water surface baseflow elevations range between 2 to 5.5 meters (Figure D9). Predicted SLR-influenced water surface elevations at this location vary from 3.1 to 6.8 meters (Figure D14), depending upon model and baseflow conditions. Note that the 3Di model is very similar to the results of the URS model under similar runoff conditions.

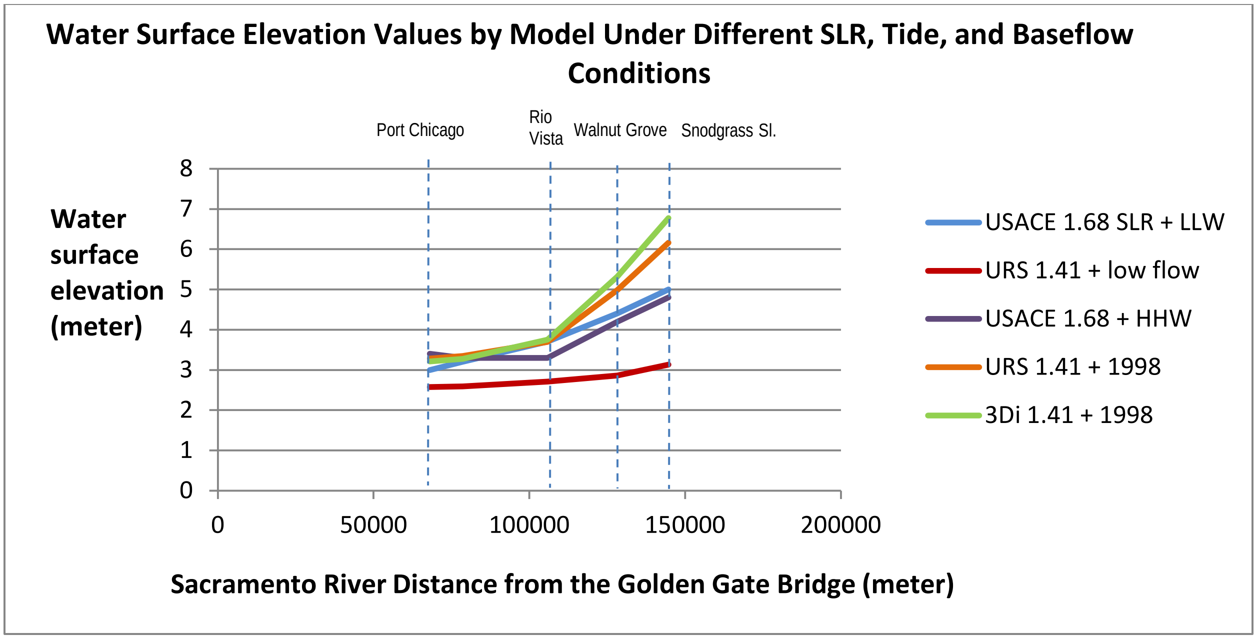


Figure D14. Combined WSE values by model choice under different SLR input values, tide and baseflow conditions.

### *E. Initial water level data for California coastal tiles*

3Di modeling parameters are adjusted to reflect differences in the geographic coverages of extreme storm events that have recently impacted the coastal areas of California. Tiles are assigned extreme waterlevels obtained from NOAA Tide Gauging Stations (NTGS) during three separate extreme storm events that impacted different portions of the coast. NTGS recordings that peaked within the same 72-hour window are considered to be the effect of the same storm event. Storm windows are adjusted to capture all local waterlevel peaks recorded within the same storm event. We use NTGS data referenced to the NAVD88 vertical datum (Table B2). We download 72-hours of water level data at 1-hour intervals for each near 100-year storm considered. In total, data is collected for three temporally separate events that began on the following dates: February 5, 1998; January 9, 2005; and December 30, 2005 and effected the Central, Southern and Northern California pseudo-meteorological zones, respectively (see Figure 18). These water levels are then assigned to the tiles that they fell in. Tiles that did not house a NOAA tidal gauging station take on water-level values from the station they are nearest to.

| NOAA Tidal Gauging Station | NOAA Station ID | UTM Zone | Storm Start Date | Storm End Date | Storm Zone | Tiles |
|---|---|---|---|---|---|---|
| La Jolla | 9410230 | 11 North | 1/9/2005 | 1/11/2005 | South | 1, 12 |
| Los Angeles | 9410660 | 11 North | 1/9/2005 | 1/11/2005 | South | 2, 3, 4 |
| Pt. San Luis | 9412110 | 10/11 North | 1/9/2005 | 1/11/2005 | South | 5, 6, 7, 8, mid 1a, mid1b |
| Monterey | 9413450 | 10 North | 1/9/2005 | 1/11/2005 | South | mid2, mid3, 2a, 2c,2d,2e |
| Pt. Reyes | 9415020 | 10 North | 2/5/1998 | 2/8/1998 | Central | 2b, 3a, 3b, 4a, 4b, 4c |
| Arena Cove | 9416841 | 10 North | 2/5/1998 | 2/8/1998 | Central | 5a, 5b, 5c, 6a |
| North Spit | 9418767 | 10 North | 12/30/2005 | 1/1/2006 | North | 7a, 8a, 8b |
| Crescent City | 9419750 | 10 North | 12/30/2005 | 1/1/2006 | North | 8c, 9a |

Table D4. NOAA Tidal Gauging Station Information and the Tiles to which the data is applied.

**Appendix D References:**


URS model:

URS Inc. (2006). "Future Delta Water Surface Elevations" (Sec. 6.5) in *Technical Memorandum: Delta Risk Management Strategy (DRMS) Phase 1 Topical Area: Flood Hazard Final*. 28-29. http://www.water.ca.gov/floodsafe/fessro/levees/drms/docs/Flood_Hazard_TM.pdf

Dynamic Solutions:

Dynamic Solutions' Inc. (2011). Sea-Level Rise Analysis Using the Extended Delta EFDC Hydrodynamic Model. Sacramento Distract, US Army Corps of Engineers. http://deltacouncil.ca.gov/sites/default/files/documents/files/CA Water Research_05092013.pdf

3Di:

Stelling, G. S. (2012). Quadtree flood simulations with sub-grid digital elevation models. *Proceedings of the ICE - Water Management*, *165*(10), 567–580. http://doi.org/10.1680/wama.12.00018

Casulli, V. and Stelling, G. S. (2011), Semi-implicit subgrid modelling of three-dimensional free-surface flows. Int. J. Numer. Meth. Fluids, 67: 441–449

Stelling, G. S. (2012). Quadtree flood simulations with sub-grid digital elevation models. *Proceedings of the ICE - Water Management*, *165*(10), 567–580. http://doi.org/10.1680/wama.12.00018